Gene Knockdown and Editing Within the Rodent Hippocampus to Inform Gene Therapy Development

by

Kirstan Gimse

A dissertation submitted in partial fulfillment of
the requirements for the degree of

Doctor of Philosophy
(Cellular and Molecular Pathology)

at the
UNIVERSITY OF WISCONSIN-MADISON
2022

Date of final oral examination: 06/10/2022

The dissertation is approved by the following members of the Final Oral Committee:

Krishanu Saha, PhD, Professor, Biomedical Engineering
Randolph Ashton, PhD, Professor, Biomedical Engineering
Marina Emborg, MD/PhD, Professor, Medical Physics
Mathew Jones, PhD, Professor, Neuroscience
Subhojit Roy, MD, PhD Professor, Pathology, UC-San Diego
Jayshree Samanta, MBBS, PhD, Professor, Comparative Biosciences

Contents

Acknowledgements

A great number of people have influenced both my life and my career over the years. I was blessed with some of the most talented educators and mentors during my time at UW Parkside. My experiences there laid a foundation for success, and I would not be who I am today without it.

First, I would like to thank Dr. Gary Wood. Thank you for seeing potential in me. You gave me the opportunity to stand out and the opportunity to be an educator. My experiences as a tutor and as a supplemental instructor for OChem were some of the most rewarding experiences of my life. I am forever grateful for these opportunities and for the guidance and encouragement you offered throughout my undergraduate career.

I would also like to extend my heartfelt gratitude to my undergraduate research advisor Dr. David Higgs. As an educator your enthusiasm for science is contagious. In the classroom you taught me how to think deeply about scientific questions and how to write concisely and persuasively. In the lab you taught me self-confidence and perseverance. Thank you for your guidance, your enthusiasm, and your confidence.

I'd also like to thank my PhD advisor, Dr. Kris Saha. Thank you for taking a chance on me and for always having confidence in my ability to develop new skills. The research I've pursued under your guidance has allowed (read: forced) me to develop skills in areas I'd previously avoided. I'm tremendously thankful for this opportunity to turn a weakness into a strength and to find joy and utility in a previously unexplored area. But also, thank you for asking hard questions, thank you for encouraging words, and thank you for the opportunity to learn, mentor and be mentored in your lab over the last 3.5 years.

And finally, thank you so very much to my friends and family and to colleagues in lab who have offered me so much support over the last few years. Amr, you are an amazing teacher, and your calm quit support and encouragement were indispensable my first year in lab. Kat, thank you for being my in-lab therapist, my communications coach and my loved and valued friend. Rianne, thank you for your friendship for the past twelve years, for sharing both laughter and tears. And Sameer- for everything, thank you.

Abstract

The hippocampus is one of the most extensively studied brain regions and plays a critical role in emotional regulation, spatial reasoning, and learning and memory. This structure is involved in a number of neuropsychiatric disorders including mood disorders, schizophrenia, epilepsy, and Alzheimer's disease. Gene expression alterations in the hippocampus are frequently observed in the context of these disorders as either causal or consequential to the diseased state making the hippocampus a potentially desirable target for gene-therapy interventions. In this thesis, mechanisms to modify gene expression in the hippocampus are explored with the goal of informing gene therapy development. Short hairpin RNAs are used to elucidate the role of *Homer1b/c* in learning and memory and the prevention of age-associated cognitive decline. Single nuclei RNA sequencing (snRNA-seq) methods are next employed to characterize the impacts of *App* editing in a mouse model of Alzheimer's disease. Finally, the delivery of gene editing machinery to hippocampus are profiled using snRNA-seq with a CRISPR-Cas9 nanocapsule. These studies thoroughly characterize cell-type specific responses to this novel nanocapsule delivery system for gene editing in the hippocampus. Altogether, the data presented here contribute to the understanding of disease etiology within the hippocampus and advance the field of gene-therapy-based therapeutics by informing best practices for safety and efficacy evaluation.

1 Understanding neuropathology in the hippocampus to inform gene-therapy

1.1 The hippocampus: a hub for emotional regulation, spatial reasoning, and learning and memory

The hippocampus is one of the most extensively studied brain regions and plays a critical role in emotional regulation, spatial reasoning, and learning and memory. This structure is involved in a number of neuropsychiatric disorders including mood disorders, schizophrenia, epilepsy and Alzheimer's disease (AD). Gene expression alterations in the hippocampus are frequently observed in the context of these disorders as either causal or consequential to the diseased state, making the hippocampus a potentially desirable target for gene therapy interventions to treat the neuropsychiatric disorders mentioned above.

In mammals, the hippocampus is a brain structure embedded deep in the temporal lobe of each cerebral cortex. The structure is most widely known for its important functions in learning and memory and spatial reasoning. However, as part of the limbic system the hippocampus also contributes to social behavior, motivation, and regulation of emotion[1-3]. Memory formation in the hippocampus is characterized by long-lasting changes in the strength of synaptic connections, long-term potentiation (LTP) – a persistent increase in the strength of connections between synapses, and long-term depression (LTD) – a persistent decrease in the strength of connections between synapses. Maintenance of both LTP and LTD beyond their early phase is dependent on significant gene expression changes in the hippocampus largely dependent on a cAMP-dependent signaling cascade involving PKA, mitogen activated protein kinases (MAPK) and the transcription factor cAMP-responsive element binding protein (CREB)[4].

The hippocampus contains the subgranular zone (SGZ; below SG in **Figure 1.1**), which is one of the few places in the brain where adult neurogenesis occurs[5]. Studies indicate that this process also contributes to cognition and plasticity in the hippocampus. Adult neurogenesis is

a tightly regulated process characterized by alterations in gene expression in response to extrinsic signals[6].

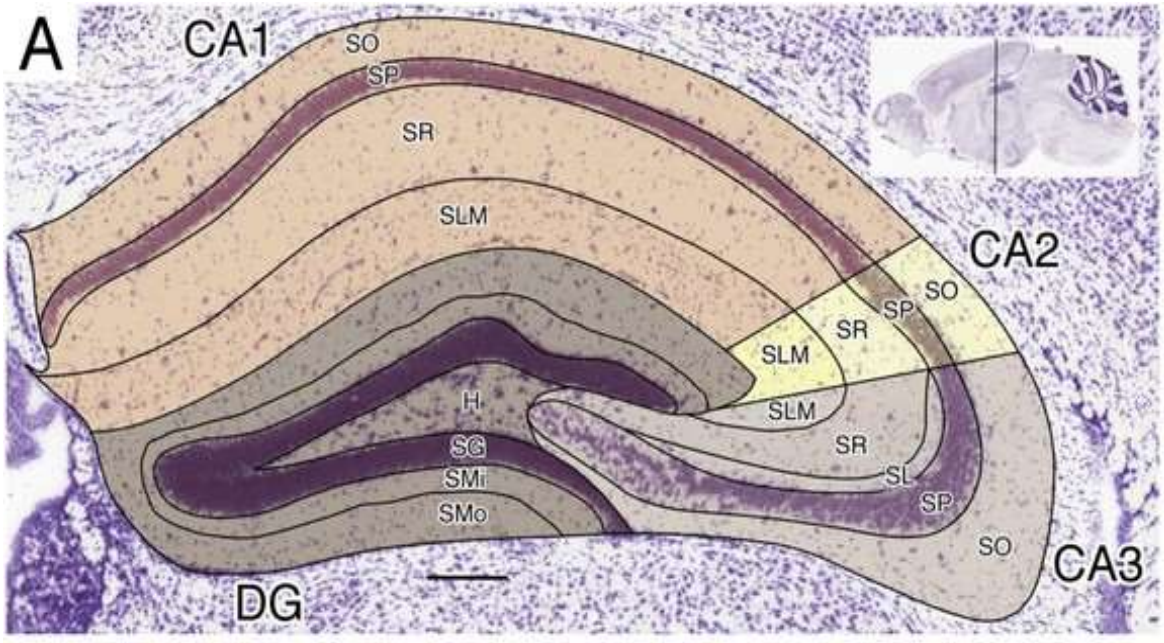

Figure 1.1. Structure and staining of the mammalian hippocampus. Nissl staining of a P56 mouse hippocampus (coronal sections 74 and 85 from the Allen Brain Atlas); Adapted from Reference #5.

1.2 Dysfunction and pathology within the hippocampus

Dysfunction in the hippocampus is associated with a wide variety of neurological maladies. Including depression, anxiety, schizophrenia, post-traumatic stress disorder, age-associated cognitive decline, AD and non-AD neurodegenerative dementias[7-11]. Gene expression alterations in the hippocampus are frequently observed in the context of these disorders as either causal or consequential to the diseased state. Alterations in transcription in the hippocampus have been shown to be associated with age-related spatial impairments and

evidence suggests artificially replacing expression of key downregulated transcripts can rescue this impairment in rodent models[12-14].

In the context of AD, recent advances in spatial transcriptomics and single cell/single nuclei RNA sequencing have revealed new molecular details on pathology within the brain. These studies found that plaque induced cellular responses upregulate complement cascades, oxidative stress pathways and immune response in astrocytes, while downregulating myelination and upregulating cytokine release in oligodendrocytes and oligodendrocyte precursors. Additional studies have shown Aβ stress in AD to cause aberrant excitatory network activity in learning and memory circuitry of the hippocampus leading to excitotoxicity and contributing to neurodegeneration[15,16]. These studies indicate unique cell-type specific mechanisms of AD pathology in many different neural cell-types initiated by excessive β-cleavage of amyloid precursor protein, APP. Recently, a gene-editing paradigm targeting *APP* has been shown to reduce β-cleavage presenting the possibility for therapeutic gene therapy targeting this gene in the hippocampus and other brain regions[17].

1.3 Gene therapy in the brain

In traditional gene therapy, a normal gene is inserted into the genome to replace an abnormal gene responsible for causing a certain disease. The application of gene therapy in the brain is particularly appealing, as drug delivery to the brain has been challenging. For example, to date, traditional pharmacological approaches for the treatment of AD have been largely unsuccessful, at best halting disease without any robust treatment of symptoms. The application of therapeutics in the brain often requires invasive procedures due to complications in passing these therapeutics across the blood brain barrier. Thus, repeat dosing

with therapeutics can be considerably problematic. Therefore, the potential of a gene therapy intervention as a one-time corrective treatment could be considerably advantageous[18].

Despite the one-shot curative potential of gene therapy, there are still a number of safety challenges that need to be addressed when investigating prospective gene therapies. In addition to traditional gene replacement therapy, potential gene therapies to target the brain in human patients include gene augmentation, RNA interference (RNAi), genome editing, and several other techniques (e.g., **Figure 1.2**)[19]. For RNAi, target genes are silenced by DICER related degradation of mRNA transcripts, while CRISPR-Cas9 genome editing targets the endogenous DNA sequence of the target gene. The modes of delivery can utilize viral vectors or non-viral vectors. For example, the CRISPR-Cas9 ribonucleoprotein can be encoded into adeno-associated viral vectors or be manufactured as Cas9 protein and guide RNAs that are delivered using synthetic nanoparticles (e.g., lipid nanoparticles, LNPs)[20].

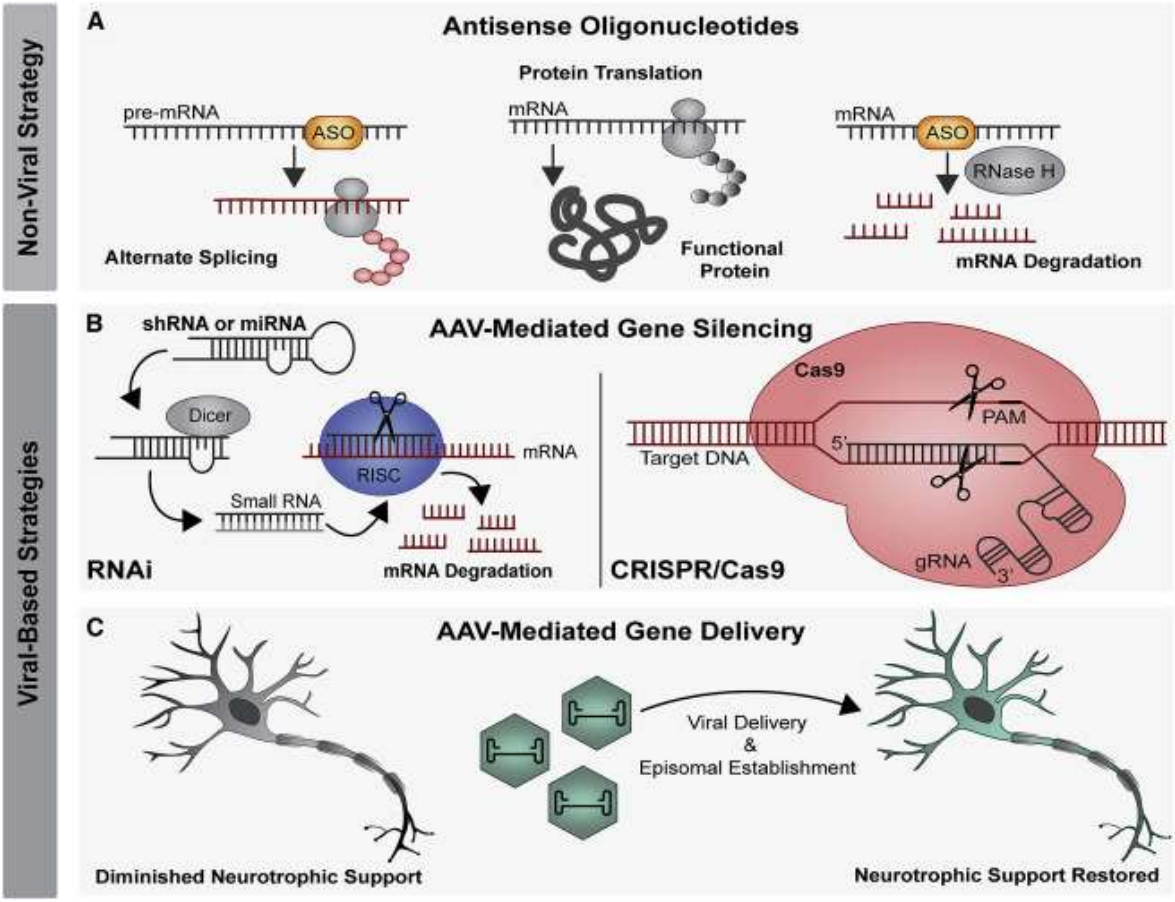

Figure 1.2. Summary of gene therapy strategies for the hippocampus. (A) Non-viral strategies include using ASOs to induce alternate splicing or RNase H-mediated degradation. (B and C) Viral strategies include (B) AAV-mediated gene silencing, through RNA interference, RNAi or CRISPR-Cas9 or (C) AAV-mediated gene delivery including neurotrophic factors can also be used as therapeutics. AAV, adeno-associated virus; ASO, antisense oligonucleotide; Cas, CRISPR-associated system; miRNA, microRNA; PAM, protospacer adjacent motif; RISC, RNA-induced silencing complex; RNAi, RNA interference; shRNA, small hairpin RNA. Adapted from reference #19.

For genome editing, safety considerations include the potential for off-target genomic editing, cell-type specific responses to editing, mRNA misregulation and transcriptional perturbations. Alterations in alternative splicing, the production of gain of function proteins, a p53 mediated stress response, and unpredicted impacts on gene expression regulation and cell

signaling can all have deleterious impacts on cellular function and survival[21,22]. Delivery of the gene therapy payload may also be off-target, hitting structures and cell types in the hippocampus that affect broad neural circuits. Thus, there are still a number of safety challenges that need to be addressed when investigating a potential gene editing based therapeutic for the hippocampus. In the hippocampus, subtle changes in gene expression or inflammatory response are likely to have large impacts on cognition, mood, and behavior.

1.4 Targeting the hippocampus with gene therapy

The work described in this thesis serves to advance our understanding of the utility and potential for gene-therapy interventions in the hippocampus. Here we have utilized recombinant adeno-associated vectors (rAAV) and RNAi to target the expression of a gene shown to be associated with age-associated cognitive decline, elucidating mechanisms of learning and memory. My work with these strategies is detailed in the next chapter. In Chapter 3, I utilized single nuclei RNA sequencing (snRNA-seq) of the mouse brain treated with genome editors to characterize the transcriptomic impacts of a novel somatic cell gene editing approach for the treatment of AD. In Chapter 4, I applied snRNA-seq to characterize the safety and efficacy of editing in the hippocampus via non-viral, nanocapsule-mediated delivery of SpyCas9 RNP in the hippocampus. Altogether, this work profiles two different types of gene therapy – RNAi and CRISPR-Cas9 gene editing – as well as viral and nonviral modes of delivering the gene therapeutic. This work advances the field of gene-therapy in the brain, informing best practices for characterizing the impacts of novel gene therapeutics targeting specifically the hippocampus.

2 Hippocampal Homer1b/c is necessary for contextual fear conditioning and group I metabotropic glutamate receptor mediated long-term depression

Work in this chapter was adapted from:

Hippocampal Homer1b/c is necessary for contextual fear conditioning and group I metabotropic glutamate receptor mediated long-term depression

Kirstan Gimse, Ryan C. Gorzek, Andrew Olin, Sue Osting, Corinna Burger
Neurobiology of Learning and Memory 156, 17-23, doi:10.1016/j.nlm.2018.10.005 (2018).

S.O. performed all intracerebral injections. R.C.G performed Western Blot analysis of PSD95. K.G. performed electrophysiology and behavioral analyses with assistance from A.O. as well as remaining Western Blot analyses. K.G analyzed the data. C.B. supervised the research. K.G. wrote the manuscript with input from all authors.

2.1 Abstract

Coiled-coil forms of Homer1, including Homer1b and c (Homer1b/c) have been shown to play a role in hippocampal learning and memory and synaptic plasticity. We have previously found that overexpression of hippocampal Homer1c is sufficient to rescue learning and memory ability in aged learning impaired rats and in *Homer1* knockout (KO) mice, and to rescue group I metabotropic glutamate receptor (mGluR1/5) mediated long-term potentiation deficits in KO mice. Here, to determine if Homer1b/c is necessary for successful learning and memory we have utilized an rAAV5 vector expressing a *Homer1b/c*-targeting short hairpin RNA to knock down the expression of hippocampal Homer1b/c in adult 4–6-month-old male Sprague Dawley rats. We have found that reduced hippocampal Homer1b/c expression elicits significant learning deficits in contextual fear conditioning, but not in the Morris water maze or novel object recognition tasks. Furthermore, we demonstrate that reduced hippocampal Homer1b/c is sufficient to completely block mGluR1/5 mediated long-term depression in the Schaffer collateral pathway. These results support a significant role for Homer1b/c in learning and synaptic plasticity; however, the exact role of each of these two protein isoforms in learning and memory remains elusive

2.2 Introduction

The synaptic scaffolding coiled-coil forms of Homer1, which include Homer1b and Homer1c (Homer1b/c), link membrane bound group I metabotropic glutamate receptors (mGluR1/5) to downstream signalling molecules[23-27]. Homer1b and Homer1c differ by a 12 amino acid addition in Homer1c[28]. Previous research in our lab and others has shown that Homer1b/c

isoforms play an important role in learning and memory[12-14,29,30]. *Homer1* knockout mice exhibit learning and memory deficits in the radial arm maze and deficits in synaptic plasticity, both of which can be rescued through recombinant adeno-associated virus (rAAV) mediated overexpression of hippocampal Homer1c[14,31]. Additionally, *Homer1c* transcripts are downregulated in the hippocampi of aged learning impaired rats when compared to aged superior learners after training in a hippocampal dependent learning task, and rAAV-mediated overexpression of hippocampal Homer1c is sufficient to improve learning and memory performance in the Morris water maze and object location memory tasks in these animals[12,13]. Importantly, disruption of associations between Homer1b/c and mGluR1/5 metabotropic impedes expression of mGluR1/5 mediated long-term depression (mGluR-LTD) and long-term potentiation (mGluR-LTP)[26,31-33].

mGluR1/5 stimulate the synthesis of proteins that modulate ionotropic receptor trafficking and expression of immediate early genes related to cognition. mGluR-LTD and mGluR-LTP both play essential roles in hippocampal learning and memory[34-38] Dysregulation of mGluR-LTD has been shown to play a role in Parkinson's disease, drug addiction, fragile-X mental retardation syndrome and Alzheimer's disease[39]

Here we sought to determine whether Homer1b/c isoforms are necessary for hippocampal learning and memory and synaptic plasticity. To this end, we utilized recombinant Adeno-associated virus (rAAV) mediated expression of a small hairpin RNA sequence targeting *Homer1b/c* (rAAV-shH1b/c) to knock down expression of Homer1b/c in the hippocampus of adult Sprague Dawley rats. We found that Homer1b/c knockdown leads to significant memory deficits in contextual fear conditioning and completely ablates expression of mGluR-LTD.

2.3 Results

2.3.1 rAAV-mediated delivery of Homer1b/c shRNA yields significant reduction in hippocampal Homer1b/c expression

We first determined the level of Homer1b/c knockdown in adult rats. rAAV-shRNA mediated expression of a sequence targeting Homer1b/c was used to knockdown Homer1b/c expression. Adult Sprague Dawley rats (3 months) were injected with rAAV-shH1b/c, rAAV-shCTL, or sham surgery. Hippocampal proteins from these animals were isolated and analyzed for Homer1b/c expression one month post-surgery. Densitometry analysis of immuno-positive bands showed a significant difference between injected groups (Fig. 2.2 $F_{(2, 13)} = 18.97$, $p = 0.0001$). An average of 50% reduction in Homer1b/c expression in total hippocampus for shH1b/c injected animals in comparison to sham injected controls was observed (Fig. 2; $p = 0.0002$). No significant differences in Homer1b/c expression were observed between sham injected and shCTL injected controls (Fig. 2.2; $p = 0.4329$). To determine whether proteins associated with Homer1b/c were affected by its downregulation, we examined levels of mGluR5 and PSD95 in the different experimental groups. No significant effect of treatment on mGluR5 expression was observed (Fig. 2.2; $F_{(2,9)} = 4.061$, $p = 0.055$. sham vs. shH1b/c: $p = 0.1$; shCTL vs. shH1b/c: $p = 0.97$; sham vs. shCTL: $p = 0.072$). Similarly, all experimental groups showed similar expression levels of PSD95 with no effect of treatment (Fig. 2.2; $F_{(2,9)} = 0.408$, $p = 0.7$). sham vs. shH1b/c: $p = 0.8$; shCTL vs. shH1b/c: $p = 0.7$; sham vs. shCTL: $p = 0.96$). Western blot analyses were also performed on hippocampal slices collected during preparation for electrophysiology on days 40 to 50 yielding similar results (data not shown).

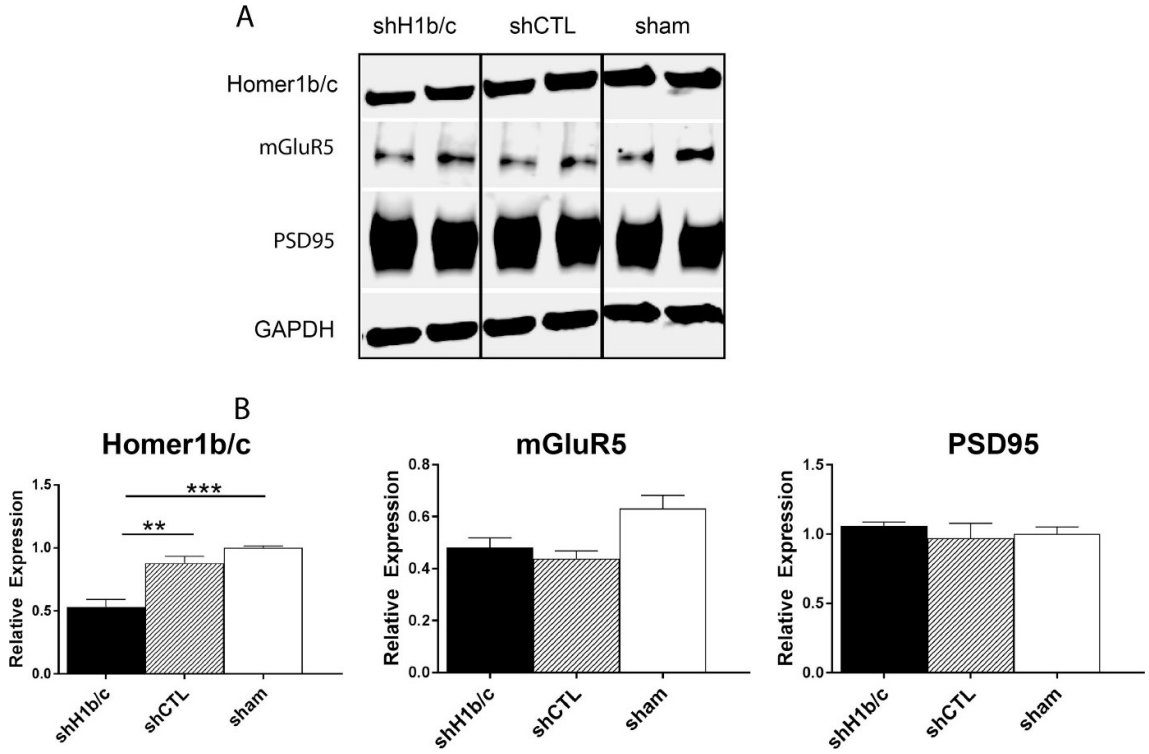

Figure 2.2 rAAV-shH1b/c significantly reduces Homer1b/c expression.
A.) Representative Western blot showing Homer1b/c reduced protein expression in rAAV-shH1b/c injected relative to rAAV-shCTL injected and sham injected controls. **B.)** Densitometry analysis of Homer1b/c expression shows a 50% reduction relative to controls with no significant differences in Homer1b/c expression in sham injected versus rAAV-shCTL injected controls (shH1b/c: n= 8, sham: n= 4 , shCTL: n= 4). No statistically significant changes were found in mGluR5 or PSD95 expression between experimental groups.

2.3.2 Reduced expression of hippocampal Homer1b/c causes learning deficits in contextual fear conditioning

To determine whether hippocampal Homer1b/c expression is necessary for successful learning and memory, animals were tested in the contextual and cued fear-conditioning tasks, the Morris water maze, and the novel object recognition task. Fear conditioning analysis indicated no significant differences in freezing behavior prior to the introduction of tone or shock (Fig. 2.3A, t= 0.14, df= 16, p= 0.89). However, animals treated with shH1b/c showed significantly less post-shock freezing on training day [a measure of short-term contextual fear

memory (Fig. 2.3B, t= 2.67, df= 16, p= 0.016)] and exhibited significant memory deficits in contextual fear conditioning on testing days 48 hours later (Fig 2.3C, t= 2.35, df= 16, p= 0.03). To determine if the observed memory deficits may be the result of early extinction, the data were analyzed in 30 second intervals. shH1b/c treated animals displayed memory deficits in contextual fear conditioning throughout the duration of the testing period indicating a deficit in either acquisition or recall (Fig. 2.3D, $F_{(1,16)} = 5.44$, p= 0.03). No significant differences were found in freezing behavior during auditory cued fear conditioning analysis (Fig 2.3E, t= 1.1, df= 16, p= 0.288). Surprisingly, no significant differences in learning ability were observed between shH1b/c injected and control animals in any of the other hippocampal dependent behavioral tasks including the Morris water maze [hidden platform (t= 1.17, df= 21 p= 0.26)], probe trial platform crossings (Fig 2.3F, t= 1.12, df= 21, p= 0.28), probe trial quadrant time (Fig 2.3G: t=1.01, df= 21, p= 0.29), and the novel object recognition task (Fig. 2.3H t= 1.71, df= 21, p= 0.10).

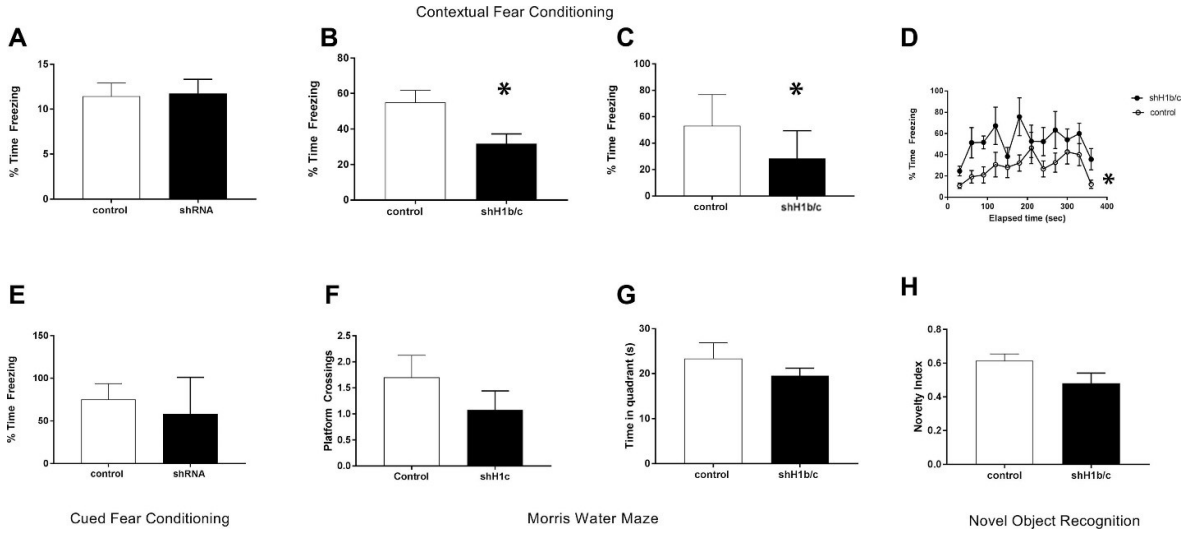

Figure 2.3 Homer1b/c knockdown causes significant memory deficits in contextual fear conditioning, but not in auditory cued fear conditioning, MWM, or novel object recognition. Figure caption continued on the next page.

Figure 2.3 Homer1b/c knockdown causes significant memory deficits in contextual fear conditioning, but not in auditory cued fear conditioning, MWM, or novel object recognition.
A.) No significant differences between groups were observed in percent of time freezing during exploration prior to training (n= 9 shH1b/c, n= 9 control). **B.)** shH1b/c treated animals showed significantly reduced post-shock freezing. **C.)** Contextual fear conditioning: rAAV-shH1b/c injected animals show significantly less freezing response upon re-exposure to an environment previously paired with an aversive stimulus than control animals. **D.)** Contextual fear conditioning was analyzed by percent of time spent freezing in 30 second intervals throughout the duration of the testing period. rAAV-shH1b/c injected animals spent significantly less time freezing throughout the duration of the testing period. **E.)** Cued fear conditioning: rAAV-shH1b/c injected and control animals show similar freezing responses when re-exposed to an auditory cue previously paired with an aversive stimulus. **F.)** MWM probe trial: no significant differences were observed between shH1b/c treated and control animals in the number of platform crossings (n= 13 shH1b/c, n= 10 control). **G.)** MWM probe trial: no significant differences were found in the time spent in the probe quadrant between shH1b/c injected and control animals. **H.)** Novel object recognition: when exposed to one novel and one familiar object, both shH1b/c injected and control animals showed increased interest in the novel object (n= 13 shH1b/c, n= 10 control).

2.3.3 Reduced expression of hippocampal Homer1b/c ablates mGluR-LTD expression

To investigate the cellular mechanisms underlying the observed memory deficits, electrophysiological recordings were performed in acute hippocampal slices to assess the impact of Homer1b/c knockdown on mGluR-LTD which has been shown to be an important process for hippocampal learning and memory[35-38,40]. Here we found that, similar to previous findings, bath application of 100μM DHPG for 10 minutes induced robust depression in control hippocampal slices from animals injected with rAAV-shCTL, (Fig. 2.4A)[41]. In contrast, bath application of DHPG in hippocampal slices from rAAV-shH1b/c injected animals did not result in LTD expression (Fig. 2.4A; main effect of treatment, $F_{(1, 10)} = 13.62$, $p= 0.004$). Traces from these slices exhibit a slight short-term depression which quickly recovers to baseline synaptic efficacy. There were no statistically significant differences in

mGluR-LTD expression between sham injected and rAAV-shCTL controls (Fig. 2.4A vs 4B, C and D; main effect of treatment, $F_{(1, 11)} = 0.17$, $p= 0.69$.)

To further characterize DHPG induced LTD we tested the impact of selective antagonists for NMDAR, mGluR1, and mGluR5 on DHPG induced LTD. Since both GFP and sham injected animals showed no difference in mGluR-LTD, we used uninjected animals as controls for these experiments. Incubation in the presence of the NMDAR receptor antagonist (2R)-amino-5-phosphonovaleric acid (APV;100 μM) before and during application of DHPG did not significantly affect induction of LTD as it has been reported (Fig. 2.4B; main effect of treatment, $F_{(1, 12)} = 0.049$, $p= 0.83$)[42]. Similar results were obtained with pre-incubation with the selective mGluR5 antagonist 2-methyl-6-(phenylethynyl) pyridine hydrochloride (MPEP;10 μM) (Fig 2.4C; main effect of treatment, $F_{(1, 10)} = 0.696$, $p= 0.42$). Induction of LTD in the presence of the mGluR1 antagonist LY 367385 (100μM) did not significantly impact the maintenance or magnitude of mGluR-LTD (Fig. 2.4D; main effect of treatment, $F_{(1, 12)} = 0.579$, $p= 0.46$), however the rate of induction was significantly reduced. (Fig. 2.4D; main effect of treatment, $F_{(1, 12)} = 7.90$, $p= 0.016$). These data are in agreement with previous reports on the mechanism of induction of mGluR-LTD[39].

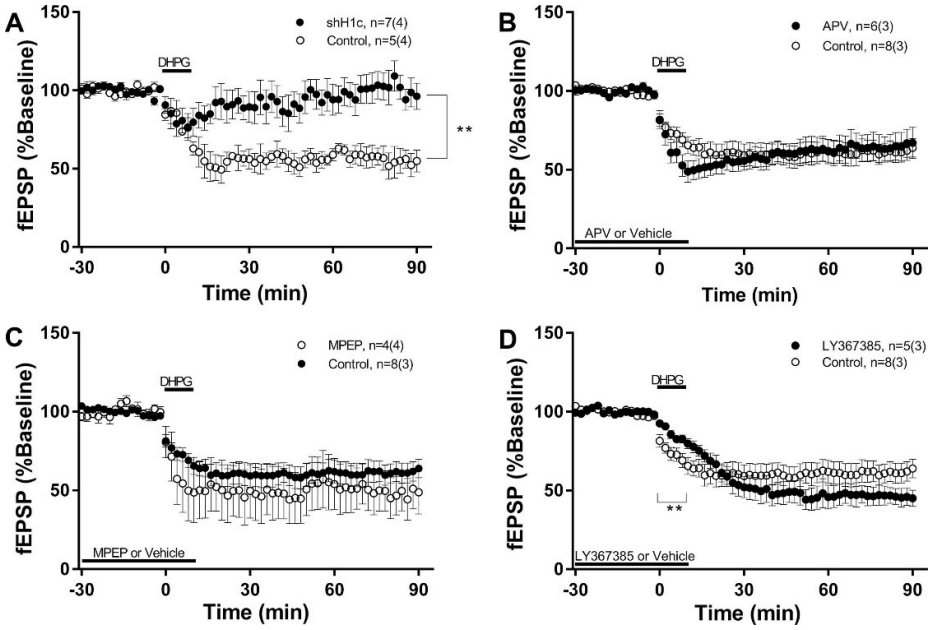

Figure 2.4 Homer1b/c is necessary for expression of mGluR-LTD.
A.) Homer1b/c knockdown blocks expression of LTD (shH1b/c: n= 7 slices (4 animals); control: n= 5(4)). **B.)** The NMDA antagonist AP5 does not prevent mGluR-LTD induction (AP5: n= 6(3); control n= 8(3)). **C.)** Incubation in MPEP during mGluR1/5 activation does not prevent mGluR-LTD (MPEP n= 4(4); control n= 8(3)). **D.)** mGluR-LTD induction in the presence of the mGluR1 antagonist LY 367385 does not significantly impact the magnitude of LTD expression (LY 367385: n= 5(3); control: n= 8(3)), but significantly reduces the rate of mGluR-LTD induction.

2.4 Discussion

This study investigated the impact of reduced hippocampal Homer1b/c expression on spatial learning and memory and synaptic plasticity. We found that knockdown of hippocampal Homer1b/c significantly reduced freezing behavior both during the post-shock periods on training day, and during testing of contextual fear conditioning 48 hours later. Significant deficits were not observed in other learning tasks, namely the MWM, novel object recognition and cued fear conditioning.

Both the acquisition and expression phases of learning in contextual fear conditioning are dependent on hippocampal mGluR1/5 signaling; therefore, we hypothesized that deficits

in mGluR1/5signaling in the absence of Homer1b/c would contribute to learning deficits in this task[43]. The results of this study support this hypothesis. Furthermore, previous studies have provided evidence for post-shock freezing to be a measure of immediate contextual fear memory. Therefore, significantly reduced post-shock freezing is further evidence of a role for Homer1b/c in contextual fear conditioning and may suggest that Homer1b/c is necessary for acquisition of contextual fear memory[44]. The lack of deficits observed in auditory cued fear conditioning were not surprising, as multiple studies have indicated that this type of memory acquisition is largely independent of the hippocampus and is primarily coded for in the amygdala[45].

Studies regarding the role of the hippocampus in novel object recognition have elicited conflicting results; many studies indicate that object recognition is encoded primarily within the perirhinal cortex[25,46-51]. There is evidence, however which indicates that the hippocampus is responsible for encoding the novel acquisition of object location. For example, endogenous hippocampal LTD dependent on both NMDAR and mGluR5 is induced in the rodent hippocampus upon exposure to configurative novelty in object-space (i.e. the presentation of either novel objects or familiar objects within a novel spatial context), but not upon exposure to novel spatial environment alone[35,36]. The finding that Homer1b/c knockdown did not elicit significant deficits in this task might indicate that any spatial coding deficits evoked by impeded mGluR1/5 signaling in the absence of Homer1b/c were obfuscated by object recognition coding within the perirhinal cortex. Alternatively, it may be that mGluR1/5 signaling mechanisms independent of Homer1b/c are sufficiently compensatory for this task or that our testing paradigm is insufficiently sensitive.

More surprising is the lack of spatial learning and memory deficits observed in the MWM. Considerable studies have been published indicating the role of the hippocampus in spatial learning and memory in the Morris water maze[52,53]. Furthermore, evidence supports a

role for group I mGluR signaling in the acquisition and retrieval learning phases of similar spatial learning tasks and positive modulators of mGluR5 have been shown to enhance MWM performance[34,54]. Additionally, overexpression of hippocampal Homer1c is sufficient to rescue MWM and OLM performance in aged learning impaired rats and radial arm maze ability in young Homer1 knockout mice[13,14]. Therefore, we initially hypothesized that disruption of mGluR1/5 signaling in the absence of Homer1b/c would yield significant learning deficits in this task. However, these current findings suggest that while Homer1c is sufficient to enhance this type of learning and rescue spatial learning deficits observable in this task in aged learning impaired rats, it may not be necessary for this type of spatial learning in young adult rats. Additionally, the discrepancy between MWM deficits observed in Homer1 knockout mice and Homer1b/c knockdown rats are likely attributable to the absence of all Homer1 isoforms, including the short-form Homer1a, as well as the global nature of this knockout. There is also a potential for the development of compensatory mechanisms developing between the time of injection and behavioral analyses, however it is necessary to allow this time to achieve maximal H1b/c knockdown.

Here we show that hippocampal Homer1b/c is necessary for the expression of mGluR-LTD. These data are in agreement with previous findings which indicate that disruptions between mGluR5 and coiled coil Homer1 proteins impedes mGluR-LTD[26]. We also confirm results from other studies indicating that blockade of NMDAR, mGluR1 or mGluR5 alone during LTD induction does not significantly affect the magnitude or length of expression. Blockade of mGluR1, however, does impact the rate of induction, suggesting that this receptor plays a key role in the early stage of LTD induction. These results are again consistent with previous characterizations of mGluR-LTD mechanism[55]. Both mGluR1/5-LTP and mGluR1/5 dependent LTD have been shown to be important for learning and memory, however evidence suggests that expression of mGluR1/5 dependent LTD may be

particularly important for maintenance of learning and memory ability in aged animals[34-38]. It may be that increased susceptibility to mGluR-LTD functions as a compensatory mechanism for the age-associated dysregulation of other synaptic plasticity mechanisms. Here we have focused on the impact of rAAV-shH1b/c on mGluR-LTD in young rats, but our future studies will focus on aged rats.

We found that downregulation of Homer1b/c did not result in decreased levels of mGluR5 or PSD95. This suggests that the phenotypes identified with Homer 1b/c knockdown are due to a decreased pool of Homer1b/c able to interact with mGluR1/5, rather than by a subsequent regulation of receptor expression[26,56]. However, this does not preclude the possibility that Homer1b/c knockdown alters the subcellular localization of mGluR5 which may also impact signaling[57]. Future studies are necessary to investigate the mechanism of Homer1b/c in LTD and learning and memory formation.

2.5 Methods

2.5.1 Animal Subjects

3-month-old male Sprague-Dawley rats were purchased from Envigo. All animals had free access to water and food. Animals were maintained on a 12-hour dark and light cycle, with behavioral tests conducted during the light cycle. All procedures concerning animals were approved by the University of Wisconsin Institutional Animal Care and Use Committee and were conducted in accordance with the U.S. National Institutes of Health "Guide for the Care and Use of Laboratory Animals." Average animal age during testing was 4–6 months old. The experimental timeline is shown in figure 2.1.

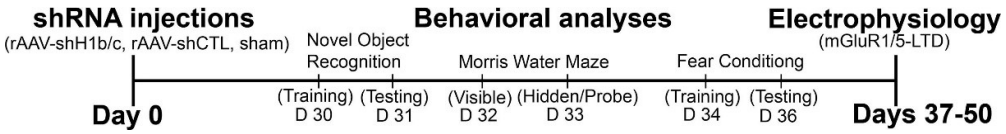

Figure 2.1 Experimental timeline

2.5.2 Viral vectors

SureSilencing shRNA plasmids were purchased from Qiagen and subcloned into rAAV. The sequence targeting Homer1b/c (shH1b/c) was: CAGGAAGTTGAGATTCGAAAT. The sequence for the control vector (shCTL) was: GGAATCTCATTCGATGCATAC. The negative control shRNA provided by Qiagen is a scrambled artificial sequence which does not match any human, mouse, or rat gene. Viral vector preparations of rAAV5 were purchased from the University of Pennsylvania Vector Core. The titer for rAAV-shH1b/c was 5×1013 vector genomes/ml; for rAAV-GFP was 2.59×1012 vg/ml. Each plasmid carries an shRNA under the control of the human U1 promoter and a GFP reporter gene under the control of the CMV promoter. We have previously shown the area and cell types transduced by this rAAV5 serotype[14,58,59]

2.5.3 Intracerebral injection of rAAV vectors

Bilateral intracerebral injections of rAAV into the rat hippocampus have been described previously in detail[13]. Two sites were injected per hippocampal hemisphere. 2µl of viral vector were injected per site. Animals were allowed to recover for one month before behavioral testing and/or electrophysiological recordings.

2.5.4 Behavioral analysis

Behavioral tests were performed in the following order: novel object recognition, Morris water maze, contextual and cued fear conditioning. All experimenters were blinded to the treatment of the subjects. For novel object recognition and Morris water maze tests n=13

shH1b/c and n=10 for sham controls were used. Fear conditioning analysis was not completed for a subset of animals due to a breakdown of the freeze monitor during experimentation: n=9 per condition.

2.5.4.1 Novel Object Recognition

We used a two-day version of the Novel Object Recognition paradigm as previously described in detail[60]. Rats were initially trained in the location of two identical objects. Each animal was placed in the enclosure and given 5 minutes to explore the area. Testing occurred 24 hours later with an identical protocol with the exception that the identity of one of the objects had been changed. In between each animal, on training and testing days, the bedding was stirred, and the toys cleaned with 70% ethanol to minimize olfactory cues.

2.5.4.2 Morris Water Maze

We used a two-day version of the Morris Water Maze consisting of one day of visible platform training followed by one day of hidden platform training and a probe trial, as described in detail[60] Visible platform training consisted of 4 consecutive trials on day 1. Hidden platform training took place on day 2. Training consisted of 4 consecutive trials. The time taken to reach the platform was recorded for each trial. The probe trial was carried out for each animal immediately following the four hidden platform trials; for this trial the time spent in the probe quadrant, as well as the number of times the animal crossed the platform area were recorded.

2.5.4.3 Fear Conditioning

Fear conditioning began with a day of training during which each animal was placed inside a white rectangular enclosure (San Diego Instruments Freeze Monitor). Each animal was then subjected to 2 minutes of silence, followed by 30 seconds of tone (2000 Hz, 80dB). During

the last 2 seconds of tone the animals were subjected to a mild foot shock (0.8 mA). This process of two-minute silent exploration time followed by 30 seconds of tone with 2 seconds of foot shock was repeated one additional time followed by a final 1 minute of silent exploration time. Contextual fear conditioning (CFC) was tested 48 hours later. For this test the animal was reintroduced to the rectangular enclosure and given 6 minutes of silent exploration time. Auditory cued fear conditioning (AFC) was tested 49 hours after training. For this test the animal was placed into a black, triangular enclosure scented with vanilla. The animal was subjected to 2 minutes of silent exploration time, followed by 30 seconds of tone, similar to the training protocol, but lacking the shock stimulus. This process was repeated one additional time and followed by a final 1 minute of silent exploration. Freezing time was measured during training and both testing protocols using the Freeze Monitor System and Freeze Monitor software (San Diego Instruments). Memory recall was assessed by measuring the percent of time spent freezing in response to the spatial or auditory stimuli on testing day. For CFC, comparisons were made between groups using the percent of time freezing over the entire 6 minute free exploration testing protocol; for AFC, assessments were made using the percent of time spent freezing during the two 30 second tone presentations. Additionally, the percent of time spent freezing during 30 second increments for CFC testing were compared to determine whether learning deficits were a result of early extinction. Post shock freezing, the percent of time freezing during both 2 minute post-shock exploration periods on training day, was also compared to further investigate the role of Homer1b/c in fear conditioning. Differences in average freezing time during training, both prior to the introduction of sound or shock stimuli and in the two-minute exploration period following the first sound/shock combination, were compared to rule out any mobility issues as a result of treatment influencing the testing results.

2.5.5 Electrophysiology

Electrophysiological analysis began one day after the completion of behavioral analyses, one animal chosen at random was analyze per day. Immediately after euthanasia the brain was removed from the skull and submerged in ice cold cutting solution (CS) [in mM]: 212 sucrose, 2.6 KCl, 1.25 NaH2PO3, 26 NaHCO3, 0.5 CaCl2, 5 MgCl2, 10 glucose. The hippocampi were sectioned transversely into 400 μm slices immersed in ice- cold CS. Slices were allowed to recover for 45 min at room temperature (RT) in 50:50 CS: artificial cerebrospinal fluid (ACSF) [in mM]: 124 NaCl, 5 KCl, 1.25 NaH2PO3, 26 NaHCO3, 2 CaCl2, 1 MgCl2, 10 glucose followed by a second 45 minute incubation at RT in ACSF. Slices were then transferred to an interface recording chamber perfused with ACSF and allowed to recover for 2 hours at 32 °C. All solutions were carboxygenated during slice preparation, recovery and recording (95/5, O2/CO2). Enameled bipolar platinum-tungsten (92:8 Pt:Y) stimulating electrodes were placed at the border of Area CA3 and Area CA1 along the Schaffer-Collateral pathway. Field excitatory post-synaptic potentials (fEPSP) were recorded from the stratum radiatum, with ACSF filled recording electrodes (2–4 MΩ). Baseline synaptic transmission was assessed for each individual slice by applying increasing stimuli (0.5–25 V, 25 nA–1.5 μA, A-M Systems model 2200 stimulus isolator, Carlsborg, WA) to determine the relationship between stimulation voltage and fEPSP slopes (Input:Output). Subsequent experimental stimuli were set to an intensity that evoked a fEPSP with a slope half that of the maximum fEPSP slope. mGluR-LTD was induced with bath application of 100μM (S)-dihydroxyphenylglycine (Tocris) in ACSF for 10 minutes. fEPSPs were recorded for 90 minutes post-LTD induction followed by a repeated measure of Input:Output relationship to confirm maintenance of slice health. Synaptic efficacy was constantly monitored (0.05 Hz). Every 2 min, sweeps were averaged; the fEPSPs were amplified (A-M Systems model 1800), digitized (Digidata 1322B, Molecular Devices,

Sunnyvale, CA) and then analyzed (pClamp, Molecular Devices). All numerical data are expressed as mean ± SEM.

2.5.6 Protein extraction and Western Blot analysis

Whole hippocampi were dissected from a subset of animals for Western blot analysis 30 days post viral vector injection. Tissue lysis and homogenization was performed with a 28-gauge insulin needle in RIPA buffer. 40µg of purified protein was separated using 4–15% gradient SDS–PAGE gels (Mini-PROTEAN TGX, Biorad, Hercules, CA) and then transferred to PVDF membranes (Trans Blot Turbo Transfer Pac, Biorad, Hercules, CA) using a Transblot Turbo Transfer System (Biorad, Hercules, CA). Primary antibodies included Homer1b/c (sc-20807, Santa Cruz, 1:1000), mGluR5 (AB5675, Millipore, Burlington, MA, 1:1000), PSD95 (3450S; Cell Signaling, 1:500) and GAPDH (MAB374, Millipore, Burlington, MA, 1:1000). IRDye 680 or 800 secondary antibodies (925–32213, 925–32212, Li-Cor, 1:5,000) were used and the membranes imaged using the Odyssey CLx imaging system (Li-Cor). Homer1b/c, mGluR5 and PSD95 bands were normalized against GAPDH expression and densitometric quantitation of immuno-positive bands was performed using Image Studio Lite image processing software (Li-Cor).

2.5.7 Statistical Analyses

Statistical analyses were performed using Prism 7.03 (Graphpad Software Inc., La Jolla CA). Significance was set at $p<.05$. For behavioral analyses, two-tailed t-tests were used to assess the significance of differences observed between shH1b/c treated and control animals, with the exception of the 30 second increment analysis of CFC which was analyzed by two-way ANOVA (treatment and time) with repeated measures (mixed model) and Bonferroni posthoc tests. Electrophysiology data were analyzed by two-way ANOVA (treatment and time) with repeated measures (mixed model) and Bonferroni posthoc tests. One-way-ANOVA followed

by Tukey's multiple comparison tests were employed for statistical analysis of Western blot data.

2.6 Acknowledgements

This research was supported by grant R01AG048172–03 to CB, NIH T32 GM081061 to KG and in part by the Core Grant for Vision Research from the NIH to the University of Wisconsin-Madison (P30 EY016665). I would like to thank Dr. Corinna Burger for guiding the research discussed in this chapter, as well as Susan Osting, Andrew Olin and Ryan Gorzek for their contributions to this research.

3 Single nuclei RNA sequencing to evaluate the transcriptomic impact of APP C-terminus editing in a mouse model of Alzheimer's disease

App C-terminus edited mouse lines were developed in Dr. Subhojit Roy's Lab at UCSD. All animal tissues used in this study were gifted from the Roy Lab.

3.1 Abstract

Alzheimer's disease (AD) is a progressive neurodegenerative disorder and the primary cause of dementia among older adults. This disease is characterized by molecular changes in several neural cell types leading to increased levels of Aβ and phosphorylated tau, inflammation, and neurodegeneration[61]. Studies indicate unique cell-type specific mechanisms of AD pathology in many different neural cell-types initiated by excessive β-cleavage of the amyloid precursor protein (APP). Recently, CRISPR/Cas9 gene editing targeting the C-terminus of APP has been shown to attenuate β-cleavage, reducing the production of neurotoxic β-amyloid (Aβ) and β-CTFs, while upregulating neuroprotective α-cleavage. Here we use single nuclei RNA sequencing (snRNA seq) to characterize the cell-type specific AD-associated transcriptional perturbations within a rodent model of AD as well as the transcriptional impacts of a potential therapeutic gene-edit for the treatment of AD. We found cell-type specific changes in the disease model which appear to recapitulate some of the key changes observed in AD and in other rodent AD models as well as transcriptomic shifts in response to edited *App* which may be advantageous in the context of AD. While more research is necessary to fully understand the implications of these transcriptomic shifts, these data illustrate the utility of snRNA seq for the characterization and evaluation of potential gene-editing based therapies and may help to advance a novel gene-editing based AD therapeutic toward clinical application.

3.2 Introduction

Alzheimer's disease (AD) is a progressive neurodegenerative disorder and the most common cause of dementia among older adults. This disease is characterized by molecular changes in

several neural cell types leading to increased levels of Aβ and phosphorylated tau, inflammation, and neurodegeneration[61]. Spatial transcriptomics and single-cell/single-nuclei RNA sequencing (scRNAseq/snRNAseq) in AD and rodent model of AD have revealed diverse cellular responses induced by plaques. These responses upregulate complement cascades, oxidative stress pathways and immune response in astrocytes, while downregulating myelination and upregulating cytokine release in oligodendrocytes and oligodendrocyte precursors. Further, unique subtypes of microglia in the context of AD had both neuroprotective and neurodegenerative activities[15,62-65]. Aβ stress in AD can cause aberrant excitatory network activity in learning and memory circuitry of the hippocampus[15,16]. These studies indicate unique cell-type specific mechanisms of AD pathology in many different neural cell-types initiated by excessive β-cleavage of the amyloid precursor protein (APP). Additionally, β-cleavage alters gene expression due to transcriptional regulation by the APP intracellular domain (AICD). When generated via the amyloidogenic pathway, AICD is stabilized and translocated to the nucleus. AICD transcriptional regulation inhibits adult hippocampal neurogenesis, induces cell-death pathways via upregulation of p53 and BIM, and contributes to neurotoxicity and hyperphosphorylation of tau by upregulation of GSK3β[63,66-70].

Recently, CRISPR/Cas9 gene editing targeting the C-terminus of APP has been shown to attenuate β-cleavage, reducing the production of neurotoxic β-amyloid (Aβ) and β-CTFs, while upregulating neuroprotective α-cleavage (Fig. 3.1a)[17]. Additionally, this edit results in a loss of APP Thr668, the phosphorylation of which is necessary for nuclear translocation of AICD, likely eliminating its activity as a transcription regulator. Preliminary data indicate that this C-terminus *App* editing in a mouse model of AD significantly reduces Aβ accumulation and may rescue spatial learning deficits. However, the cellular changes

underlying these learning differences have yet to be characterized. Here we use snRNA seq of *App*-edited AD mouse model brains to characterize cell-type specific AD-associated transcriptional perturbations within this disease model.

3.3 Results

3.3.1 Transcriptomic profiling of APP-NLGF, WT and APP-NLGF-ΔC mouse brains

A previously established AD mouse model, APP-NLGF, developed by Saito et al, harbors modification to the endogenous mouse *App* gene that allow for the recapitulation of AD pathology without App overexpression. The modified endogenous *App* gene includes a humanized Aβ region, as well as Swedish, Iberian, and Artic mutations[71,72]. My collaborators in the Roy lab (UC-San Diego) have since modified this model using CRISPR-Cas9 genome editing of mouse embryos. Two mouse colonies were generated. One colony harbored a homozygous insertion of single T base (InsT) through indels produced by a Cas9-induced double strand break in the C-terminal *App* coding region (Fig. 3.1). The other colony harbored a homozygous deletion of 5 bases at the same Cas9 double strand break. Both edits result in a frameshift, and therefore a premature truncation of the App protein. Both of these edits have been previously shown to result in a truncated App protein that is preferentially processed by the non-amyloidogenic pathway resulting in reduced production of Aβ and increased expression of neuroprotective APPα (Fig. 3.1b)[17]. Single nuclei RNA seq was used to examine the transcriptional profiles of neural cells from two APP-NLGF, two WT, two Del5 and two InsT mouse brains.

3.3.2 Identification and quantification of cell-types

After quality control filtering (Methods), we analyzed the transcriptional profiles of 86,897 nuclei, 19,737 from two APP-NLGF; 23,058 from two InsT; 24,660 from two Del5 and 19,442 from two WT mouse brains. We first performed initial unbiased uniform manifold approximation and projection (UMAP) clustering on all samples[73]. This analysis yielded 43 unique cell clusters, which we subsequently categorized into seven major cell-types according to their individual transcriptome profiles and previously reported cell-type markers[74-79] (Fig. 3.2, and Sup. Fig 3.1). To facilitate analysis, adjacent and/or overlapping clusters of the same cell-type were regrouped into single clusters, ultimately yielding 20 clusters: 11- glutamatergic neurons (N_Glu), 4- GABAergic neurons (N_Gaba), 1- oligodendrocytes (Olig), 1- microglia (Micro), and 1- brain endothelial cells (Endo) (Fig 3.2a).

We next investigated the abundance of each cell type across the four genotypes (Fig. 3.2c, d and Supp. Table 3.1). Here we found a significant increase in the proportion of microglia from the APP-NLGF disease model in contrast to WT ($F_{(3,4)} = 0.6.68$, $p = 0.048$), while no significant differences were observed in the proportion of microglia from either Del5 or InsT mouse brains. We also compared the proportions of sample in each subcluster and found no significant differences in these proportions between the four genotypes (Supp. Fig. 3.2, Supp. Table 3.1).

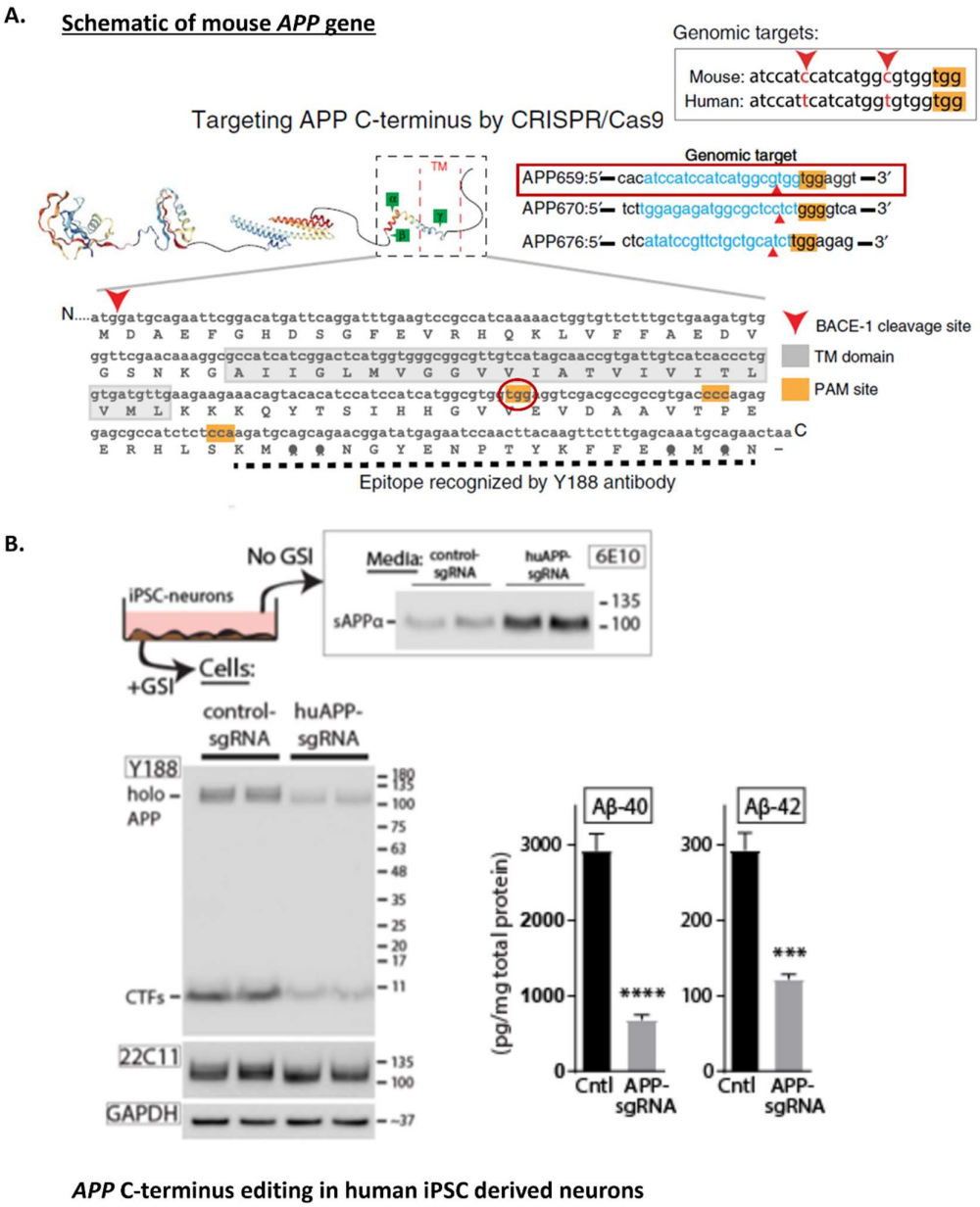

Figure 3.1 Editing of the APP C-terminus yields a truncated APP protein preferentially processed by the non-amyloidogenic pathway. A.) Schematic of the mouse *App* gene with SpyCas9 PAM sites highlighted in yellow. Cut-site shown to generate therapeutic truncated APP protein circled in red. Similar sequence in human *APP* gene used for editing in human cells also shown. **B.)** Western blot analysis of proteins extracted from edited and control hiPSC-neurons cultured with γ-secretase inhibitor or extracted from the media of edited and control hiPSC w/o g-secretase inhibitor show decreased Aβ production and increased secretion of sAAPα in edited cells. Adapted from reference #17.

3.3.3 Differential expression and gene set enrichment analysis

We then investigated cell-type specific transcriptomic differences between the APP-NLFG and WT mouse brain and how those differences are impacted by the altered APP C-terminus in InsT and Del5 mouse brains. Setting our thresholds at FDR (false discovery rate/adjusted p-value) < 0.05 and log2FC > 0.25, we identified 657 differentially expressed genes (DEGs) between APP-NLFG and WT brains: 83 in brain endothelial cells, 66 in microglial cells, 50 in dual receptor expressing neurons, 53 in GABAergic neurons, 60 in glutamatergic neurons 424 in oligodendrocytes and 5 in oligodendrocyte precursor cells. None of these DEGs were common to all cell-types suggesting cell-type specificity in differential expression. However, 17 DEGs were common to all three neuronal subtypes. Additionally, 17 microglial DEGs have previously been identified in disease-associated microglia (DAM) in Alzheimer's disease[80-82].

To identify potential functional consequences of these gene expression differences, we performed gene set enrichment analysis (GSEA) using the BioCarta canonical pathways database (GSEA). To avoid potential false positives, we limited our results to those with FDR < 0.25 and nominal p-value < 0.05. In our disease model we found significant negative enrichment in cell-signaling, cell-cycle and gene-expression regulatory pathways within microglial cells; oligodendrocytes exhibited positive enrichment in cell-cycle pathways and negative enrichment in cell-signaling, immune, stress and inflammatory response pathways, and brain endothelial brain cells showed negative enrichment in the Ask1-NEF stress response pathway (Fig. 3.3a). While there was no direct overlap in pathway enrichment between microglia and oligodendrocytes, leading edge analysis indicated a number of genes related to calcium signaling (*Prkca, Prkar1b, Camk2a, Calm1*) in the core enrichment subsets for pathways in both of these cell-types, suggesting dysregulation of calcium signaling in these cell-types. Aberrant calcium signaling and perturbed calcium homeostasis in

oligodendrocytes and microglia have been shown to play a prominent role in AD pathology[83,84]

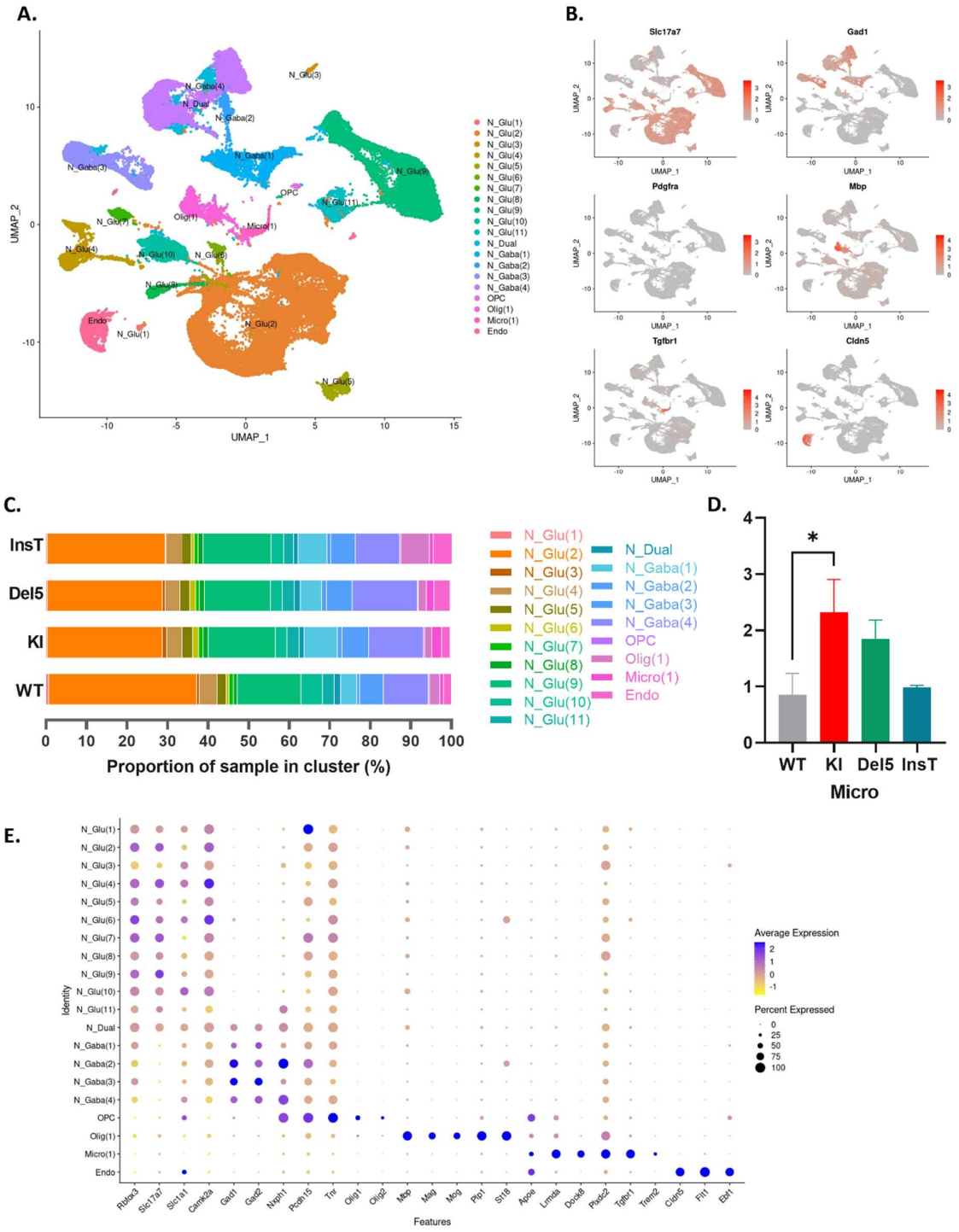

Fig. 3.2 Identification of cell-types. Figure caption on the following page

Figure 3.2 Identification of cell-types. A.) UMAP projection of 86,897 single nuclei transcriptomes (19,737 from 2 APP-NFGL, 23,058 from 2 InsT, 24,660 from 2 Del5 and 19,442 from two wild type mouse brains. **B.)** Feature map illustrating expression level and location of key marker genes for each cell-type Slc17a7 indicated glutamatergic neurons, Gad1 indicates GABAergic neurons, Pdgfra indicates oligodendrocyte progenitor cells, Mbp indicates oligodendrocytes, Tgfbr1 indicates microglia and Cldn5 indicates brain endothelial cells. **C.)** Stacked bar graph illustrating the percentage of samples in each cluster across the four genotypes. **D.)** Bar graph showing a significant increase in the proportion of microglia from APP-NLGF samples. E.) Dot plot showing the expression levels of well-known cell-type specific marker genes. Slc17a7, Slc1a1, and Camk2a indicate glutamatergic neurons, Gad1, Gad2 and Nxph1 indicate GABAergic neurons, Pcdh15, Tnr, Olig1 and Olig2 indicate oligodendrocyte progenitor cells, MBP, Mag, Mog, Pip1, and St18 indicate oligodendrocytes, ApoE is primarily expressed in astrocytes but can also be expressed in other glial cells and neurons. Lrmda, Dock8, Plxdc2, Tgfbr1 and Trem2 indicate microglia. Cldn5, Flt1, and Ebfr1 indicate brain endothelial cells.

Differential expression and gene set enrichment analyses were also performed on InsT and Del5 mouse brain cell-types in comparison to both WT and APP-NLGF cell-types. In Del5 samples compared with WT, we found that brain endothelial cells showed a similar enrichment in the Ask1 signaling pathway observed in the disease model. Additionally, these samples showed negative enrichment in several cell-signaling, immune response and apoptotic pathways within GABAergic neurons. Oligodendrocytes from InsT samples showed negative enrichment in gene-expression and cytoskeletal remodeling pathways, positive enrichment in the TCR immune response pathway and a mix of positive and negative enrichment in cell-signaling pathways when compared to oligodendrocytes from WT samples. When compared to APP-NLGF, Del5 samples showed positive enrichment in the Act1-NEF signaling pathway and OPCs showed negative enrichment in the Act1-Nef, MAPK, and VIP, MAPK-KC pathways.

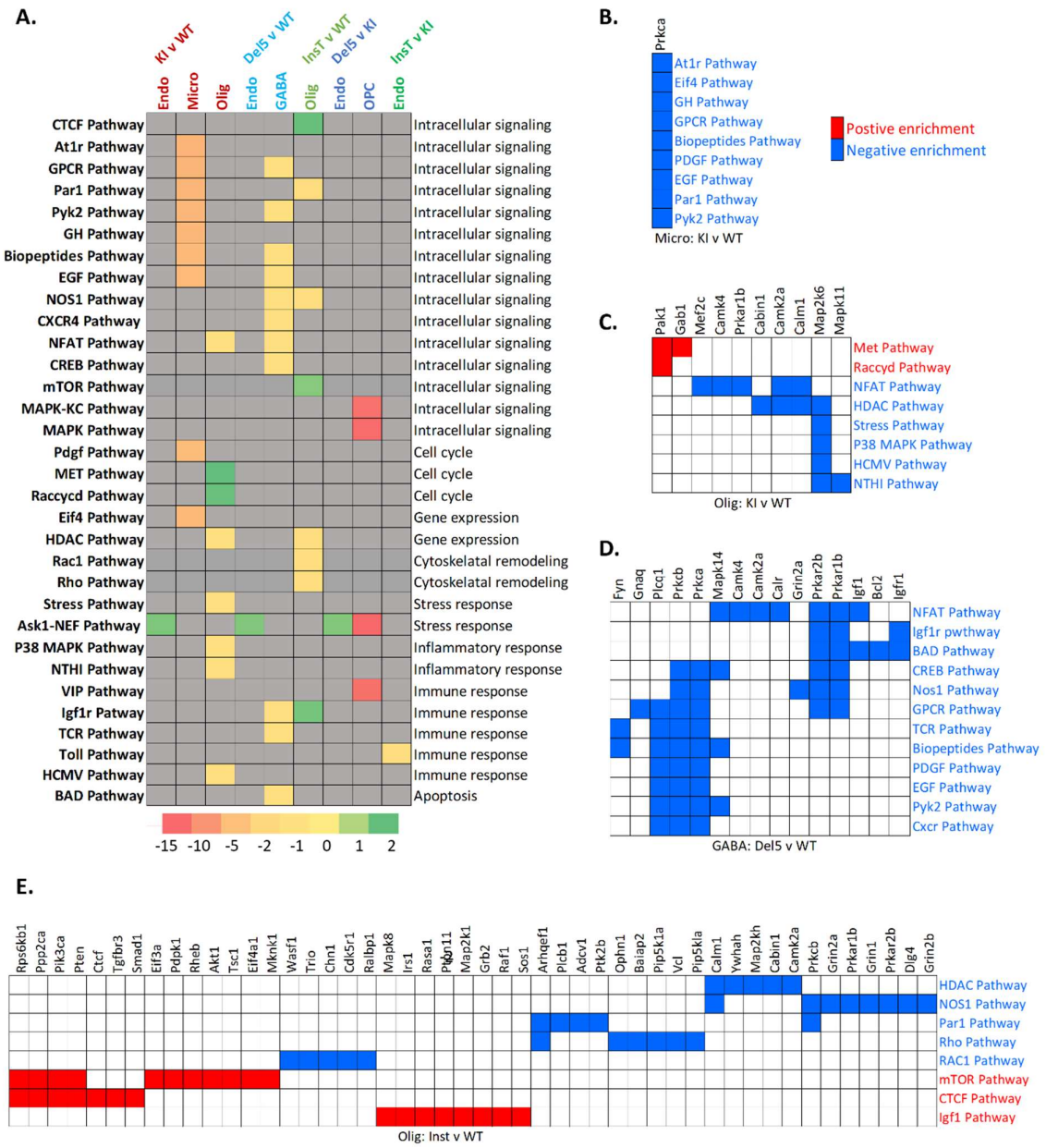

Figure 3.3 Gene set enrichment analysis. A.) Heat map of NES scores for enriched pathways across cell-types and genotypes. **B.)** Leading edge analysis highlighting upregulated (red boxes) or downregulated (blue boxes) genes that represent the core enrichment subset of DEGs within positively enriched (red text) or negatively enriched (blue text) pathways within APP-NLGF microglial cells in contrast to WT microglial cells. **C.)** Leading edge analysis highlighting upregulated or downregulated genes that represent the core enrichment subset of DEGs within positively or negatively enriched pathways within APP-NLGF oligodendrocytes in contrast to WT oligodendrocytes. **D.)** Leading edge analysis within Del5 GABAergic neurons in contrast to WT GABAergic neurons. **E.)** Leading edge analysis within InsT oligodendrocytes in contrast to WT oligodendrocytes.

3.4 Discussion

The DEGs and differentially expressed pathways identified in this study elucidate molecular changes in the APP-NLGF AD mouse model, and the potential to prevent these changes through genome editing. Notably, we observed altered gene expression in microglial cells that mimic known changes observed in DAMs in both DEG identity and directionality of the expression change[85]. Additionally, down regulation of genes involved in calcium signaling in APP-NLGF oligodendrocytes and microglia could be related to aberrant regulation of calcium homeostasis and dysregulated calcium signaling in these cells that has been associated with AD pathogenesis. C-terminal editing in the disease model had limited impacts on pathway enrichment in the disease model. InsT samples showed downregulation of the Toll pathway in endothelial cells when contrasted with the disease model and Del5 samples showed downregulation in pathways largely associated with inflammation, stress response and apoptosis in OPCs and brain endothelial cells. This could suggest some rescue of inflammation in these samples.

The implications of pathway enrichment analysis in APP-NLGF-DC animals in contrast to WT is not immediately obvious. Here we see several pathways differentially expressed in oligodendrocytes in InsT animals and in GABAergic neurons in Del5 animals. Many of these changes appear to be potentially advantageous in the context of Alzheimer's disease. NFAT, Igf1r, NOS1, GPCR and EGF signaling pathways have all been shown to be associated with AD pathology and neurodegeneration[86-90]. Additionally, these cells show downregulation in immune response and apoptotic pathways such as Cxcr, and TCR pathways and down regulation of the protein Fyn which has been implicated in AD by its interactions with Tau[91]. However, the downregulation of these pathways observed here is in

contrast to WT samples, not the disease model. Furthermore, downregulation of the CREB pathway could have negative impacts on learning and memory and synaptic plasticity, and downregulation of this pathway is a known contributor to hippocampal memory deficits in age-associated cognitive decline and AD pathology. Therefore, more thorough investigation is necessary to understand the magnitude and precise implication of this edit- which may vary with more localized application in contrast to the germline modification in this model and may also have different impacts on human neural cell-types than what is observed in mice.

Comparisons of the DEGs identified in these cell-types could be further cross analyzed with single cell data generated from other AD single cell/single nuclei analyses to assess differences and similarities between this and other models and human disease data, as well as to further assess the implications of differential gene expression in the edited samples. Additionally, more thorough investigation into pathway enrichment utilizing additional gene set databases such as the GO, Reactome, WikiPathways and Hallmark gene set databases followed by pathway enrichment mapping may generate deeper understanding of the functional consequences of this edit.

A notable limitation in this study is that we did not identify any astrocytic cell clusters in our single cell analysis, additionally the only neuronal subtypes identified were glutamatergic, GABAergic and those expressing both vGlut and GAD1. It is possible that we did not recover nuclei from astrocytes while performing our nuclear isolation. They are potentially more vulnerable to loss during freezing, shipping, and tissue processing. However, we were able to identify astrocytes in snRNA data sets of nuclei isolated from fresh hippocampi. Another possibility is that the astrocytes did not specifically cluster by cell-type and are intermixed among the other clusters. This is likely to be the case for additional neuronal subtypes. This can be determined by isolating specific clusters, such as all the clusters identified as glutamatergic neurons, or a individual subclusters, and re-clustering the

subsetted data. This will allow for greater resolution and is often employed for exploring neuronal subtype. This process will very likely reveal missing neuronal subtypes and may also help identify and separate astrocytes from the other cell-types. A second approach is to use specific sets of cell-type markers to cluster the data, rather than performing unbiased UMAP clustering.

Gene editing within the brain has tremendous potential for the treatment of neurodegenerative disorders. However, thorough characterization of the impacts of any potential therapeutic gene edit is essential for safety considerations in downstream clinical applications. Genome editing has a potential for risks including off-target editing effects, inflammatory responses as well as unpredictable impacts on gene regulation. Single cell analyses offer the potential to fully characterize the impact of potential therapeutic edits in an unbiased manner. Here we used single-nuclei RNA sequencing to characterize a potentially therapeutic edit of the C-terminus of APP in an Alzheimer's disease model background. We have elucidated DEGs, and differentially enriched pathways between WT, disease model and edited disease model which offer deeper understanding into the consequences of these edits and can be used to guide future applications.

3.5 Methods

3.5.1 Mouse brain tissue

Flash frozen brain hemispheres were provided by the Roy lab, 2 hemispheres were used for each genotype from two separate animals, one male, one female. Nuclei were then isolated following 10X Genomics nuclear isolation protocol for adult brain tissue with some modifications. In brief, frozen hemispheres were transferred directly to 5 ml of chilled lysis buffer inside the chamber of a 7ml glass Dounce homogenizer. The homogenizer was placed on ice for 5 minutes after which 3-5 passes were made with the smaller diameter pestle to

begin homogenization of the tissue. The homogenizer with buffer and tissue was then placed back on ice for 10 minutes after which 3-5 passes were made with the larger diameter pestle completing the tissue homogenization and releasing the nuclei. Nuclei were then filtered, washed and centrifuged to separate nuclei from cellular debris according to 10X protocol. Myelin removal was not performed on nuclei from hippocampal tissue, but rather sucrose density gradient centrifugation was utilized to complete purification of nuclei according to 10X protocol.

3.5.2 Single-nuclei RNA Sequencing:

Single- nuclei RNA-sequencing was performed by the UW-Madison Biotechnology Center Gene Expression Center. The 10x Genomics Chromium Next GEM Single Cell 3′ Library v3.1 Single Cell Gene Expression Assay was used to target 10 000 cells per sample with a sequencing depth of 70,000 reads per cell according to the manufacturer's recommendations (10x Genomics).

3.5.3 Single-nuclei RNA-sequencing analysis:

Alignments, pre-processing, quality control and integration of data sets:

Alignments were performed with 10X Genomics Cell Ranger 6.1.2. GRCm39 using the cell ranger count pipeline with the GRCm39 *Mus musculus* genome from the Ensembl database as the reference genome. By default, cellranger count only counts reads aligned to exons. Since single-nuclei RNA assays capture unspliced pre-mRNAs containing intronic reads in addition to mature mRNA the include-introns flag was added to the cellranger count command to ensure these reads were counted, as is recommended for snRNA seq analysis by 10X genomics. Default quality control filtering settings in Cell Ranger were utilized as the first round of quality control[92]. After alignments and filtering in Cell Ranger a second round of quality control filtering was performed with Seurat version 4.1.1. To exclude potential

dead cells and cell debris, we filtered out nuclei with ≤ 500 UMIs, ≤ 200 genes, ≥ 20,000 genes and ≥ 10% mitochondrial genes.

Integrative analysis:

The data were then integrated following the workflow outlined in the Seurat guided analysis. We first log-normalized the filtered matrices and identified highly variable features for each sample using the *FindVariableFeatures* function with default parameters. We then used the *FindIntegrationAnchors* function to identify variable features conserved across the data sets and used these anchors to integrate the datasets using the *IntegrateData* function. We subsequently scaled the integrated matrix and performed linear dimensional reduction using the *RunPCA* function. We then used an elbow plot to visualize the percentage of variance explained by each principal component and opted to use the first 20 principal components for graph-based clustering. Next, we performed UMAP and *K*-nearest neighbor clustering using the function *RunUMAP* with the parameter dims = 20 and the functions *FindNeighbors* and *FindClusters* with the parameter resolution = 0.6.

Differential Expression Analysis:

Differentially expressed genes were identified for each cluster in contrast to the all other clusters by the Wilcoxon rank-sum test using the function *FindAllMarkers* with the parameters logfc.threshold = 0.25 and min.pct = 0.10. These genes along with the expression of previously established cell-type marker genes were used to identify cluster cell-types.

Differential expression analysis to identify cell-type specific impacts of genotype were performed using the function *FindMarkers.* Comparisons were made between a single cell-type (i.e. glutamatergic neurons) from a given genotype (i.e. Del5) in contrast to the same cell-type from either wild-type or APP-NFGL. This function also uses the Wilcoxon rank-sum test. Significance threshold was set at logfc.threshold = 0.25, min.pct = 0.10 and adjusted p-

value < 0.05 (adjusted p-value is also known as FDR and is the Bonferroni corrected p=value of the significance of differential expression considering all other features of the dataset).

Similar cell-type specific differential expression analysis with *FindMarkers* was also used to generate differential expression lists used in GSEA analysis. Since GSEA functions best when ranked expression is included for all or most expressed genes the logfc.threshold for this analysis was set at 0 and min.pct = 0.10.

Gene Set Enrichment Analysis was performed using GSEA version 4.2.3 and the pre-ranked GSEA analysis. Gene lists with log2 fold change and p-values were generated using the *FindMarkers* function in Seurat as described above. Ranked gene lists in .rnk format were generated using log2FC and p-adj values by eVITTA easyGSEA[93]. Ranked gene lists were compared to 72 canonical pathway mouse gene sets contained within the Biocarta database.

Statistical analysis

Differential expression statistics were generated by Seurat using the Wilcoxon rank-sum test with Bonferroni correction expressed in adjusted p-values. Pathway enrichment analyses statistics were generated by GSEA. All other statistical analyses were performed with Graph Pad Prism9. One-way ANOVAs were performed to evaluate the differences between means across the genotype groups with multiple comparisons using the Tukey's HSD.

Acknowledgments: We would like to thank the Roy lab for their help with this study and for providing the transgenic mouse brains used in this analysis.

4 Transcriptomic profiling of the mouse brain after intracerebral injection of Cas9 nanocapsule genome editors

Intracerebral injections described in this study were performed in Dr. Jon Levine's Lab by Jesi Felton or Dr. Mathew Flowers. Nanocapsules were generated in Dr. Sarah Gong's Lab by Dr. Yuyuan Wang. Single nuclei RNA sequencing was performed by the UW Madison Biotechnology Gene Expression Center.

4.1 Abstract

Evaluating the editing efficiency and cell-type specificity of genome editors is a critical task for developing somatic cell genome editing strategies, especially for those that target the brain. Standard methods rely on deep sequencing at the on-target site combined with immunohistochemistry within treated animal model systems to enumerate the types of edited cells in select tissues after administering genome editors. In particular, animal reporter systems that express fluorescent proteins after successful on-target genomic editing provide robust platforms to evaluate the number of edited cells but typically incorporate limited opportunities to co-register cell-type markers with the reporter protein. Thus, molecular characterization of an edited cell typically is limited to 2-4 cell-type markers that can be imaged simultaneously with the fluorescent reporter. Here, we report on a new method to deeply characterize the transcriptome of edited cells within the brain of Ai14-tdTomato reporter mice. We performed single nuclei RNA sequencing (snRNA-seq) on nuclei isolated from the hippocampi after intracranial injection of nanoparticle genome editors into the hippocampus. We utilized a previously developed biodegradable nanocage (NC) capable of delivering preassembled SpyCas9 protein-gRNA ribonucleoprotein complexes (RNPs). RNPs targeting the Ai14 loxP-STOP cassette were encapsulated into these NCs and delivered into the hippocampus via intracranial injection. After performing snRNA-seq, we observe the capture of ~500-15000 unique transcripts per nuclei and robust *Ai14-tdTomato* reporter expression in nuclei from neuronal, glial, and oligodendrocytic cells. Additionally, differential cell-type specific transcriptomic shifts were identified primarily in immune and cell signaling pathways between treatment with recombinant adeno-associated viral vectors (rAAV) or NC. Overall, transcriptional profiling provides a high-resolution and complementary method to examine the cellular outcomes from genome editing within animal

reporter systems, which has high potential to inform the clinical development of genome editing therapeutics.

4.2 Introduction

CRISPR/Cas9 based genome editing has rapidly become one of the most promising tools for treating human genetic diseases. This tool holds particular promise for the treatment of neurodegenerative disorders where conventional pharmacological treatments have been largely unsuccessful and where a necessity for invasive delivery mechanisms can make repeat dosing considerably problematic[18]. However, there are still a number of safety challenges that need to be addressed when evaluating potential gene-editing based therapies.

For genome editing, safety considerations include the potential for off-target genomic editing, cell-type specific responses to editing, mRNA misregulation and transcriptional perturbations. Alterations in alternative splicing, the production of gain of function proteins, a p53 mediated stress response, and unpredicted impacts on gene expression regulation and cell signaling can all have deleterious impacts on cellular function and survival[21,22]. Standard methods for evaluating editing efficiency and cell-type specificity often rely on deep sequencing at the on-target and predicted off-target sites, combined with immunohistochemistry within treated animal model systems to enumerate the types of edited cells in select tissues after administering genome editors. Animal reporter systems that express fluorescent proteins after successful on-target genomic editing provide robust platforms to evaluate the number of edited cells, but typically incorporate limited opportunities to co-register cell-type markers with the reporter protein[94-96]. Thus, molecular characterization of an edited cell is typically limited to 2-4 cell-type markers that can be imaged simultaneously with the fluorescent reporter, limiting the scope of cell-type identification and the ability to detect immune response or transcriptional perturbations.

Here we have utilized single nuclei RNA sequencing to deeply characterize the transcriptome of edited cells within the hippocampus of Ai14-tdTomato reporter mice to thoroughly characterize the safety and efficacy of editing in the hippocampus via non-viral, nanocapsule-mediated delivery of SpyCas9 RNP. We utilized a previously developed biodegradable nanocage (NC) capable of delivering preassembled SpyCas9 protein-gRNA ribonucleoprotein complexes (RNPs)[97]. RNPs targeting the Ai14 loxP-STOP cassette were encapsulated into these NCs and delivered into the hippocampus via intracranial injection.

Our transcriptomic analysis identified nine major cell-types of the hippocampus (glutamatergic neurons, GABAergic neurons, astrocytes, oligodendrocytes, pericytes, ependymocytes and vascular smooth muscle cells), largely mirroring previously published single cell characterization in the hippocampus[98]. We observed broad reporter activation in response to Cas9 and positive-control administration of rAAV-Cre, particularly within glutamatergic neurons. Additionally, we identified differential tropism and differential cell-type specific transcriptomic shifts, primarily within immune and cell-signaling pathways, between treatment with NC and rAAV. Overall, transcriptional profiling provides a high-resolution and complementary method to examine the cellular outcomes from genome editing within animal reporter systems, which has high potential to inform the clinical development of genome editing therapeutics.

4.3 Results

4.3.1 Single-nucleus transcriptomic profiling of genome-edited and control Ai14 mouse hippocampi

To characterize the impact of NC-mediated gene editing with a genetically integrated reporter, we utilized a well-established Ai14 mouse model[99] (Fig. 4.1a). These mice harbor a modification at the Rosa26 locus containing a *loxP*-flanked STOP cassette (three repeats of

the SV40 polyA sequence) upstream of a tdTomato coding sequence (Fig. 4.1b). This allele was originally designed for Cre-mediated recombination at the *loxP* sites leading to excision of the stop cassette to promote expression of *Ai14-tdTomato* transcripts. To employ this model as a reporter for Cas9-induced genome editing, we utilized a guide RNA sequence (sgAi14-targeting) which targets three distinct areas of the Ai14 stop cassette. Multiple double strand breaks at any two of the three sites is predicted to delete the intervening sequence and remove the STOP cassette, thereby allowing transcription of *tdTomato* to occur. Use of this guide sequence has previously been shown to activate tdTomato expression in this allele within a similar mouse model (Ai9, which included a downstream selection cassette that should not affect tdTomato expression from this allele)[94]. We have previously utilized the Ai14 model with this sgAi14-targeting guide sequence to identify edited cells in the retina and muscle upon injection of NCs.

To perform genome editing, Cas9 ribonucleoprotein (RNP) containing sgAi14-targeting RNA were encapsulated by polymeric nanocapsules (NC-Cas9) and sterotactically injected into the hippocampi of adult Ai14 mice. We then used unbiased high-throughput single nuclei RNA sequencing (Fig. 4.1a) to examine the transcriptional profiles of these hippocampi (n = 4). These profiles were compared to control hippocampi from uninjected (n = 1), and PBS injected (n =1) Ai14 mice, Ai14 mice injected with nanocapsules containing RNP with scrambled non-targeting guide (NC-scram, n = 2), as well as Ai14 mice sterotactically injected with recombinant adeno-associated viral vectors expressing Cre-recombinase (rAAV-Cre, n = 2) (Fig. 1a and 1c.). To verify the activity of the sgAi14-targeting guide RNA and the ability of our analysis to capture *Ai14-tdTomato* transcripts using our workflow, we isolated mouse fibroblasts from the tail tips of Ai14 mice. These cells were then edited *in vitro* via nucleofection of RNPs loaded with sgAi14-targeting sgRNA. tdTomato expression in the nucleofected fibroblasts was verified with

immunofluorescence microscopy and flow cytometry (Fig. 1d). Further, flow cytometry analysis indicated that an average of 15.3% (n = 3) of these fibroblasts were tdTomato+ (Sup. Fig. 4.1), which is consistent with prior studies of nucleofection of RNP with the Ai14 model[94,97].

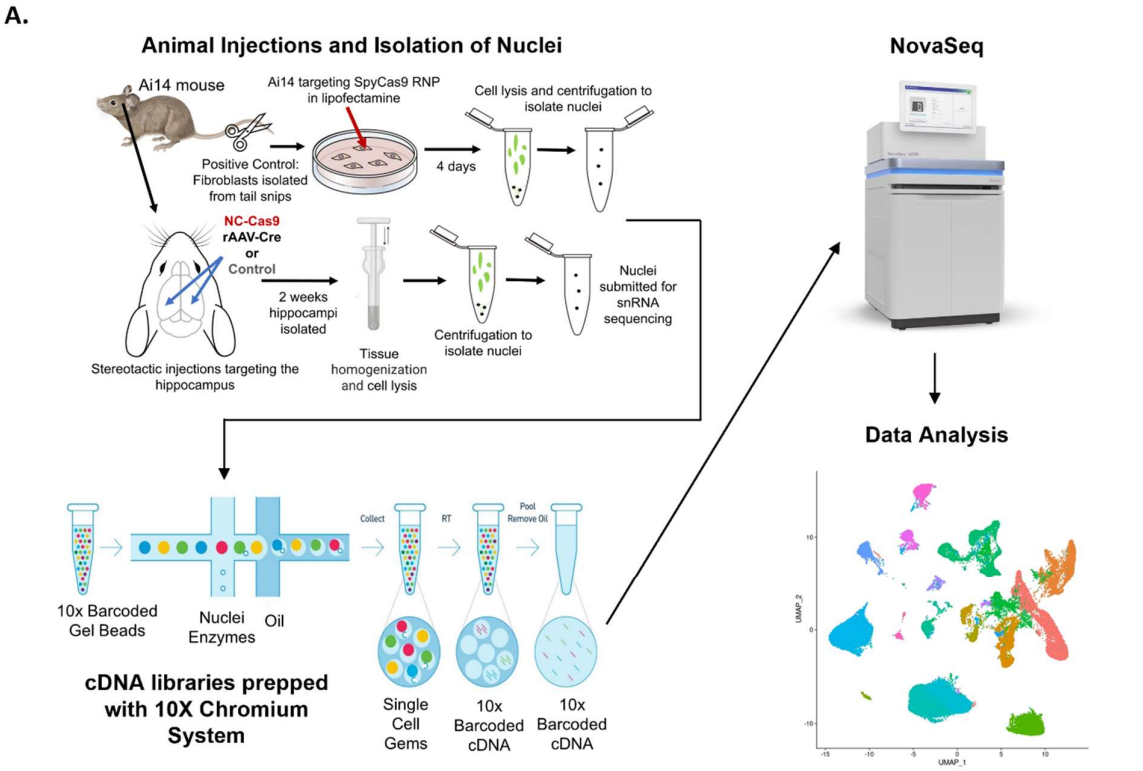

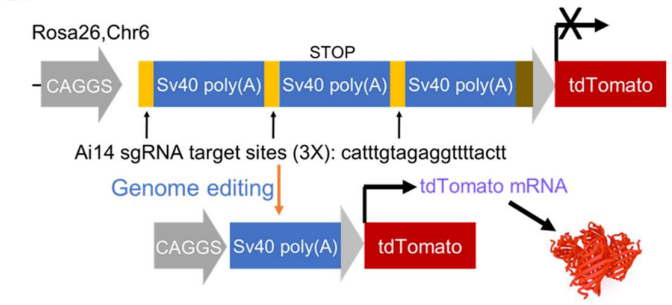

C.

Treatment	Hippocampi	Nuclei (after QC)
NC-Ai14	n = 4	29737
rAAV-Cre	n = 2	16572
NC-Scrambled	n = 2	16951
PBS	n = 1	9350
Uninjected	n = 1	4045

Figure 4.1 Single nuclei sequencing of mouse hippocampi treated with genome editors. **A**.) Overview of experimental workflow: stereotactic injection was used to deliver NC-Cas9, NC-scram, rAAV-Cre or PBS to the hippocampus of Ai14 mice, an uninjected control, WT control and *in vitro* edited Ai14 mouse fibroblasts were also analyzed). **B.)** Schematic of the Ai14 stop cassette upstream of the tdTomato targeting region and the regions targeted by the Ai14-targeting gRNA. **C.)** Summary of the hippocampal samples, treatment and nuclei used for this analysis.

4.3.2 Identification and analysis of cell types across treatments

A custom Ai14 reference genome was generated with the mkref function in 10X Genomics Cell Ranger 6.1.2 by appending the tdTomato coding region of the Ai14 transgene to the GRCm39 Mus musculus genome[92]. The cellranger count pipeline was then used to align single nuclei sequencing reads to the Ai14 reference genome. Default setting in the cellranger count pipeline were utilized for filtering and cell calling in the first round of quality control. Subsequent single nuclei analyses were performed with Seurat version 4.1.1 in R and R studio version 4.2.0. Here we performed a second round of quality control to exclude potential dead cells and cell debris, filtering out nuclei with ≤ 500 unique molecular indexes (UMIs), ≤ 200 genes, ≥ 20,000 genes and ≥ 10% mitochondrial genes (Methods). After quality control, we analyzed the transcriptional profiles of 76,755 nuclei, 39,737 from four NC-Cas9 treated Ai14 hippocampi, 15,090 from four control Ai14 hippocampi and 16,572 from two rAAV-Cre treated AI14 hippocampi (Fig. 4.1c). Importantly, to ensure the specificity of *Ai14-tdTomato* transcript detection in our downstream analysis, snRNA sequencing was performed on nuclei isolated from a wild-type mouse brain hemisphere. The resulting WT cDNA libraries were aligned to the Ai14 reference genome and queried for *Ai14-tdTomato*+ nuclei. No *Ai14-tdTomato*+ nuclei were detected in these wild-type samples.

We first performed initial unbiased uniform manifold approximation and projection (UMAP) clustering on all samples[73]. This analysis permitted visualization of the entire dataset in lower dimension, and a two-dimensional plot is shown in Fig. 4.2a. This process identifies features expressing high cell to cell variability, uses these features to define clusters of cells with similar feature expression patterns and then projects this high dimensional data

into two-dimensional space. We initially observed 37 unique cell clusters, which we subsequently categorized into nine major cell-types (glutamatergic neurons, GABAergic neurons, astrocytes, oligodendrocytes, pericytes, ependymal cells and vascular smooth muscle cells) according to their individual transcriptome profiles and previously reported markers of cell types in the mouse hippocampus[74-79] (Fig. 4.2b, c, and Supp. Fig. 4.2). To facilitate analysis, small adjacent and/or overlapping clusters of the same cell-type were regrouped into single clusters ultimately yielding 22 clusters (Fig. 4.2a). The distribution of these clusters were 8 subtypes of glutamatergic neurons (N_Glu), GABAergic neurons (N_Gaba), three subtypes of oligodendrocytes (Olig), two subtypes of astrocytes (Astro), three subtypes of microglia (Micro), choroid plexus cells (CPC), ependymal cells (EPC), pericytes (Prcyts), and vascular smooth muscle cells (vSMC). High expression of marker genes for each of these cell types are shown in Fig. 4.2b and are largely restricted to specific cell types. Globally distinguishing marker genes for nine cell types are shown in Fig. 2c.

We next investigated the abundance of each of the nine major cell-types across the three treatment groups (Fig. 4.3). Only very slight variations in cell-type and cluster proportions were observed between the different control samples (NC-scram (n=2), PBS injected (n=1), and uninjected (n=1), therefore these samples were considered as one "Control" group for all subsequent cell-type and cluster abundance comparisons (Supp. Table 4.3). Significant differences between the treatment groups were identified in cell-type proportions for glutamatergic neurons ($F_{(2,7)} = 7.629$; $p = 0.017$), oligodendrocytes ($F_{(2,7)} = 5.816$; $p = 0.33$), and astrocytes ($F_{(2,7)} = 4.867$; $p = 0.047$). Treatment with either NC-Cas9 or rAAV-Cre resulted in ~15% decrease in the proportion of glutamatergic neurons; with significance in the NC-Cas9 treatment group (NC-Cas9 mean diff = -16.01, $p = 0.019$; rAAV-Cre mean diff = -14.25, $p = 0.072$). Astrocytes also decreased in response to both NC-Cas9 and rAAV-Cre treatment, ~5%, with significance in the NC-Cas9 treatment (NC-Cas9

mean diff = -5.60%, p = 0.041; rAAV-Cre mean diff = -3.70%, p = 0.28). Oligodendrocytes were increased ~20% in both NC-Cas9 and rAAV-Cre groups in comparison to control, again with significance in the NC-Cas9 treatment (NC-Cas9 mean diff = 21.65%, p = 0.03; rAAV-Cre mean diff = 15.10%, p = 0.20). No significant differences in cell-type proportions were observed between NC-Cas9 and rAAV-Cre treatment groups.

Clustering analysis identified eight separately clustering subtypes of glutamatergic neurons [N_Glu(1) – N_Glu(8)], three subtypes of oligodendrocytes [Olig(1) – Olig(3)], two subtypes of astrocytes[(Astro(1) and Astro(2)], and three subtypes of microglia [Micro(3)]. In order to determine if treatment with NC-Cas9 or rAAV-Cre resulted in population shifts within these subtypes, we compared the proportions of samples within subtype clusters. Here we found significant reduction in the proportion of samples represented in the microglial subtype Micro(3) (Fig. 4.3c; $F_{(2,7)} = 7.771$, p = 0.017). This cluster was significantly reduced in NC-Cas9 treated samples in comparison to both Control (mean diff = -0.24, p = 0.035) and rAAV-Cre treated samples (mean diff = -0.30, p = 0.027).

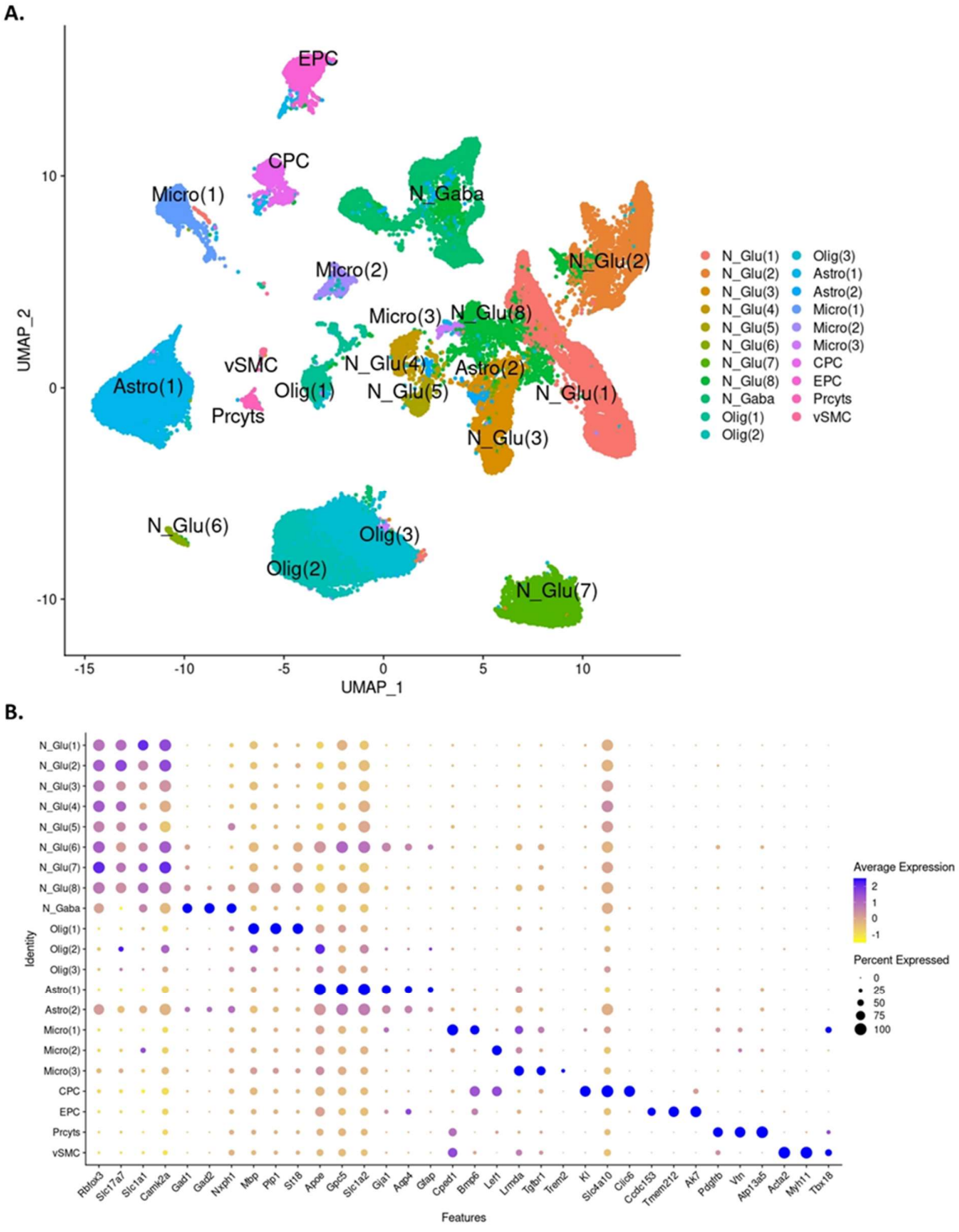

Figure 4.2 Cell types in treated mouse hippocampi (continued on the next page)

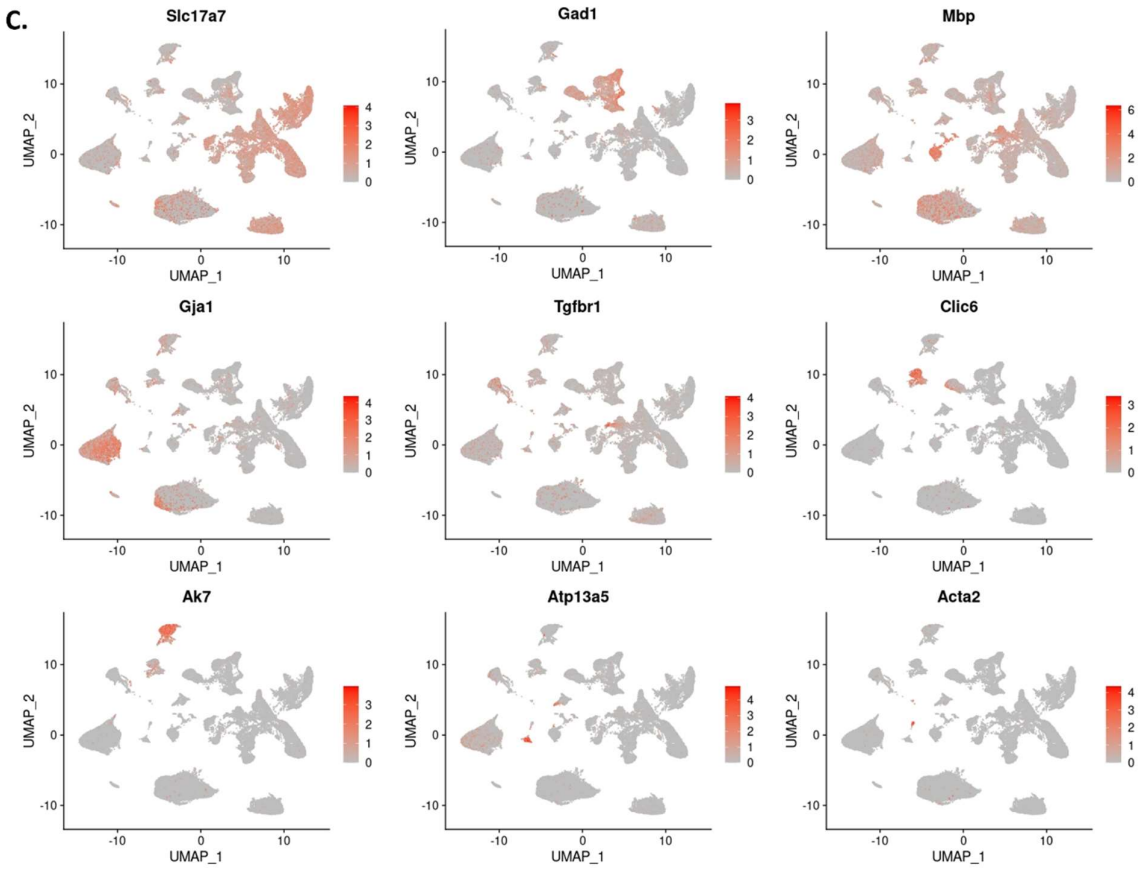

Figure 4.2 Identification of Cell Types. A.) UMAP projection of 76,655 single-nuclei transcriptomes of Ai14 treated hippocampi (39,737 from 4 NC-Cas9 treated hippocampi, 15,090 from 4 control treated hippocampi and 16,572 from 2 rAAV-Cre treated hippocampi.) Identified clusters are: 8 subtypes of glutamatergic neurons [N_Glu(1) – N_Glu(8), GABAergic neurons (N_Gaba), 3 subtypes of oligodendrocytes [Olig(1)-Olig(3)], 2 subtypes of astrocytes [Astro(1)-Astro(2)], 3 subtypes of microglia [Micro(1)-Micro(3)], choroid plexus cells (CPC), pericytes (Prcyts) and vascular smooth muscle cells (vSMC). **B.)** Dot plot illustrating the expression levels of well-known cell-type specific marker genes in each cluster. Dot color indicates the average scaled expression level of cells within that cluster. Data is scaled such the average expression level of a gene across the whole data set = 0 and the standard deviation =1. Negative expression levels indicate expression levels below the average of the entire data set, positive expression levels indicate expression levels higher than the average of the data set. Lower expression levels are indicated by more yellow circles while higher are indicated by darker purple circles. Rbfox3 indicates neuronal cells, Slc17a7, Slc1a1, and Camk2a indicate glutamatergic neurons, Gad1, Gad2 and Nxph1 indicate GABAergic neurons, MBP, Pip1, St18 indicate Oligodendrocytes, ApoE is primarily expressed in astrocytes but can also be expressed in other glial cells and neurons. Gpc5, Slc1a2, Gja1 Aqp4 and Gfap indicate astrocytes, Cped1, Bmp6, Lef1, Lrmda, Tgfbr1 and Trem2 indicate microglial cells, KI, Slc4a10 and Clic6 indicate choroid plexus cells, Ccdc153, Tmem212 and Ak7 indicate ependymal cells, and Acta2, Myh11 and Tbx18 indicate vascular smooth muscle cells. **C.)** Feature Plot showing the location and scaled level of expression of one key marker gene for each cell type in the UMAP. Grey indicates expression levels ≤ average expression of the entire data set; darker red indicated increased expression of the marker gene.

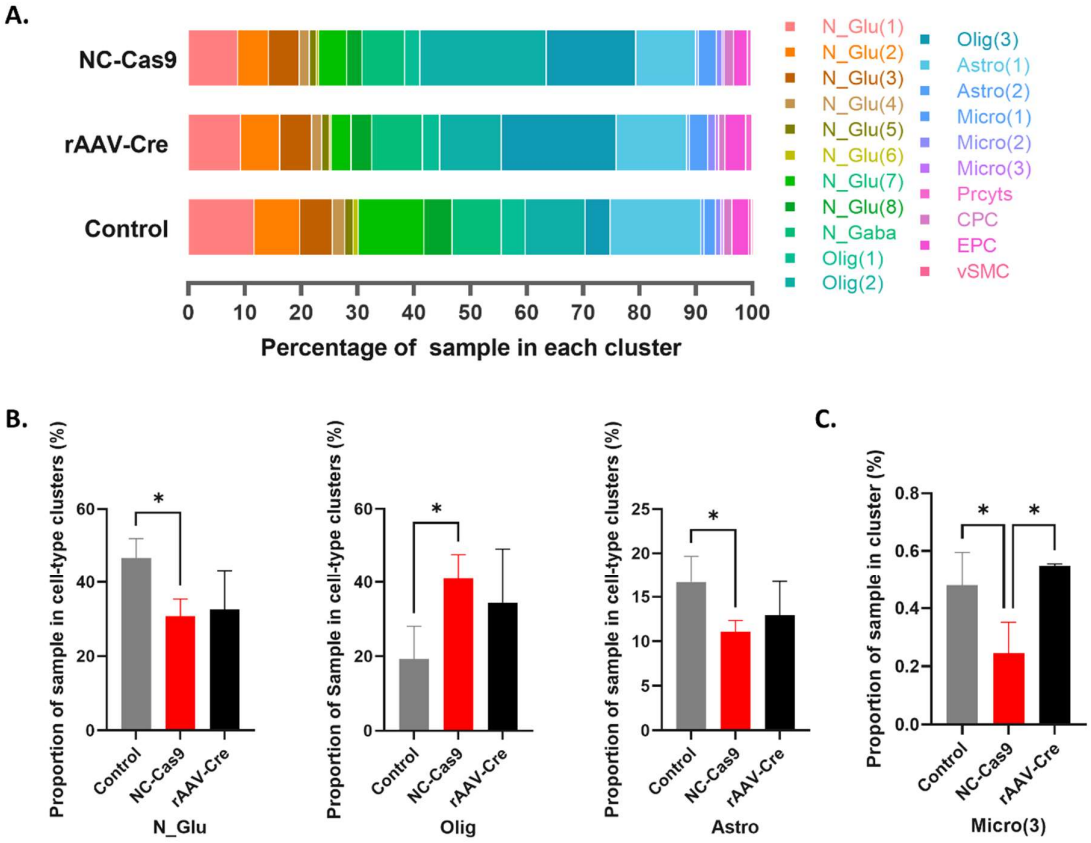

Figure 4.3 NC-Cas9 shifts in cell-types upon treatment with nanoparticle genome editors versus control treatments A.) Stacked bar graph illustrating the percentage of samples in each cluster across treatment groups. **B.)** Bar graphs illustrating major cell-types where significant shifts in proportions were observed between treatment groups. Both NC-Cas9 and rAAV-Cre treatments showed decreased percentages in glutamatergic neurons and astrocytes and increased oligodendrocytes. Glutamatergic neurons were decreased by roughly 10%, astrocytes by roughly 5% and oligodendrocytes were increased by roughly 20% in both NC-Cas9 and rAAV-Cre treated samples, these differences were significant for NC-Cas9 treated samples. **C.)** Bar graph illustrating cell subtypes where significant shifts in proportions were observed across the treatment groups. A significant reduction in cluster Micro(3) was observed in response to NC-Cas9, but not rAAV-Cre treated samples. No other subtype clusters showed significant proportional shifts in response to treatment.

4.3.3 Analysis of differential reporter expression across treatments

To assess the editing efficiency of NC-Cas9 we compared the number of *tdTomato*+ nuclei between Control, NC-Cas9 and rAAV-Cre treated groups and used differential expression analysis to evaluate differences in *tdTomato* expression levels between Control and NC-Cas9 or rAAV-Cre treated groups. As with cell-type and cluster proportions, only very slight variations in proportion of *tdTomato*+ cells or in *tdTomato* expression level were observed between the different control conditions overall, within major cell-types, or within subtype clusters. Therefore, all control conditions were treated as one "Control" group for all subsequent comparisons of *tdTomato* expression. NC-scram treated hippocampi had 15.9 and 15.1% *tdTomato*+ nuclei; uninjected and PBS injected controls had 16.9 and 17.8% *tdTomato*+ nuclei, respectively.

Overall, 28.6% of nuclei from NC-Cas9 treated hippocampi were *tdTomato* positive in contrast to 16.3% percent of nuclei from control treated hippocampi. Hippocampi treated with the positive control, rAAV-Cre recombinase, had a slightly higher percentage of *tdTomato* positive nuclei at 31.6%. There was very little difference in the percent of *tdTomato*+ nuclei between NC-scram, uninjected and PBS injected controls. NC-scram treated hippocampi had 15.9 and 15.1% *tdTomato*+; uninjected and PBS injected controls had 16.9 and 17.8% *tdTomato*+ nuclei, respectively. The capture of these transcripts indicates leakiness of the Ai14 loxP-STOP allele. Differential expression analysis of nuclei from NC-Cas9 and rAAV-Cre treated hippocampi showed a 1.5- and a 1.7-fold increase in *tdTomato* expression, respectively, in comparison to Controls (p-adj = 0 for both comparisons).

To assess cell-type specificity in nanocapsule or rAAV targeting, we compared the percent of *Ai14- tdTomato*+ nuclei in each of the 9 major cell-types (Fig. 4.4b). Significant differences among treatment groups were observed in glutamatergic neurons ($F_{(2,7)} = 5.754$, p

= 0.033) and vascular smooth muscle cells ($F_{(2,2)} = 44.54$, p = 0.022). The percentage of *tdTomato*+ glutamatergic nuclei were increased in both NC-Cas9 (mean diff = 20.26, p = 0.064) and rAAV-Cre (mean diff = 26.33, p = 0.052), however, neither direct comparison of means passed the 95% significance threshold. Vascular smooth muscle cells showed a significantly higher percentage of *tdTomato*+ nuclei in rAAV-Cre treated samples in comparison to both Control (mean diff = 20.8, p = 0.027) and NC-Cas9 (Fig. 4.4d, mean diff = 17.75, p= 0.027). For several samples of this cell-type were represented at < 3 cells per sample which may skew the expression results for this cluster (Supp. Table 4.3).

Within cell subtype clusters, all clusters showed an increase in the percentage of *tdTomato*+ nuclei from hippocampi treated with NC-Cas9 or with rAAV-Cre. N_Glu(2) showed significant differences among treatment groups ($F_{(2,7)} = 6.646$, p = 0.024) with roughly 20% more *tdTomato*+ nuclei in NC-Cas9 (mean diff = 16.35, p = 0.054) and rAAV-Cre (mean diff = 22.22, p = 0.035) (Fig4.4a). This increase was significant in the rAAV-Cre treatment group. N_Glu(7) also showed significant differences among the treatment groups ($F_{(2,7)} = 4.831$, p = 0.048), also with roughly 20% more *tdTomato*+ nuclei from NC-Cas9 (mean diff = 15.95, p = 0.12) and rAAV-Cre (mean diff = 20.85, p = 0.093); however neither direct comparison of means passed the 95% significance threshold (Fig. 4.4a). Significant differences were also observed for the astrocyte subtype Astro(1) ($F_{(2,7)} = 5.035$, p = 0.044). However, this group showed a considerably larger increase in percentage of *tdTomato*+ nuclei in response to rAAV-Cre (mean diff = 31.45, p = 0.037) than to NC-Cas9 (mean diff = 11.00, p = 0.41) (Fig. 4.4a).

Differential expression analysis between individual clusters from Control and NC-Cas9 treated samples showed a significant increase in *tdTomato* expression levels in 16 of the 22 clusters in response to NC-Cas9 treatment (Supp. Table 4.1). For most clusters, this increase in expression was modest (between 1.1 and 1.5), however a subtype of

oligodendrocytes, Olig(2) showed a more robust increase in *tdTomato* expression at 2.6-fold. Statistically significant differential expression of *tdTomato* in response to NC-Cas9 treatment was not observed in clusters Olig(3), Micro(2), Micro(3), EPC, Pericytes, or vSMC. A similar, modest yet significant, increase in *tdTomato* expression was observed in response to treatment with rAAV-Cre in all clusters apart from Astro(2), Pericytes and vSMC. rAAV-Cre treatment elicited more robust increases in expression in clusters CPC (FC = 1.6), Micro(2) (FC = 2.0), Astro(1) (FC = 2.2) and Olig(2) (FC = 2.1) (Fig. 4.43 and Supp. Table 4.2).

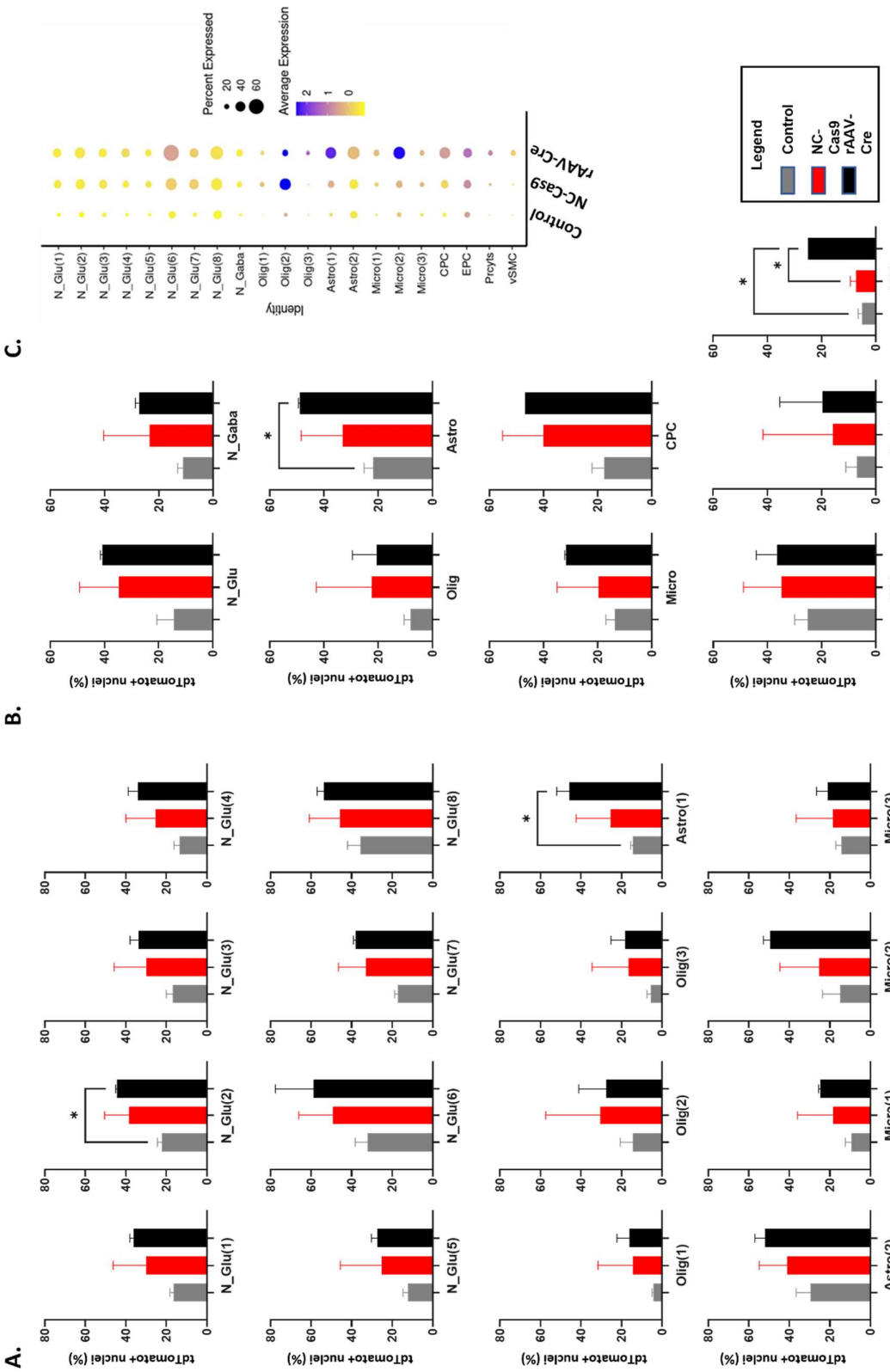

Figure 4.4: tdTomato expression across treatment and clusters Figure caption on next page

Figure 4.4: *tdTomato* reporter expression across treatments. A.) Bar graphs indicating the percent of *tdTomato*+ nuclei in each cluster **B.)** Bar graphs indicating the percent of *tdTomato*+ nuclei in 9 major cell-types. **C.)** Dot plot illustrating scaled reporter expression levels as well as percentage of cells expressing *tdTomato* in all clusters across the three treatment groups.

4.3.4 Identification of pathways affected by treatment with NC-Cas9 or rAAV-Cre

To investigate potential transcriptomic changes in response to treatment, we compared individual clusters from control treated hippocampi to those from NC-Cas9 or rAAV-Cre treated hippocampi using differential expression and gene set enrichment analysis (GSEA), using the BioCarta mouse canonical pathways database[73,100,101]. To avoid potential false positives, we limited our results to those with false discovery rates (FDR) < 0.25 and nominal p-value < 0.05. Here we found significant downregulation in five cell signaling and immune response related pathways across three clusters in NC-Cas9 treated samples (Fig. 4.5). Reduced expression of *Camk2a* was identified in the leading-edge subset in all three downregulated pathways for cluster N_Glu(4) as well as in the HDAC pathway in Micro(3). Reduced *Ppp3ca* expression contributed to the leading-edge subset for downregulation of the VIP pathway in Micro(3), N_Glu(4) and N_Glu(7).

Comparisons between clusters from hippocampi treated with rAAV-Cre and control treated hippocampi showed more enriched pathways than were observed in response to NC-Cas9. Here we found enrichment in 14 pathways, across six clusters including Micro(3), N_Gaba, and four glutamatergic subtype clusters. Several of the upregulated pathways are related to inflammation and immune response (Fig. 4.5). Micro(3) showed enrichment in nine pathways associated with immune response, inflammation, cell-signaling and proliferation. Nearly all these pathways have been shown to be associated with activated microglia, pro-inflammatory response, neurotoxicity and neurodegeneration[102-109]. Of note, is the overexpression of *Stat1* observed in nuclei of this cluster from rAAV-Cre treated samples

which is implicated in the leading-edge subset for all but two of these enriched pathways (Fig. 4.5b). *Stat1* is also found in the leading-edge subset for two of the enriched pathways in cluster N_Glu(1) (Fig. 4.5b), both enriched pathways in N_Glu(7), and MAPK pathway enrichment in N_Glu(6) and N_Glu(8). Stat1 is a transcription factor that has been shown to be activated in neurons in response to viral infection. This transcription factor is a driver of microglia activation and neuroinflammation and has been shown to regulate pro-apoptotic factors in neurons[110-112].

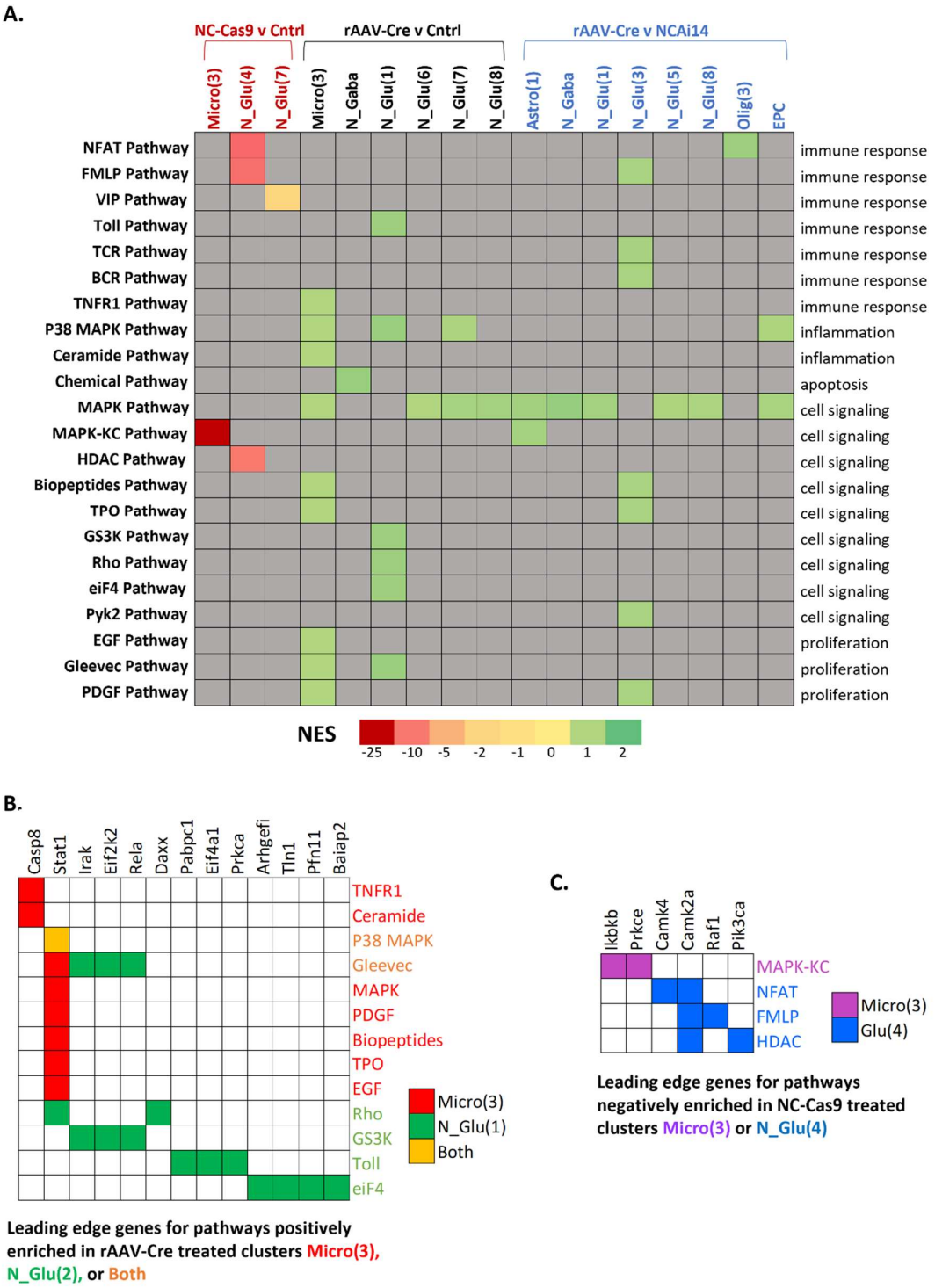

Figure 4.5 Pathway enrichment in NC-Cas9 and rAAV-Cre treated nuclei: caption continued on the next page

Figure 4.5 Pathway enrichment in NC-Cas9 and rAAV-Cre treated nuclei. A.) Heatmap of normalized enrichment scores for enriched pathways in clusters across treatment groups. Negative enrichment scores indicate downregulation of genes associated with that pathway while positive values indicate upregulated pathways. **B.)** Leading edge analysis of positively enriched pathways in Micro(3) and N_Glu(2) treated with rAAV-Cre. Red text indicates pathways enriched in Micro(3), green text for pathways enriched in N_Glu(1), yellow text enrichment in both cell subtypes. Red boxes indicate upregulated genes that contribute to core enrichment for the pathway in Micro(3), green for core enrichment genes in N_Glu(1) and yellow boxes for both cell subtypes. **C.)** Leading edge analysis of negatively enriched pathways in Micro(3) and N_Glu(4) treated with rAAV-Cre Purple text indicates pathways negatively enriched in Micro(3), blue text for N_Glu(4). Purple boxes indicate downregulated genes contributing to core enrichment in the pathway in Micro(3) and blue boxes for N_Glu(4).

4.4 Discussion

4.4.1 Resolving genome editing efficiency NC-Cas9in hippocampal cell types

We observed broad reporter activation by Cas9 and Cre recombinase delivery to the hippocampus. Treatment with either NC-Cas9 or rAAV-Cre resulted in a robust increase in *tdTomato* expression in the hippocampus of Ai14 mice, with increases in the total percent of *tdTomato*+ nuclei of 12.3% for NC-Cas9 treated hippocampi and 15.3% for treatment with rAAV-Cre as well as significant fold-change increases in expression of 1.5 and 1.7, respectively.

When comparing Cre recombinase mediated and Cas9-mediated reporter activation, there are limitations on the fidelity of reporting of genome editing events. For Cas9-induced genome editing at this reporter allele, NC-Cas9*Ai14-tdTomato* expression under-reports genomic editing as excision of one or more SV40 polyA sequences in the stop cassette requires at least two Cas9 double strand breaks (Fig. 4.1). One to two base target edits containing indels arising from the DNA repair a single double strand break by Cas9 have been detected in previous studies[94,97], but do not produce large deletions in the STOP

cassette. Therefore, single cuts at this locus resulting in insertions or deletions are unlikely to activate expression of *tdTomato* reporter transcripts. Moreover, it is possible that excision of only one of the three SV40 polyA sequence is not sufficient to lift existing transcriptional repression, creating the possibility that only Cas9 edits flanking two or more SV40 polyA sequences result in increased *tdTomato.* It has been previously reported that tdTomato expression only reports about 40% of Cas9 editing at this locus, however this analysis was at the level of protein expression and may not precisely correlate to *Ai14-tdTomato* transcript expression[94]. Given these limitations on exactly correlating *tdTomato* transcript level and presence to editing at the genetic level, we conclude that the range of reporter outcomes in the hippocampus with the NC-Cas9 are similar to the positive control with Cre recombinase delivered using rAAV serotype 9.

Treatment with NC-Cas9 appears to have the highest editing efficiency in glutamatergic neurons which show a 20.26% increase in *tdTomato*+ nuclei. Choroid plexus cells also showed roughly a 20% increase in the number of tdTomato+ nuclei after treatment with NC-Cas9. One limitation with this dataset is that this cell-type was not represented in all samples potentially skewing expression results for this cluster (Supp. Table 4.2). Oligodendrocytes, GABAergic neurons, and astrocytes had more edited *tdTomato*+ cells, ranging from 10-15% more positive nuclei in these clusters than control treated animals. rAAV-Cre appears to have a similar tropism to glutamatergic neurons and oligodendrocytes as NC-Cas9, with similar increases in *tdTomato*+ nuclei in these clusters. However, this AAV9 vector seems to have a much higher affinity to astrocytes and microglia than NC-Cas9 with a 27% and an 18% increase in *tdTomato*+ nuclei in these clusters, respectively, in contrast to an 11% and 6% increase in these clusters from NC-Cas9 treated samples. Previous studies with AAV9 delivery to the brain also indicate high tropism for astrocytes and microglia[113,114]. Given that roughly 90% of neurons in the hippocampus are glutamatergic[115],

this data suggests that this nanocapsule could be an effective option for targeting therapeutic gene edits to hippocampal neurons.

4.4.2 Pathways responding to treatment with NC-Cas9 or rAAV-Cre

Overall, the samples treated with the rAAV-Cre viral vectors has more differentially enriched pathways in multiple cell types than other samples in our dataset. Treatment with rAAV-Cre resulted in enrichment of multiple pathways in astrocytes, oligodendrocytes, glutamatergic neurons and GABAergic neurons. Of particular note are the pathways upregulated in cluster Micro(3). Many of these pathways suggest activation of a proinflammatory response in this subset of microglia. MAPK signaling in microglia has been shown to initiate inflammatory cytokine release, and inhibition of this signaling pathway can reduce microglial inflammatory response and subsequent neuronal damage[102,108]. TNFR1 signaling has also been shown to promote microglial inflammation and neurotoxicity [107]. Furthermore, *Stat1* and *Casp8* represent core enrichment genes for many of these pathways both of which have been implicated in driving activation of proinflammatory microglia and neurotoxicity[103-106,109,111]. Pathways associated with proliferations such as EGF, and PDGF pathways are also upregulated in Micro(3). Activated, proinflammatory microglia have high proliferative capacity (microglia proliferation). These data suggest that treatment with rAAV-Cre results in persistent activation in this subset of microglia that is not observed in NC-Cas9 or Control treated hippocampi. Chronic activation of microglia results cumulative neuronal loss over time and has been strongly implicated in neurodegeneration in neurodegenerative diseases, traumatic brain injury and hypoxia[116-121]. Immune response, inflammatory pathways, and stress response pathways are also enriched in glutamatergic neurons after rAAV-Cre treatment. Many proinflammatory and apoptotic signaling genes contribute to core enrichment in these pathways, such as *Daxx, Irak1, Eif2ak and Rela. Stat1*is also seen in the leading-edge subset in several of these pathways and has been shown to induce apoptosis in

neurons[110,112]. Pathways related to innate immune response have been detected in other edited cell types, retinal pigmented epithelial cells and hematopoietic stem/progenitor cells[122,123].

While treatment with NC-Cas9 resulted in fewer enriched pathways across fewer clusters, it is important to note that the magnitude of the normalized enrichment scores for these pathways were far higher than those observed in rAAV-Cre enriched pathways. The most significantly downregulated pathway is the MAPK-KC pathway in cluster Micro(3). This pathway is a MAPK signaling pathway containing many of the same genes of the proinflammatory pathways upregulated in Micro(3) after rAAV-Cre treatment, such as p38, MAPK, and EGF. The leading-edge subset for downregulation of this pathway in NC-Cas9 treated Micro(3) includes *Ikbkb* and *Prkce,* both of which have been shown to be associated with microglia induced neurotoxicity, neuroinflammation and neuronal death[124-126]. This would seem to suggest that microglia in cluster Micro(3) have low levels of activation, which could potentially be advantageous for the utilization of nanocapsules for therapeutic gene editing in the hippocampus. However, these microglial cells are less reactive than those from the control treated samples, and thus, there is the possibility that too little responsiveness in microglia after nanocapsule facilitated editing could leave the area susceptible to neurodegeneration via alternative mechanisms. For example, in the context of Alzheimer's disease, the TREM2 R47H mutation leads to reduced activation in microglia due to defective TREM2 signaling, resulting in a significant reduction in plaque clearance and increase neuronal dystrophy and ultimately neurodegeneration[65,127].

Three additional immune response and cell-signaling pathways are found to be downregulated in two glutamatergic subsets in NC-Cas9 treated hippocampi. Core enrichment for these pathways are dominated by *CamKII* and the calcineurin subunit coding genes *Ppp3a*, and *Ppp3cc.* CamKII and calcineurin signaling in the hippocampus play essential roles in synaptic plasticity and learning and memory[128,129]. However, they are also

implicated in excitotoxicity leading to neuronal cell death in neurological disorders[129-131]. Therefore, as with the downregulated pathways in Micro(3), this response could prove to be advantageous for nanocapsule-mediated editing in the hippocampus, minimizing excitotoxicity induced neuronal death, or it could implicate deficits in synaptic signaling in response to nanocapsule-mediated gene editing. Both NC-Cas9 and rAAV-Cre treatment resulted in a moderate reduction in the proportion of glutamatergic neurons and an increase in oligodendrocytes, suggesting some degree of inflammatory response and neuronal death as a result of treatment. However, there does not appear to be any significant differences in this effect between the two treatments.

Deeply characterizing the tropism and delivery characteristics of delivery vehicles is likely to be important preclinical data to establish the safety of potential genome editing therapeutics. A p53 response has been noted in prior studies of CRISPR edited cells[132]. We find that these pathways are not significantly enriched in our edited cells. Further, we see no gene expression signatures associated with proliferation at this timepoint, indicating that tumorigenesis process is not observed specifically in the edited cells. These gene expression signatures from potential unintended translocations or chromothripsis were not seen. Longer term studies will be required to fully rule out these adverse outcomes from genome editing.

4.4.3 Conclusions and future steps

Here we have demonstrated the utility of snRNA seq to characterize the safety, efficacy and cell-type specificity of gene-editing based therapeutics. This work has the potential to inform best practices for evaluating novel delivery vectors and potential gene-editing based therapeutics. We are currently investigating the spatial distribution of NC-Cas9 mediated editing in the hippocampus and the striatum with RNAscope *in situ* hybridization assay. The results of this study will serve to buttress our snRNA seq analysis of this editor in the hippocampus, while also providing information on the distribution of editing throughout the

hippocampus and the striatum. Additional experiments are being performed to evaluate NC-Cas9 mediated gene editing in non-human primates targeting the endogenous *APP* gene in Rhesus macaques. These studies should provide greater insight into the utility of this vector for genome editing in the brain for the treatment of human neuropsychiatric disease.

4.5 Methods

4.5.1 Nanoparticle preparation:

NC-Cas9 were prepared as described in reference #9.No targeting ligands were employed for these studies. sgRNA were synthesized by Synthego company with the following modifications: 2'-O-Methyl at 3 first and last bases, 3' phosphototioate bonds between first 3 and last 2 bases

4.5.2 Viral vectors:

AAV9 particles produced from pENN.AAV.CMVs.Pl.Cre.rBG (#105537) at a titer $\geq 1\times10^{13}$ vg/mL purchased from addgene.

4.5.3 Animal subjects:

Ai14 mice were obtained from The Jackson Laboratory. The care, use and treatment of all animals were performed in accordance with protocols approved by the University of Wisconsin- Madison Animal Care and Use Committee. All mice had free access to water and food, were maintained under a tightly controlled temperature (21 ± 5°C), humidity (35–45%) and light/dark (12/12 h) cycle conditions. Animals were between 3 and 5 months at the time of injection.

4.5.4 Intracerebral injections:

Mice were anaesthetized by intraperitoneal injection of a ketamine (120 mg/kg), xylazine (10 mg/kg), and acepromazine (2 mg/kg) cocktail. Thermal stability was maintained by placing mice on a temperature-regulated heating pad during the injection and for recovery purposes. Brain injections were performed using stereotactic methods in a Stoelting stereotactic frame equipped with a Stoelting Quintessential Stereotax Injector (QSI). The right or left hippocampus was targeted at coordinates AP -2.06 mm, ML ±1.35 mm, DV -1.7 mm using a 10 µl Hamilton syringe and 32-gauge 1 inch Hamilton small hub RN needle. The injections were delivered at a rate of 0.2 µl/min, and the tip of the needle remained in place at the injection site for 5 minutes post-injection, after which it was gently withdrawn. After infusion, the operation field was cleaned with sterile saline and closed with surgical glue.

The solutions delivered were 1.5 µl of PBS, 1.5 µl of NC-no ligand with RNP containing Ai14 guide, NC-no ligand with RNP containing non-targeting guide at concentrations of 20 µM RNP suspended in PBS, or 1.5 µl of ready-to-use AAV9 particles produced from pENN.AAV.CMVs.Pl.Cre.rBG (#105537) at a titer ≥ 1×10^{13} vg/mL purchased from addgene.

4.5.5 Hippocampal dissections and isolation of nuclei:

Dissection of the hippocampus from mouse brains was performed as described previously with moderate adaptions[133]. In brief: animals were anesthetized to a surgical plane via isoflurane inhalation, they were then immediately sacrificed with cervical dislocation and the brain rapidly removed and placed into a semi-frozen slurry of carboxygenated (95/5, O_2/CO_2) cutting solution (CS) (in mM: 212 sucrose, 2.6 KCl, 1.25 NaH_2PO_3, 26 $NaHCO_3$, 0.5 $CaCl_2$, 5 $MgCl_2$, 10 glucose). The hippocampi were then dissected from the brain on ice while bathed in ice cold CS and placed directly into 5ml of Hibernate AB media (Hibernate A, 2% B27 and .5mM GlutaMax, BrainBits).

Nuclei were then isolated from the hippocampi following 10X Genomics nuclear isolation protocol for adult brain tissue with some modifications. In brief, hippocampi were transferred to 5 ml of chilled lysis buffer inside the chamber of a 7ml glass Dounce homogenizer. The homogenizer was placed on ice for 5 minutes after which 3-5 passes were made with the smaller diameter pestle to begin homogenization of the tissue. The homogenizer with buffer and tissue was then placed back on ice for 10 minutes after which 3-5 passes were made with the larger diameter pestle completing the tissue homogenization and releasing the nuclei. Nuclei were then filtered, washed and centrifuged to separate nuclei from cellular debris according to 10X protocol. Myelin removal was not performed on nuclei from hippocampal tissue, but rather sucrose density gradient centrifugation was utilized to complete purification of nuclei according to 10X protocol.

4.5.6 Single-nuclei RNA Sequencing:

Single- nuclei RNA-sequencing was performed by the UW-Madison Biotechnology Center Gene Expression Center. The 10x Genomics Chromium Next GEM Single Cell 3′ Library v3.1 Single Cell Gene Expression Assay was used to target 10 000 cells per sample with a sequencing depth of 70,000 reads per cell according to the manufacturer's recommendations (10x Genomics).

4.5.7 Single-nuclei RNA-sequencing analysis:

<u>Alignments, pre-processing, quality control and integration of data sets:</u>

Alignments were performed using 10X Genomics Cell Ranger 6.1.2. We first created a custom reference genome for the Ai14 mouse model by attaching the *Ai14-tdTomato* transgene sequence beginning at the 5’ end of tdTomato coding region, continuing through the Woodchuck Hepatitis Virus Posttranscriptional Regulatory Element (WPRE) and terminating at the 3’ end of the bovine growth hormone polyadenylation signal (bGH-PolyA)

to the GRCm39 *Mus musculus* genome from the Ensembl database following the steps outlined in the 10X genomics Cell Ranger make custom reference genome tutorial. Alignments were then performed with the cellranger count pipeline. By default, cellranger count only counts reads aligned to exons. Since single-nuclei RNA assays capture unspliced pre-mRNAs containing intronic reads in addition to mature mRNA the include-introns flag was added to the cellranger count command to ensure these reads were counted, as is recommended for snRNA seq analysis by 10X genomics. Default quality control filtering settings in Cell Ranger were utilized as the first round of quality control[92]. After alignments and filtering in Cell Ranger a second round of quality control filtering was performed with Seurat version 4.1.1. To exclude potential dead cells and cell debris, we filtered out nuclei with ≤ 500 UMIs, ≤ 200 genes, ≥ 20,000 genes and ≥ 10% mitochondrial genes.

Integrative analysis:

The data were then integrated following the workflow outlined in the Seurat guided analysis. We first log-normalized the filtered matrices and identified highly variable features for each sample using the *FindVariableFeatures* function with default parameters. We then used the *FindIntegrationAnchors* function to identify variable features conserved across the data sets and used these anchors to integrate the datasets using the *IntegrateData* function. We subsequently scaled the integrated matrix and performed linear dimensional reduction using the *RunPCA* function. We then used an elbow plot to visualize the percentage of variance explained by each principal component and opted to use the first 20 principal components for graph-based clustering. Next, we performed UMAP and *K*-nearest neighbor clustering using the function *RunUMAP* with the parameter dims = 20 and the functions *FindNeighbors* and *FindClusters* with the parameter resolution = 0.6.

Differential Expression Analysis:

Differential Expression Analysis:

Differentially expressed genes were identified for each cluster in contrast to the all other clusters by the Wilcoxon rank-sum test using the function *FindAllMarkers* with the parameters logfc.threshold = 0.25 and min.pct = 0.10. These genes along with the expression of previously established cell-type marker genes were used to identify cluster cell-types.

Differential expression analysis to evaluate cell-type and cluster specific differences in the level of *tdTomato* expression between treatments were performed using the function *FindMarkers* with the feature specified as *Ai14-tdTomato.* Comparisons were made between a single cell-type or cluster (i.e. glutamatergic neurons or Olig(2)) from either rAAV-Cre or NC-Cas9 in contrast to the same cell -type or cluster from Control. This function also uses the Wilcoxon rank-sum test. Significance threshold was set at logfc.threshold = 0.25, min.pct = 0.10 and adjusted p-value < 0.05 (adjusted p-value is also known as FDR and is the Bonferroni corrected p=value of the significance of differential expression considering all other features of the dataset).

Differential expression analysis to identify cell-type or cluster specific transcriptomic impacts of treatment were also performed using the function *FindMarkers.* Comparisons were made between a single cell-type or cluster from either NC-Cas9 or rAAV-Cre in contrast to the same cell -type or cluster from Control. This function uses the Wilcoxon rank-sum test. Significance threshold was set at logfc.threshold = 0.25, min.pct = 0.10 and adjusted p-value < 0.05 (adjusted p-value is also known as FDR and is the Bonferroni corrected p=value of the significance of differential expression considering all other features of the dataset).

Similar cell-type specific differential expression analysis with *FindMarkers* was also used to generate differential expression lists used in GSEA analysis. Since GSEA functions best

when ranked expression is included for all or most expressed genes the logfc.threshold for this analysis was set at 0 and min.pct = 0.10.

Gene Set Enrichment Analysis was performed using GSEA version 4.2.3 and the pre-ranked GSEA analysis. Gene lists with log2 fold change and p-values were generated using the *FindMarkers* function in Seurat as described above. Ranked gene lists in .rnk format were generated using log2FC and p-adj values by eVITTA easyGSEA[93]. Ranked gene lists were compared to 72 canonical pathway mouse gene sets contained within the Biocarta database.

Statistical analysis

Differential expression statistics were generated by Seurat using the Wilcoxon rank-sum test with Bonferroni correction expressed in adjusted p-values. Pathway enrichment analyses statistics were generated by GSEA. All other statistical analyses were performed with Graph Pad Prism9. One-way ANOVAs were performed to evaluate the differences between means across the genotype groups with multiple comparisons using the Tukey's HSD.

Acknowledgements: I would like to thank all of our collaborators for their help in this study: the Gong lab for the manufacture of the nanocapsules utilized in these experiments, the Levine lab for their help performing the intracerebral injections and the Roy and Emborg labs for their input and feedback in discussing results and experimental design.

5 Looking forward: the future of gene-therapy in the hippocampus

5.1 Summary and conclusions

As discussed in chapter 1, the hippocampus is a complex and important brain structure with integral roles in behaviour, emotional regulation, and learning and memory. This structure is particularly vulnerable to damage via traumatic brain injury, hypoxic ischemia, and inflammation[1]. These injuries often result in persistent changes in gene expression within the hippocampus continuing degenerative processes and dysregulation long after the original insult has passed[1,9,112,131,134,135]. This structure is also profoundly affected by Alzheimer's disease and other non-AD dementias, as well as psychiatric disorders such anxiety and depression, schizophrenia, and post-traumatic stress disorders[1,8,11,134,136-138]. Alterations in gene expression in these diseases, whether causal or consequential to the diseased state, often contribute to pathogenesis and exacerbate the diseased state. This is particularly true in the context of Alzheimer's disease where altered gene expression in multiple cell-types has been shown to increase amyloid burden and the development of fibrillary fibres, amplify inflammation and contribute to excitotoxicity and neuronal death[1,10,11,15,16,61,74,121,139].

Due to the aforementioned integral role of the hippocampus in behavior, cognition and emotional regulation, damage to this structure can have significant impact on an individual's quality of life. Damage to the hippocampus and other brain regions in Alzheimer's disease leads to memory deficits, significant changes in mood and behavior and ultimately a complete inability to communicate, recognize loved ones or care for oneself. The progression of this disease takes a tremendous emotional toll on the individual affected as well as their loved ones and care givers.

The gravity of degeneration and other disorders within the hippocampus as well as the difficulty in treating many of these disorders with traditional pharmacologics makes it an appealing target for gene-therapy interventions. In this thesis, I have aimed to advance our

current understanding of the utility and potential for gene-therapy based therapeutics in the hippocampus. The data outlined in these chapters illustrates the importance of gene expression regulation in the hippocampus. In chapter 2, I illustrate the molecular mechanisms of age-related transcriptional perturbations in age-associated cognitive decline. Using RNAi, I knockdown expression of *Homer1b/c,* a gene whose expression is dysregulated in age-associated cognitive decline[12]. I show that this knockdown in young animal recapitulates some of the memory deficits observed in aged-impaired animals and determine a role for this protein in the expression of mGluR1/5-mediated LTD[140]. This work illustrates a potential for gene-therapy based regulation of gene expression to influence mechanisms of learning and memory in the hippocampus.

Not only do the important functions of the hippocampus contribute to its appeal as a target for gene-therapy, they also necessitate the utmost caution when considering gene-editing based therapeutics. In chapter 3, I use single nuclei RNA sequencing to characterize cell-type specific transcriptional perturbation in a rodent model of AD, as well as characterizing the transcriptomic impacts of a novel somatic cell gene editing approach for the treatment of AD. Here, I show cell-type specific changes in the disease model which appear to recapitulate some of the key changes observed in AD and in other rodent AD models. Additionally, I've shown that editing in this disease model results in transcriptomic shifts which may be advantageous in the context of AD. While more research is necessary to fully understand the implications of these transcriptomic shifts. These data illustrate the utility of snRNA seq for the characterization and evaluation of potential gene-editing based therapies and may help to advance a novel gene-editing based AD therapeutic toward clinical application.

In addition to evaluating the impacts of a gene therapy modification (gene knockout, gene correction, transcriptional repression etc), important safety consideration must be

accounted for when considering the vector used to deliver gene editing material to the hippocampus. For certain therapies, cell-type specificity could have major impacts on the safety of the gene-therapy based therapeutics. Additionally, delivery vectors and Cas9 editing machinery itself have the potential to elicit immune an immune response[21]. Furthermore, the efficiency of delivery is an important consideration for the efficacy of gene-therapy approach. In Chapter 4, I applied snRNA-seq to characterize the safety and efficacy of editing in the hippocampus via non-viral, nanocapsule-mediated (NC) delivery of SpyCas9 RNP in the hippocampus. Here I show that nanocapsule-mediated editing resulted in robust expression of our reporter, particularly within glutamatergic neurons. Additionally, I have shown differential cell-type specific perturbations in immune response and cell-signalling pathways between NC and rAAV vectors. This data again demonstrates the utility of snRNA seq as a tool for evaluating the safety and efficacy of gene-editing based therapeutics and illustrates differences in tropism and immune response in NC and AAV9 vectors. This work advances the field of gene-therapy in the brain, informing best practices for characterizing the impacts of novel gene therapeutics, specifically in the hippocampus.

5.2 Future steps: characterizing the spatial distribution of gene editing in the hippocampus

The structure of the hippocampus is spatially diverse; the population of cell-types as well as the characteristics of those cell-types vary between regions. For example, the hippocampal dentate gyrus harbors neural precursor cells and is one of the few regions of the brain where adult neurogenesis occurs[6]. Depending on the target and desired gene-editing or gene-therapy outcome, spatially specific editing may be desirable. Alternatively, it may be desirable to utilize a vector that is capable of a broad spatial distribution. It is also possible that different gene therapy interventions will have different impacts within the same cell-type depending on the spatial context of the intervention. Therefore, in addition to characterizing editing

efficiency, cell-type specificity and transcriptomic impact of potential gene-therapy based interventions, it is also important to evaluate the spatial distribution of delivery and spatial variations in response to treatment.

Currently, we are investigating this aspect of nanocapsule-facilitated editing in both the striatum and the hippocampus of Ai14 mice. For this analysis we are utilizing RNAscope, an *in situ* RNA hybridization with single cell resolution and single molecule sensitivity capable of simultaneously characterizing the expression of up to 12 RNA targets (Fig. 5.1)[141,142]. The results of this study will serve to buttress our snRNA seq analysis of this editor in the hippocampus, while also providing information on the distribution of editing throughout the hippocampus and the striatum.

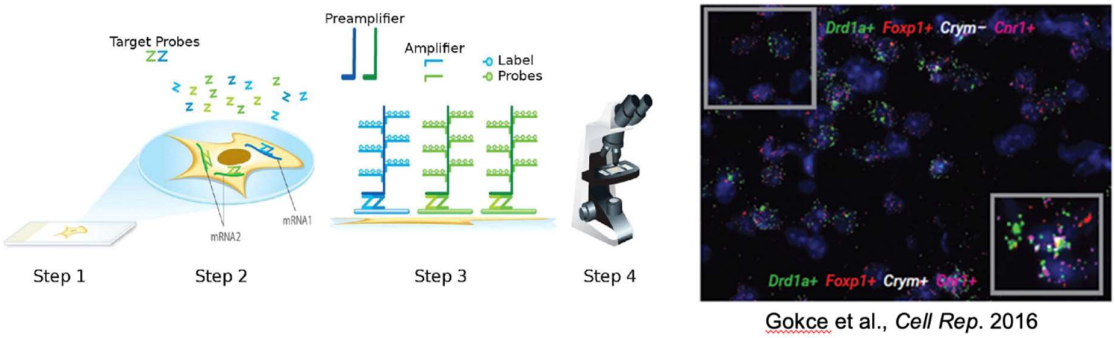

Gokce et al., *Cell Rep*. 2016

Figure 5.1 Schematic and example of RNAscope: RNAscope probes hybridize to RNA targets in slide affixed tissue slices. The signal is then amplified with preamplifier and amplifier scaffolding to which labelled probes can bind. Imaging is used to quantify the RNA signal within the spatial context. Amplifiers and probes can then be cleaved for the next round of staining and imagine allowing for characterization of up to 12 RNA targets. Example of RNAscope identification of novel cell-types in the striatum. Adapted from Reference #141 and #142.

5.3 Cross-species characterization of gene editing: human cell models

Despite the tremendous value of animal models in translational research, there are often important human specific aspects of disease processes that are not recapitulated, and mechanisms of gene expression regulation and cell signaling may not be conserved across species. Therefore, I intend to extend our investigation of the impacts *APP* editing into human cell lines. Our goal is to apply the genome editor against human *APP* in human cell specific monocultures (glia, microglia, neurons, and neural stem cells). Then, we will characterize the cell-type specific impact of this edit using RNA seq, ATACseq, and proteomics. This work will identify human gene regulatory networks (GRNs) associated with those found in our mouse studies as well as elucidate human specific GRNs that would be changed upon editing *APP* in the brain. This research will help to elucidate cell-type specific molecular mechanisms of AD pathology and evaluate the safety and efficacy of a potential genomic editing therapeutic approach in the treatment of AD.

Future steps for characterizing the consequences of therapeutic *APP* editing will aim to explore the impacts of this edit in a multicellular environment. Our current snRNA seq study is elucidating GRNs impacted by editing *in vivo* in mouse model AD brains where important cellular cross-talk between glia and neurons remains intact. By applying the human genome editor in co-cultures of human induced pluripotent cell (hiPSC) derived neurons, astrocytes and microglia and/or hiPSC derived brain organoids we can further explore the potential for differences in response across species and more thoroughly assess the safety and efficacy of this edit for the treatment of Alzheimer's disease. This study has the potential to elucidate novel mechanism of Alzheimer's disease pathology, highlight differences in GRNs

across species, inform best practices for therapeutic gene editing characterization and to advance a novel gene-editing-based therapeutic for Alzheimer's disease treatment.

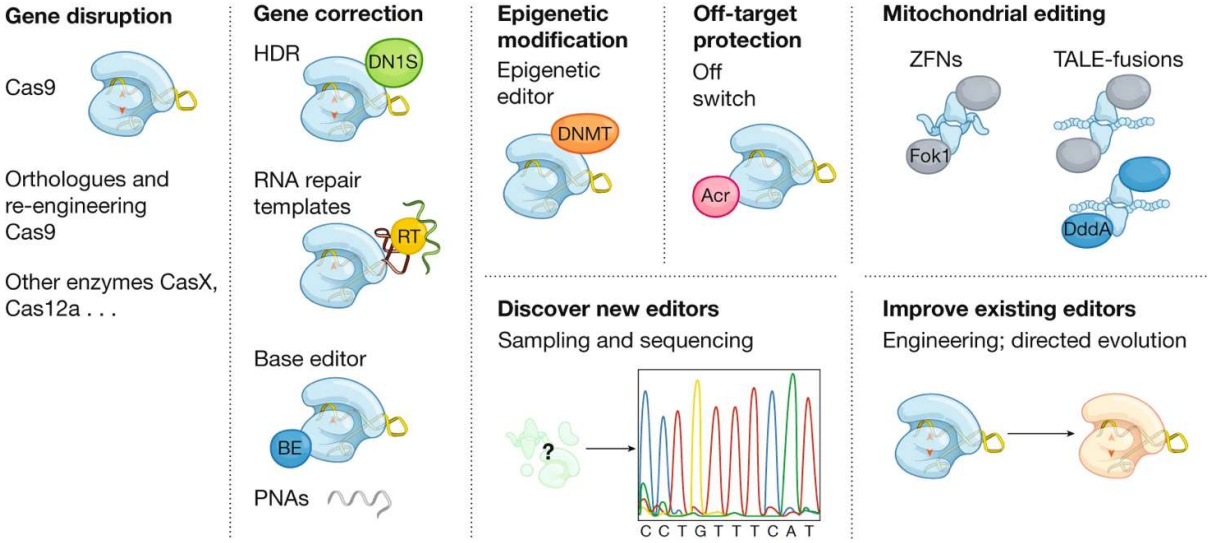

Figure 5.2 Different types of gene editors have a variety of functions and targets. Adapted from reference #143. Overview of different gene editors and their various functions and targets as well as goals for the discovery and engineering of new editors, which could facilitate more nuanced gene-therapy approaches in the hippocampus.

Finally, while the focus of this thesis has primarily been on viral expression of RNAi for permanent knockdown of gene-expression or CRISPR/Cas9 based editing to result in the loss of expression in genome regions, there have been many advances in CRISPR/Cas technology that allow for more nuanced modulation of gene expression (Fig. 5.2)[143]. Future analysis of gene editing in the hippocampus will likely explore the utility of gene expression modulation via novel genome editors. One potential application is targeting adult neurogenesis in the hippocampus. Deficits in adult neurogenesis contribute to age-associated cognitive decline, memory deficits in AD, and are a key feature in major depressive disorder. The process of neurogenesis is stimulated by extrinsic factors which stimulate the activity of transcription factors and epigenetic regulators[6]. It may be possible to combat age-associated cognitive decline, repair memory deficits and combat depression by targeting this pathway, potentially utilizing a CRISPR based epigenetic editor.

Supplemental Figures and Tables

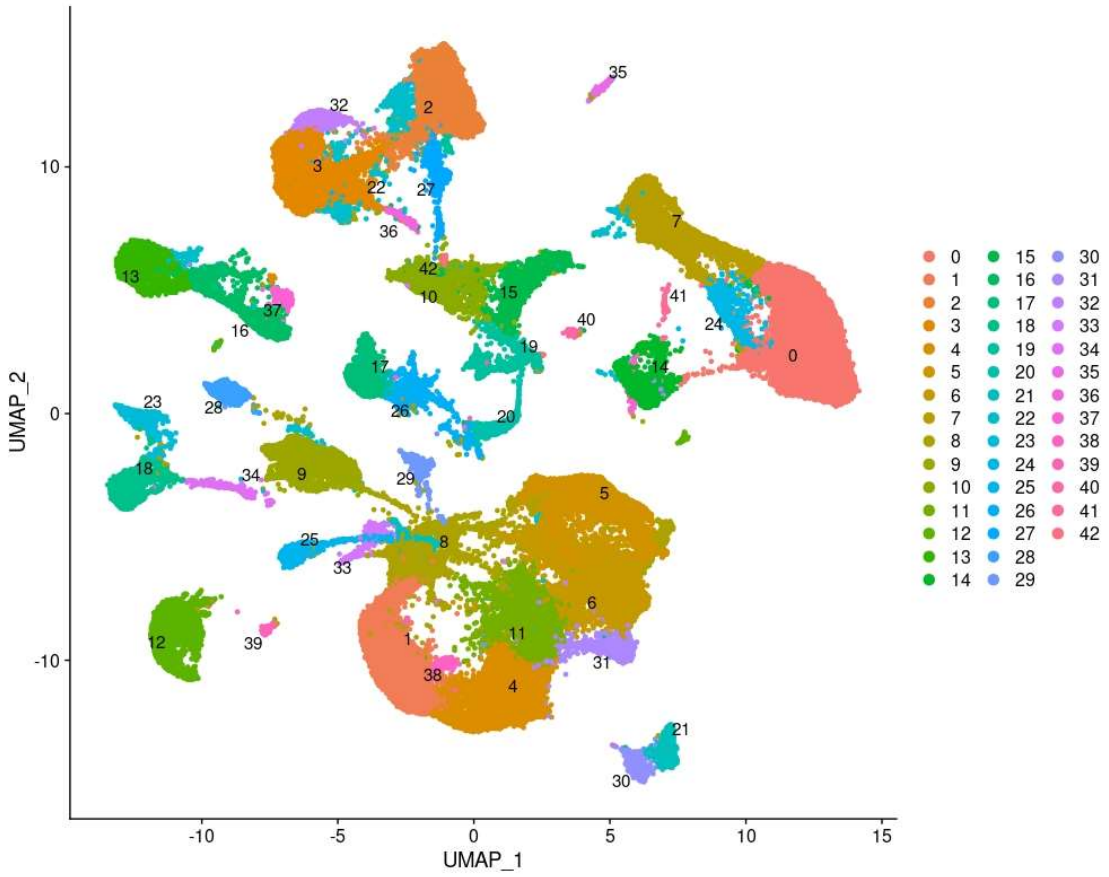

Supplemental Figure 3.1: UMAP projection depicting all the clusters in Figure 3.2a identified by Seurat clustering (resolution parameter = 0.6) prior to cell-type identification and subsequent grouping of adjacent clusters of the same cell type. Identification of cell type and subsequent grouping ultimately resulted in 20 final clusters.

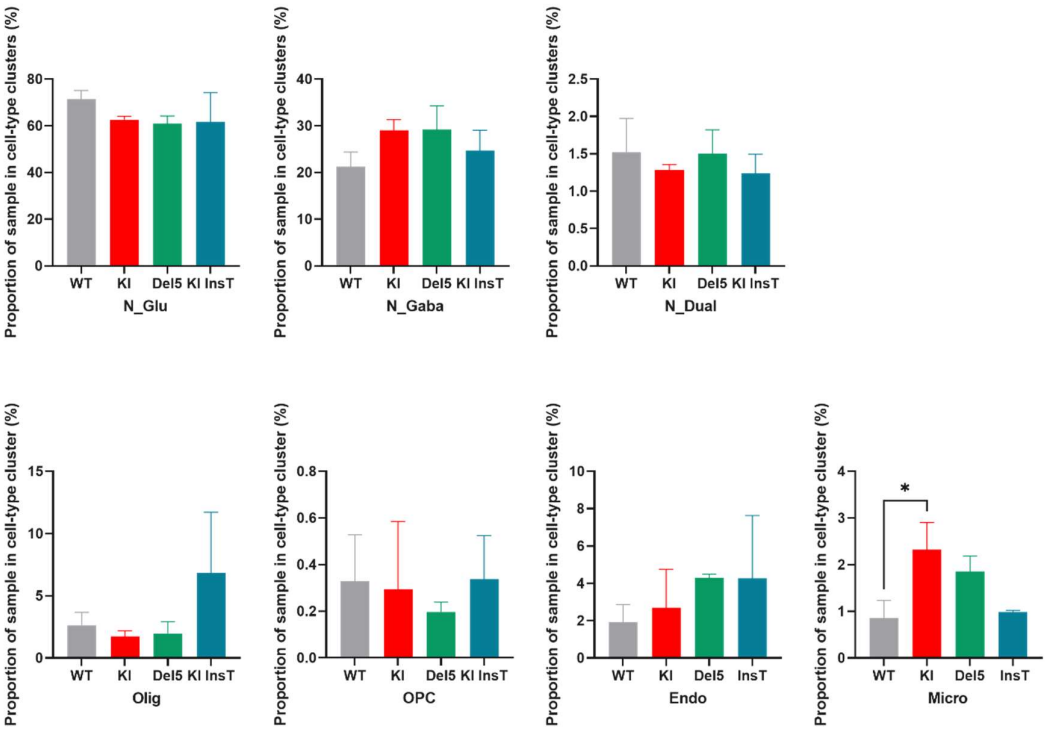

Supplemental Figure 3.2 The proportion of samples in cell-types: Bar graphs indicating the average proportion of sample in each cell-type by genotype. No significant differences were observed between the genotypes for any cell type apart from microglial cells

Sample Type:	WT	WT	Del5	Del5	KI InsT	KI InsT	KI	KI
Sample ID:	A0487B	A0848B	A0953	A0958	A8021	A0570	A0964	A2059
Cluster								
Endo	288	103	606	455	204	822	329	147
Micro(1)	125	48	285	178	104	125	152	323
Olig(1)	212	281	361	144	360	1271	111	243
OPC	21	39	23	25	22	58	7	59
N_Gaba(4)	1408	748	1937	2013	1206	1276	1102	1554
N_Gaba(3)	684	437	652	906	658	753	566	730
N_Gaba(2)	90	52	175	152	69	147	87	141
N_Gaba(1)	431	347	742	537	379	1256	416	1198
N_Dual	205	100	236	140	152	131	106	146
N_Glu(11)	334	214	362	357	250	303	232	361
N_Glu(10)	676	368	397	326	442	268	257	301
N_Glu(9)	1818	1249	2378	1633	1805	2078	1437	1824
N_Glu(8)	102	59	172	144	102	157	141	117
N_Glu(7)	126	109	121	96	162	72	88	136
N_Glu(6)	46	70	177	164	89	64	39	240
N_Glu(5)	236	211	241	378	244	307	157	370
N_Glu(4)	463	394	589	322	623	262	330	410
N_Glu(3)	73	42	133	18	48	9	24	202
N_Glu(2)	3727	3382	4027	2986	3729	2978	2321	3270
N_Glu(1)	66	58	46	26	56	17	26	37
Total	11131	8311	13660	11000	10704	12354	7928	11809

Supplemental Table 3.1: Table indicating the cell counts for each sample within each cluster in Figure 3.2a.

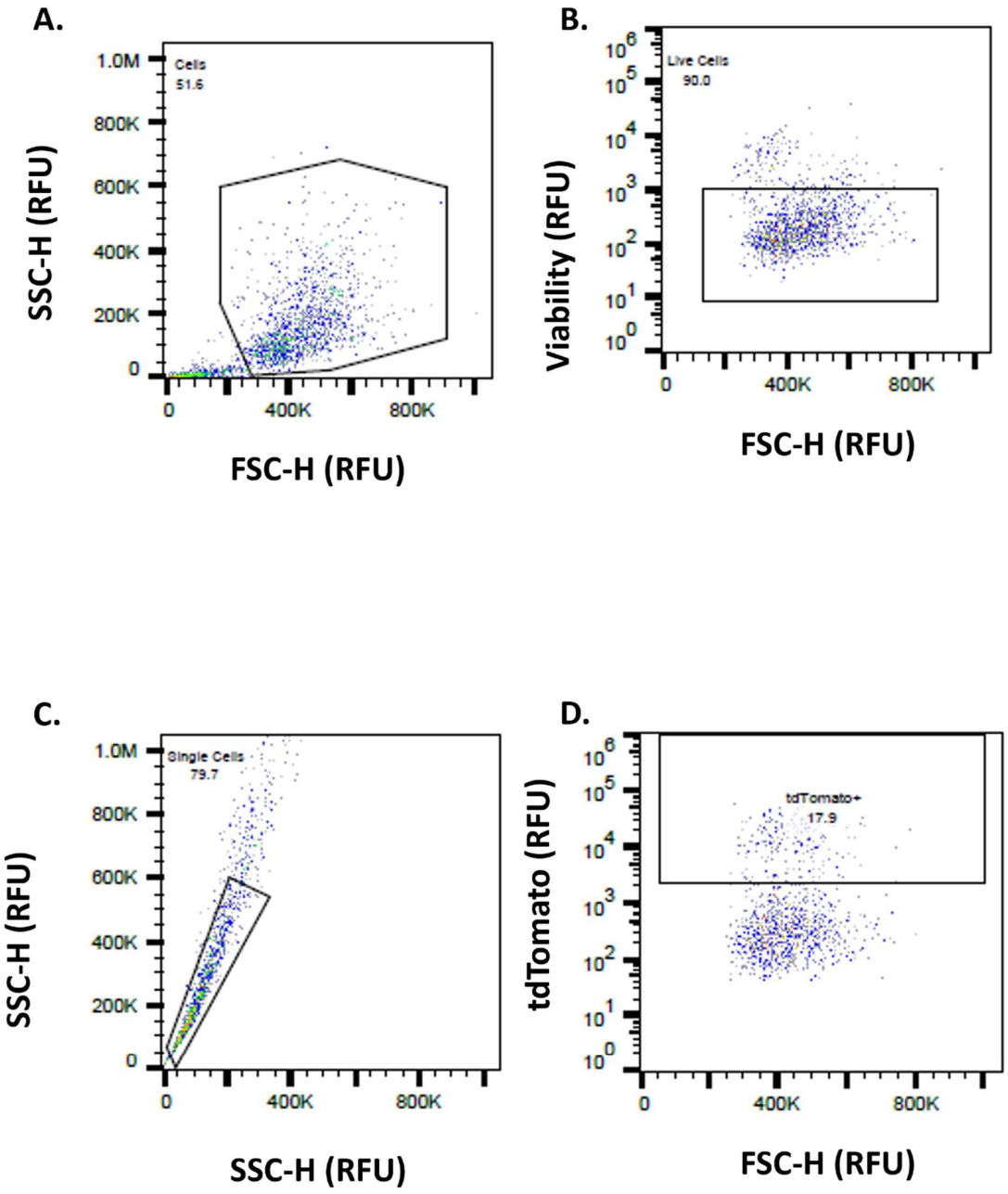

Supplemental Figure 4.1 Flow cytometric analysis of tdTomato expression in *in vitro* edited Ai14 fibroblasts. A representative flow cytometry analysis of tdTomato in *in vitro* edited Ai14 fibroblasts illustrating gating strategy used for analysis. Panel A indicates gating to isolated cells from debris, panel B indicates gating to isolate live cells from dead, panel C indicates gating used to isolate single cells from clumped multiplets and paned D indicates gating used for tdTomato expression. This analysis found 17.9% of the cells to be tdTomato positive. In total 3 groups were edited *in vitro* and analyzed with flow cytometry with an average of 15.3% tdTomato positive cells after editing.

	p_val	avg_log2FC	Fold Change	p_val_adj
N_Glu(1)	5.45E-44	0.168805387	1.124127274	1.19E-39
N_Glu2)	8.94E-37	0.170081069	1.125121706	1.96E-32
N_Glu(3)	6.18E-22	0.145300512	1.105961	1.35E-17
N_Glu(4)	1.97E-07	0.125729572	1.091059342	0.004312
N_Glu(5)	4.75E-07	0.222128441	1.166453212	0.010397
N_Glu6	0.001117	0.311976015	1.241406853	1
N_Glu7	1.25E-68	0.400605775	1.320062077	2.73E-64
N_Glu(8)	1.83E-07	0.105116227	1.075581038	0.004012
N_Gaba	3.11E-32	0.150576755	1.11001314	6.8E-28
Olig(1)	3.96E-28	0.563084591	1.477424688	8.66E-24
Olig(2)	2.96E-187	1.38251469	2.607224275	6.47E-183
Olig(3)	2.98E-01	-0.011	0.992404375	1.00E+00
Astro(1)	1.67E-46	0.348149556	1.272926885	3.66E-42
Astro(2)	1.25E-68	0.400605775	1.320062077	2.73E-64
Micro(1)	4.14E-06	0.20881932	1.155741955	0.090707
Micro(2)	0.009752	0.131882707	1.095722679	1
Micro(3)	0.273863	0.397600391	1.317315021	1
CPC	3.75E-09	0.233928695	1.176033123	8.20E-05
EPC	0.000129	0.128414182	1.093091509	1
Prcytes	0.048823	0.474916545	1.38983782	1
vSMC	5.55E-01	0.077333	1.055065817	1.00E+00

Supplemental Table 4.1 Differential expression analysis by cluster of *tdTomato* in NC-Cas9 vs control treated animals. p-val indicates the unadjusted p values for significance of the differential expression. avg_log2FC indicates the log base 2 of the average fold change in *tdTomato* expression between the two groups – NC-Cas9 vs control: positive values indicate an increase in tdTomato in NC-Cas9 treated clusters, negative values indicate a decrease. Fold change indicates the fold change in *tdTomato* expression in NC-Cas9 vs control treated samples. p_val_adj indicated the adjusted p-value of the significance of the differential expression based on Bonferroni correction using all features in the dataset. Adjusted p-value is also known as false discovery rate (FDR) and is the metric used for significance cut off in all differential expression analyses within this thesis.

	p_val	avg_log2FC	Fold Chang	p_val_adj
N_Glu(1)	1.09E-44	0.166675311	1.122469	2.39E-40
N_Glu2)	2.11E-39	0.222766199	1.166969	4.62E-35
N_Glu(3)	1.06E-16	0.083880206	1.059865	2.32E-12
N_Glu(4)	2.24E-13	0.320058022	1.248381	4.89E-09
N_Glu(5)	1.31E-05	0.203451567	1.15145	0.287024
N_Glu(6)	1.25E-08	0.660893381	1.581061	0.000274
N_Glu(7)	2.59E-32	0.401544194	1.320921	5.67E-28
N_Glu(8)	3.11E-15	0.206338237	1.153756	6.80E-11
N_Gaba	3.08E-39	0.174247906	1.128376	6.75E-35
Olig(1)	2.24E-16	0.397795636	1.317493	4.91E-12
Olig(2)	1.60E-23	1.074973304	2.106683	3.50E-19
Olig(3)	1.55E-21	0.828999018	1.776452	3.40E-17
Astro(1)	8.25E-187	1.108067278	2.155567	1.81E-182
Astro(2)	0.00141	0.400823807	1.320262	1
Micro(1)	5.83E-13	0.377313583	1.298921	1.28E-08
Micro(2)	2.92E-15	1.010204712	2.014197	6.39E-11
Micro(3)	0.137217	0.387327981	1.307969	1
CPC	2.33E-15	0.691351322	1.614795	5.10E-11
EPC	1.74E-07	0.28997246	1.222617	0.003811
Prcyts	0.000147	0.829078569	1.77655	1
vSMC	0.069393	0.427581232	1.344977	1

Supplemental Table 4.2 Differential expression analysis by cluster of *tdTomato* in rAAV-Cre vs control treated animals. p-val indicates the unadjusted p values for significance of the differential expression. avg_log2FC indicates the log base 2 of the average fold change in *tdTomato* expression between the two groups – rAAV vs control: positive values indicate an increase in tdTomato in NC-Cas9 treated clusters, negative values indicate a decrease. Fold change indicates the fold change in *tdTomato* expression in NC-Cas9 vs control treated samples. p_val_adj indicated the adjusted p-value of the significance of the differential expression based on Bonferroni correction using all features in the dataset. Adjusted p-value is also known as false discovery rate (FDR) and is the metric used for significance cut off in all differential expression analyses within this thesis.

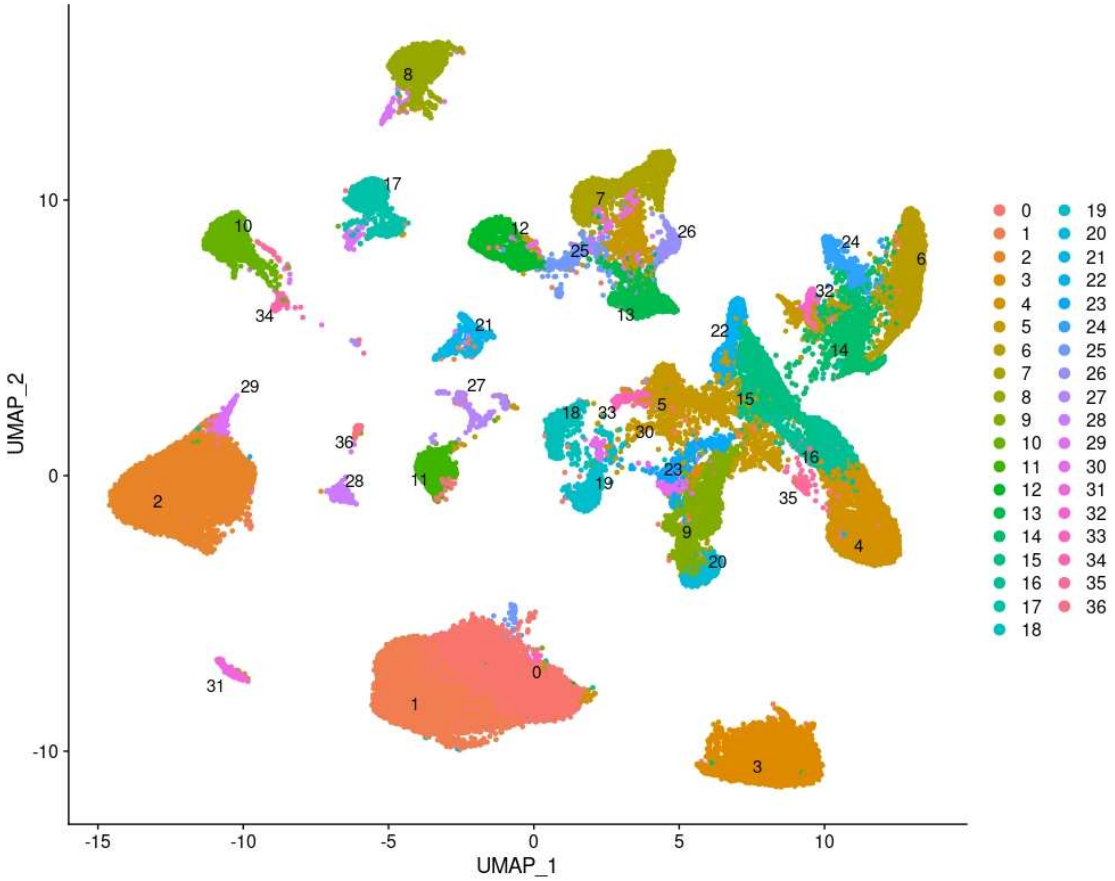

Supplemental Figure 4.2 UMAP projection of all Seurat identified clusters (resolution parameter = 0.6) prior to cell-type identification and grouping of adjacent clusters of the same cell-type. Cell-type identification and grouping yielded 22 final clusters.

Sample ID:	S1	S10	S11	S12	S14	S2	S4	S7	S8	S9
Sample Type:	NC-Cas9	NC-Cas9	rAAV-Cre	rAAV-Cre	PBS	NC-Scram	Uninjected	NC-Cas9	NC-Scram	NC-Cas9
Cluster										
Olig(3)	136	2487	953	1895	286	77	60	210	1274	3103
Olig(2)	894	1143	683	513	379	813	391	2557	1694	604
Astro(1)	216	844	1210	785	1284	938	839	943	1597	1345
N_Glu(7)	176	121	456	183	337	973	633	705	1245	246
N_Glu(1)	220	546	967	682	1174	751	453	780	1165	1087
N_Glu(8)	78	213	385	218	563	315	236	153	334	341
N_Glu(2)	121	316	815	521	713	541	332	526	826	721
N_Gaba	109	625	852	1107	1403	438	227	591	773	1316
EPC	35	219	382	444	432	165	92	146	249	468
N_Glu(3)	92	638	306	165	912	359	162	390	401	657
Micro(1)	54	391	150	215	355	28	94	175	182	465
Olig(1)	59	236	268	162	248	294	249	287	364	183
CPC	2	188	0	244	345	106	0	63	48	454
N_Glu(4)	28	200	101	55	289	129	79	134	160	239
N_Glu(5)	24	102	116	123	169	102	48	106	139	168
Micro(2)	4	154	87	153	171	27	22	36	97	179
Prcyts	7	92	94	86	74	22	24	35	33	101
Astro(2)	6	45	33	42	96	35	16	28	27	80
N_Glu(6)	19	11	43	17	42	74	61	24	65	31
Micro(4)	9	47	44	12	45	25	26	14	42	30
vSMC	1	8	1	35	33	1	1	1	23	68
Total	2290	8626	7946	7657	9350	6213	4045	7904	10738	11886

Supplemental Table 4.3 Table indicating the cell counts in each cluster for each sample in Figure 4.2a

Bibliography

1 Anand, K. S. & Dhikav, V. Hippocampus in health and disease: An overview. *Ann Indian Acad Neurol* **15**, 239-246, doi:10.4103/0972-2327.104323 (2012).

2 Tracy, A. L., Jarrard, L. E. & Davidson, T. L. The hippocampus and motivation revisited: appetite and activity. *Behav Brain Res* **127**, 13-23, doi:10.1016/s0166-4328(01)00364-3 (2001).

3 Rubin, R. D., Watson, P. D., Duff, M. C. & Cohen, N. J. The role of the hippocampus in flexible cognition and social behavior. *Front Hum Neurosci* **8**, 742, doi:10.3389/fnhum.2014.00742 (2014).

4 Bliss, T. V. & Cooke, S. F. Long-term potentiation and long-term depression: a clinical perspective. *Clinics (Sao Paulo)* **66 Suppl 1**, 3-17, doi:10.1590/s1807-59322011001300002 (2011).

5 Wheeler, D. W. *et al.* Hippocampome.org: a knowledge base of neuron types in the rodent hippocampus. *Elife* **4**, doi:10.7554/eLife.09960 (2015).

6 Toda, T. & Gage, F. H. Review: adult neurogenesis contributes to hippocampal plasticity. *Cell Tissue Res* **373**, 693-709, doi:10.1007/s00441-017-2735-4 (2018).

7 Bettio, L. E. B., Rajendran, L. & Gil-Mohapel, J. The effects of aging in the hippocampus and cognitive decline. *Neurosci Biobehav Rev* **79**, 66-86, doi:10.1016/j.neubiorev.2017.04.030 (2017).

8 Heckers, S. & Konradi, C. Hippocampal neurons in schizophrenia. *J Neural Transm* **109**, 891-905, doi:DOI 10.1007/s007020200073 (2002).

9 Andrus, B. M. *et al.* Gene expression patterns in the hippocampus and amygdala of endogenous depression and chronic stress models. *Mol Psychiatry* **17**, 49-61, doi:10.1038/mp.2010.119 (2012).

10 Small, S. A., Schobel, S. A., Buxton, R. B., Witter, M. P. & Barnes, C. A. A pathophysiological framework of hippocampal dysfunction in ageing and disease. *Nat Rev Neurosci* **12**, 585-601, doi:10.1038/nrn3085 (2011).

11 Moodley, K. K. & Chan, D. The hippocampus in neurodegenerative disease. *Front Neurol Neurosci* **34**, 95-108, doi:10.1159/000356430 (2014).

12 Burger, C. *et al.* Changes in transcription within the CA1 field of the hippocampus are associated with age-related spatial learning impairments. *Neurobiol Learn Mem* **87**, 21-41, doi:10.1016/j.nlm.2006.05.003 (2007).

13 Gerstein, H., Lindstrom, M. J. & Burger, C. Gene delivery of Homer1c rescues spatial learning in a rodent model of cognitive aging. *Neurobiology of Aging* **34**, 1963-1970, doi:10.1016/j.neurobiolaging.2013.02.006 (2013).

14 Gerstein, H., O'Riordan, K., Osting, S., Schwarz, M. & Burger, C. Rescue of synaptic plasticity and spatial learning deficits in the hippocampus of Homer1 knockout mice by recombinant Adeno-associated viral gene delivery of Homer1c. *Neurobiol Learn Mem* **97**, 17-29, doi:10.1016/j.nlm.2011.08.009 (2012).

15 Chen, W. T. *et al.* Spatial Transcriptomics and In Situ Sequencing to Study Alzheimer's Disease. *Cell* **182**, 976-991 e919, doi:10.1016/j.cell.2020.06.038 (2020).

16 Saura, C. A., Parra-Damas, A. & Enriquez-Barreto, L. Gene expression parallels synaptic excitability and plasticity changes in Alzheimer's disease. *Front Cell Neurosci* **9**, 318, doi:10.3389/fncel.2015.00318 (2015).

17 Sun, J. *et al.* CRISPR/Cas9 editing of APP C-terminus attenuates beta-cleavage and promotes alpha-cleavage. *Nat Commun* **10**, 53, doi:10.1038/s41467-018-07971-8 (2019).

18 Sun, J. & Roy, S. Gene-based therapies for neurodegenerative diseases. *Nat Neurosci* **24**, 297-311, doi:10.1038/s41593-020-00778-1 (2021).

19 Amado, D. A. & Davidson, B. L. Gene therapy for ALS: A review. *Mol Ther* **29**, 3345-3358, doi:10.1016/j.ymthe.2021.04.008 (2021).

20 Musunuru, K. *et al.* In vivo CRISPR base editing of PCSK9 durably lowers cholesterol in primates. *Nature* **593**, 429-434, doi:10.1038/s41586-021-03534-y (2021).

21 Broeders, M., Herrero-Hernandez, P., Ernst, M. P. T., van der Ploeg, A. T. & Pijnappel, W. Sharpening the Molecular Scissors: Advances in Gene-Editing Technology. *iScience* **23**, 100789, doi:10.1016/j.isci.2019.100789 (2020).

22 Tuladhar, R. *et al.* CRISPR-Cas9-based mutagenesis frequently provokes on-target mRNA misregulation. *Nat Commun* **10**, 4056, doi:10.1038/s41467-019-12028-5 (2019).

23 Duncan, R. S., Hwang, S. Y. & Koulen, P. Effects of Vesl/Homer proteins on intracellular signaling. *Exp Biol Med (Maywood)* **230**, 527-535, doi:10.1177/153537020523000803 (2005).

24 Kammermeier, P. J. Endogenous homer proteins regulate metabotropic glutamate receptor signaling in neurons. *J Neurosci* **28**, 8560-8567, doi:10.1523/JNEUROSCI.1830-08.2008 (2008).

25 Aggleton, J. P. & Brown, M. W. Contrasting hippocampal and perirhinal cortex function using immediate early gene imaging. *Q J Exp Psychol B* **58**, 218-233, doi:10.1080/02724990444000131 (2005).

26 Ronesi, J. A. & Huber, K. M. Homer interactions are necessary for metabotropic glutamate receptor-induced long-term depression and translational activation. *J Neurosci* **28**, 543-547, doi:10.1523/JNEUROSCI.5019-07.2008 (2008).

27 Tu, J. C. *et al.* Homer binds a novel proline-rich motif and links group 1 metabotropic glutamate receptors with IP3 receptors. *Neuron* **21**, 717-726, doi:10.1016/s0896-6273(00)80589-9 (1998).

28 Xiao, B. *et al.* Homer regulates the association of group 1 metabotropic glutamate receptors with multivalent complexes of homer-related, synaptic proteins. *Neuron* **21**, 707-716, doi:10.1016/s0896-6273(00)80588-7 (1998).

29 Klugmann, M. *et al.* AAV-mediated hippocampal expression of short and long Homer 1 proteins differentially affect cognition and seizure activity in adult rats. *Mol Cell Neurosci* **28**, 347-360, doi:10.1016/j.mcn.2004.10.002 (2005).

30 Menard, C. & Quirion, R. Successful cognitive aging in rats: a role for mGluR5 glutamate receptors, homer 1 proteins and downstream signaling pathways. *PLoS One* **7**, e28666, doi:10.1371/journal.pone.0028666 (2012).

31 O'Riordan, K., Gerstein, H., Hullinger, R. & Burger, C. The role of Homer1c in metabotropic glutamate receptor-dependent long-term potentiation. *Hippocampus* **24**, 1-6, doi:10.1002/hipo.22222 (2014).

32 Cortese, G. P., Olin, A., O'Riordan, K., Hullinger, R. & Burger, C. Environmental enrichment improves hippocampal function in aged rats by enhancing learning and memory, LTP, and

mGluR5-Homer1c activity. *Neurobiol Aging* **63**, 1-11, doi:10.1016/j.neurobiolaging.2017.11.004 (2018).

33 Hullinger, R., O'Riordan, K. & Burger, C. Environmental enrichment improves learning and memory and long-term potentiation in young adult rats through a mechanism requiring mGluR5 signaling and sustained activation of p70s6k. *Neurobiol Learn Mem* **125**, 126-134, doi:10.1016/j.nlm.2015.08.006 (2015).

34 Balschun, D. *et al.* A specific role for group I mGluRs in hippocampal LTP and hippocampus-dependent spatial learning. *Learn Mem* **6**, 138-152 (1999).

35 Goh, J. J. & Manahan-Vaughan, D. Endogenous hippocampal LTD that is enabled by spatial object recognition requires activation of NMDA receptors and the metabotropic glutamate receptor, mGlu5. *Hippocampus* **23**, 129-138, doi:10.1002/hipo.22072 (2013).

36 Goh, J. J. & Manahan-Vaughan, D. Spatial object recognition enables endogenous LTD that curtails LTP in the mouse hippocampus. *Cereb Cortex* **23**, 1118-1125, doi:10.1093/cercor/bhs089 (2013).

37 Kemp, A. & Manahan-Vaughan, D. Hippocampal long-term depression and long-term potentiation encode different aspects of novelty acquisition. *Proc Natl Acad Sci U S A* **101**, 8192-8197, doi:10.1073/pnas.0402650101 (2004).

38 Manahan-Vaughan, D. & Braunewell, K. H. Novelty acquisition is associated with induction of hippocampal long-term depression. *Proc Natl Acad Sci U S A* **96**, 8739-8744, doi:10.1073/pnas.96.15.8739 (1999).

39 Luscher, C. & Huber, K. M. Group 1 mGluR-dependent synaptic long-term depression: mechanisms and implications for circuitry and disease. *Neuron* **65**, 445-459, doi:10.1016/j.neuron.2010.01.016 (2010).

40 Di Prisco, G. V. *et al.* Translational control of mGluR-dependent long-term depression and object-place learning by eIF2alpha. *Nat Neurosci* **17**, 1073-1082, doi:10.1038/nn.3754 (2014).

41 Palmer, M. J., Irving, A. J., Seabrook, G. R., Jane, D. E. & Collingridge, G. L. The group I mGlu receptor agonist DHPG induces a novel form of LTD in the CA1 region of the hippocampus. *Neuropharmacology* **36**, 1517-1532, doi:10.1016/s0028-3908(97)00181-0 (1997).

42 Huber, K. M., Roder, J. C. & Bear, M. F. Chemical induction of mGluR5- and protein synthesis--dependent long-term depression in hippocampal area CA1. *J Neurophysiol* **86**, 321-325, doi:10.1152/jn.2001.86.1.321 (2001).

43 Gravius, A., Barberi, C., Schafer, D., Schmidt, W. J. & Danysz, W. The role of group I metabotropic glutamate receptors in acquisition and expression of contextual and auditory fear conditioning in rats - a comparison. *Neuropharmacology* **51**, 1146-1155, doi:10.1016/j.neuropharm.2006.07.008 (2006).

44 Wood, S. C. & Anagnostaras, S. G. Interdependence of measures in pavlovian conditioned freezing. *Neurosci Lett* **505**, 134-139, doi:10.1016/j.neulet.2011.10.006 (2011).

45 Selden, N. R., Everitt, B. J., Jarrard, L. E. & Robbins, T. W. Complementary roles for the amygdala and hippocampus in aversive conditioning to explicit and contextual cues. *Neuroscience* **42**, 335-350, doi:10.1016/0306-4522(91)90379-3 (1991).

46 Bachevalier, J. & Nemanic, S. Memory for spatial location and object-place associations are differently processed by the hippocampal formation, parahippocampal areas TH/TF and perirhinal cortex. *Hippocampus* **18**, 64-80, doi:10.1002/hipo.20369 (2008).

47 Baxter, M. G. & Murray, E. A. Opposite relationship of hippocampal and rhinal cortex damage to delayed nonmatching-to-sample deficits in monkeys. *Hippocampus* **11**, 61-71, doi:10.1002/1098-1063(2001)11:1<61::AID-HIPO1021>3.0.CO;2-Z (2001).

48 Beason-Held, L. L., Rosene, D. L., Killiany, R. J. & Moss, M. B. Hippocampal formation lesions produce memory impairment in the rhesus monkey. *Hippocampus* **9**, 562-574, doi:10.1002/(SICI)1098-1063(1999)9:5<562::AID-HIPO10>3.0.CO;2-X (1999).

49 Broadbent, N. J., Squire, L. R. & Clark, R. E. Spatial memory, recognition memory, and the hippocampus. *Proc Natl Acad Sci U S A* **101**, 14515-14520, doi:10.1073/pnas.0406344101 (2004).

50 Brown, M. W. & Aggleton, J. P. Recognition memory: what are the roles of the perirhinal cortex and hippocampus? *Nat Rev Neurosci* **2**, 51-61, doi:10.1038/35049064 (2001).

51 Clark, R. E., Zola, S. M. & Squire, L. R. Impaired recognition memory in rats after damage to the hippocampus. *J Neurosci* **20**, 8853-8860 (2000).

52 Morris, R. G., Garrud, P., Rawlins, J. N. & O'Keefe, J. Place navigation impaired in rats with hippocampal lesions. *Nature* **297**, 681-683, doi:10.1038/297681a0 (1982).

53 Sutherland, D. E., Gillingham, K. & Moudry-Munns, K. C. Results of pancreas transplantation in the United States for 1987-90 from the United Network for Organ Sharing (UNOS) Registry with comparison to 1984-87 results. *Clin Transplant* **5**, 330-341 (1991).

54 Ayala, J. E. *et al.* mGluR5 positive allosteric modulators facilitate both hippocampal LTP and LTD and enhance spatial learning. *Neuropsychopharmacology* **34**, 2057-2071, doi:10.1038/npp.2009.30 (2009).

55 Volk, L. J., Daly, C. A. & Huber, K. M. Differential roles for group 1 mGluR subtypes in induction and expression of chemically induced hippocampal long-term depression. *J Neurophysiol* **95**, 2427-2438, doi:10.1152/jn.00383.2005 (2006).

56 Mao, L. *et al.* The scaffold protein Homer1b/c links metabotropic glutamate receptor 5 to extracellular signal-regulated protein kinase cascades in neurons. *J Neurosci* **25**, 2741-2752, doi:10.1523/JNEUROSCI.4360-04.2005 (2005).

57 Giuffrida, R. *et al.* A reduced number of metabotropic glutamate subtype 5 receptors are associated with constitutive homer proteins in a mouse model of fragile X syndrome. *J Neurosci* **25**, 8908-8916, doi:10.1523/JNEUROSCI.0932-05.2005 (2005).

58 Burger, C. *et al.* Recombinant AAV viral vectors pseudotyped with viral capsids from serotypes 1, 2, and 5 display differential efficiency and cell tropism after delivery to different regions of the central nervous system. *Mol Ther* **10**, 302-317, doi:10.1016/j.ymthe.2004.05.024 (2004).

59 Hullinger, R., Ugalde, J., Puron-Sierra, L., Osting, S. & Burger, C. The MRI contrast agent gadoteridol enhances distribution of rAAV1 in the rat hippocampus. *Gene Ther* **20**, 1172-1177, doi:10.1038/gt.2013.47 (2013).

60 Hullinger, R. & Burger, C. Learning impairments identified early in life are predictive of future impairments associated with aging. *Behav Brain Res* **294**, 224-233, doi:10.1016/j.bbr.2015.08.004 (2015).

61 De Strooper, B. & Karran, E. The Cellular Phase of Alzheimer's Disease. *Cell* **164**, 603-615, doi:10.1016/j.cell.2015.12.056 (2016).

62 Keren-Shaul, H. *et al.* A Unique Microglia Type Associated with Restricting Development of Alzheimer's Disease. *Cell* **169**, 1276-1290 e1217, doi:10.1016/j.cell.2017.05.018 (2017).

63 Jiang, M. *et al.* Amyloid precursor protein intracellular domain-dependent regulation of FOXO3a inhibits adult hippocampal neurogenesis. *Neurobiol Aging* **95**, 250-263, doi:10.1016/j.neurobiolaging.2020.07.031 (2020).

64 Zhou, Y. *et al.* Human and mouse single-nucleus transcriptomics reveal TREM2-dependent and TREM2-independent cellular responses in Alzheimer's disease. *Nat Med* **26**, 131-142, doi:10.1038/s41591-019-0695-9 (2020).

65 Zhou, Y., Ulland, T. K. & Colonna, M. TREM2-Dependent Effects on Microglia in Alzheimer's Disease. *Front Aging Neurosci* **10**, 202, doi:10.3389/fnagi.2018.00202 (2018).

66 Alves da Costa, C. *et al.* Presenilin-dependent gamma-secretase-mediated control of p53-associated cell death in Alzheimer's disease. *J Neurosci* **26**, 6377-6385, doi:10.1523/JNEUROSCI.0651-06.2006 (2006).

67 Chang, K. A. *et al.* Phosphorylation of amyloid precursor protein (APP) at Thr668 regulates the nuclear translocation of the APP intracellular domain and induces neurodegeneration. *Mol Cell Biol* **26**, 4327-4338, doi:10.1128/MCB.02393-05 (2006).

68 Coronel, R. *et al.* Physiological effects of amyloid precursor protein and its derivatives on neural stem cell biology and signaling pathways involved. *Neural Regen Res* **14**, 1661-1671, doi:10.4103/1673-5374.257511 (2019).

69 D'Andrea, L., Stringhi, R., Di Luca, M. & Marcello, E. Looking at Alzheimer's Disease Pathogenesis from the Nuclear Side. *Biomolecules* **11**, doi:10.3390/biom11091261 (2021).

70 Wang, X. *et al.* FoxO mediates APP-induced AICD-dependent cell death. *Cell Death Dis* **5**, e1233, doi:10.1038/cddis.2014.196 (2014).

71 Saito, T. *et al.* Single App knock-in mouse models of Alzheimer's disease. *Nature Neuroscience* **17**, 661-+, doi:10.1038/nn.3697 (2014).

72 Mehla, J. *et al.* Age-dependent behavioral and biochemical characterization of single APP knock-in mouse (APP(NL-G-F/NL-G-F)) model of Alzheimer's disease. *Neurobiology of Aging* **75**, 25-37, doi:10.1016/j.neurobiolaging.2018.10.026 (2019).

73 Hao, Y. *et al.* Integrated analysis of multimodal single-cell data. *Cell* **184**, 3573-3587 e3529, doi:10.1016/j.cell.2021.04.048 (2021).

74 Lau, S. F., Cao, H., Fu, A. K. Y. & Ip, N. Y. Single-nucleus transcriptome analysis reveals dysregulation of angiogenic endothelial cells and neuroprotective glia in Alzheimer's disease. *Proc Natl Acad Sci U S A* **117**, 25800-25809, doi:10.1073/pnas.2008762117 (2020).

75 Bonham, L. W., Sirkis, D. W. & Yokoyama, J. S. The Transcriptional Landscape of Microglial Genes in Aging and Neurodegenerative Disease. *Front Immunol* **10**, 1170, doi:10.3389/fimmu.2019.01170 (2019).

76 Ximerakis, M. *et al.* Single-cell transcriptomic profiling of the aging mouse brain. *Nat Neurosci* **22**, 1696-1708, doi:10.1038/s41593-019-0491-3 (2019).

77 Del-Aguila, J. L. *et al.* A single-nuclei RNA sequencing study of Mendelian and sporadic AD in the human brain. *Alzheimers Res Ther* **11**, 71, doi:10.1186/s13195-019-0524-x (2019).

78 Al-Dalahmah, O. *et al.* Single-nucleus RNA-seq identifies Huntington disease astrocyte states. *Acta Neuropathol Commun* **8**, 19, doi:10.1186/s40478-020-0880-6 (2020).

79 MacDonald, A. *et al.* Single Cell Transcriptomics of Ependymal Cells Across Age, Region and Species Reveals Cilia-Related and Metal Ion Regulatory Roles as Major Conserved Ependymal Cell Functions. *Front Cell Neurosci* **15**, 703951, doi:10.3389/fncel.2021.703951 (2021).

80 Olah, M. *et al.* Single cell RNA sequencing of human microglia uncovers a subset associated with Alzheimer's disease. *Nat Commun* **11**, 6129, doi:10.1038/s41467-020-19737-2 (2020).

81 Sobue, A. *et al.* Microglial gene signature reveals loss of homeostatic microglia associated with neurodegeneration of Alzheimer's disease. *Acta Neuropathol Commun* **9**, 1, doi:10.1186/s40478-020-01099-x (2021).

82 Yang, H. S. *et al.* Natural genetic variation determines microglia heterogeneity in wild-derived mouse models of Alzheimer's disease. *Cell Rep* **34**, 108739, doi:10.1016/j.celrep.2021.108739 (2021).

83 Brawek, B. *et al.* Impairment of in vivo calcium signaling in amyloid plaque-associated microglia. *Acta Neuropathol* **127**, 495-505, doi:10.1007/s00401-013-1242-2 (2014).

84 Mattson, M. P. & Chan, S. L. Neuronal and glial calcium signaling in Alzheimer's disease. *Cell Calcium* **34**, 385-397, doi:10.1016/s0143-4160(03)00128-3 (2003).

85 Butovsky, O. & Weiner, H. L. Microglial signatures and their role in health and disease. *Nat Rev Neurosci* **19**, 622-635, doi:10.1038/s41583-018-0057-5 (2018).

86 Tavassoly, O., Sato, T. & Tavassoly, I. Inhibition of Brain Epidermal Growth Factor Receptor Activation: A Novel Target in Neurodegenerative Diseases and Brain Injuries. *Mol Pharmacol* **98**, 13-22, doi:10.1124/mol.120.119909 (2020).

87 Zhao, J., Deng, Y., Jiang, Z. & Qing, H. G Protein-Coupled Receptors (GPCRs) in Alzheimer's Disease: A Focus on BACE1 Related GPCRs. *Front Aging Neurosci* **8**, 58, doi:10.3389/fnagi.2016.00058 (2016).

88 Balez, R. & Ooi, L. Getting to NO Alzheimer's Disease: Neuroprotection versus Neurotoxicity Mediated by Nitric Oxide. *Oxid Med Cell Longev* **2016**, 3806157, doi:10.1155/2016/3806157 (2016).

89 Sohrabi, M., Floden, A. M., Manocha, G. D., Klug, M. G. & Combs, C. K. IGF-1R Inhibitor Ameliorates Neuroinflammation in an Alzheimer's Disease Transgenic Mouse Model. *Front Cell Neurosci* **14**, 200, doi:10.3389/fncel.2020.00200 (2020).

90 Abdul, H. M., Furman, J. L., Sama, M. A., Mathis, D. M. & Norris, C. M. NFATs and Alzheimer's Disease. *Mol Cell Pharmacol* **2**, 7-14 (2010).

91 Nygaard, H. B., van Dyck, C. H. & Strittmatter, S. M. Fyn kinase inhibition as a novel therapy for Alzheimer's disease. *Alzheimers Res Ther* **6**, 8, doi:10.1186/alzrt238 (2014).

92 Zheng, G. X. *et al.* Massively parallel digital transcriptional profiling of single cells. *Nat Commun* **8**, 14049, doi:10.1038/ncomms14049 (2017).

93 Cheng, X., Yan, J., Liu, Y., Wang, J. & Taubert, S. eVITTA: a web-based visualization and inference toolbox for transcriptome analysis. *Nucleic Acids Res* **49**, W207-W215, doi:10.1093/nar/gkab366 (2021).

94 Staahl, B. T. *et al.* Efficient genome editing in the mouse brain by local delivery of engineered Cas9 ribonucleoprotein complexes. *Nat Biotechnol* **35**, 431-434, doi:10.1038/nbt.3806 (2017).

95 Swiech, L. *et al.* In vivo interrogation of gene function in the mammalian brain using CRISPR-Cas9. *Nat Biotechnol* **33**, 102-106, doi:10.1038/nbt.3055 (2015).

96 Yamaguchi, H., Hopf, F. W., Li, S. B. & de Lecea, L. In vivo cell type-specific CRISPR knockdown of dopamine beta hydroxylase reduces locus coeruleus evoked wakefulness. *Nat Commun* **9**, 5211, doi:10.1038/s41467-018-07566-3 (2018).

97 Chen, G. *et al.* A biodegradable nanocapsule delivers a Cas9 ribonucleoprotein complex for in vivo genome editing. *Nat Nanotechnol* **14**, 974-980, doi:10.1038/s41565-019-0539-2 (2019).

98 Zeisel, A. *et al.* Brain structure. Cell types in the mouse cortex and hippocampus revealed by single-cell RNA-seq. *Science* **347**, 1138-1142, doi:10.1126/science.aaa1934 (2015).

99 Madisen, L. *et al.* A robust and high-throughput Cre reporting and characterization system for the whole mouse brain. *Nat Neurosci* **13**, 133-140, doi:10.1038/nn.2467 (2010).

100 Mootha, V. K. *et al.* PGC-1alpha-responsive genes involved in oxidative phosphorylation are coordinately downregulated in human diabetes. *Nat Genet* **34**, 267-273, doi:10.1038/ng1180 (2003).

101 Subramanian, A. *et al.* Gene set enrichment analysis: a knowledge-based approach for interpreting genome-wide expression profiles. *Proc Natl Acad Sci U S A* **102**, 15545-15550, doi:10.1073/pnas.0506580102 (2005).

102 Kim, S. H., Smith, C. J. & Van Eldik, L. J. Importance of MAPK pathways for microglial pro-inflammatory cytokine IL-1 beta production. *Neurobiol Aging* **25**, 431-439, doi:10.1016/S0197-4580(03)00126-X (2004).

103 Burguillos, M. A. *et al.* Caspase signalling controls microglia activation and neurotoxicity. *Nature* **472**, 319-324, doi:10.1038/nature09788 (2011).

104 Kavanagh, E. *et al.* Deletion of caspase-8 in mouse myeloid cells blocks microglia pro-inflammatory activation and confers protection in MPTP neurodegeneration model. *Aging (Albany NY)* **7**, 673-689, doi:10.18632/aging.100805 (2015).

105 Viceconte, N. *et al.* Neuromelanin activates proinflammatory microglia through a caspase-8-dependent mechanism. *J Neuroinflammation* **12**, 5, doi:10.1186/s12974-014-0228-x (2015).

106 Zhang, C. J. *et al.* TLR-stimulated IRAKM activates caspase-8 inflammasome in microglia and promotes neuroinflammation. *J Clin Invest* **128**, 5399-5412, doi:10.1172/JCI121901 (2018).

107 Papazian, I. *et al.* Fundamentally different roles of neuronal TNF receptors in CNS pathology: TNFR1 and IKKbeta promote microglial responses and tissue injury in demyelination while TNFR2 protects against excitotoxicity in mice. *J Neuroinflammation* **18**, 222, doi:10.1186/s12974-021-02200-4 (2021).

108 Qu, W. S. *et al.* Inhibition of EGFR/MAPK signaling reduces microglial inflammatory response and the associated secondary damage in rats after spinal cord injury. *J Neuroinflammation* **9**, 178, doi:10.1186/1742-2094-9-178 (2012).

109 Kaminska, B., Mota, M. & Pizzi, M. Signal transduction and epigenetic mechanisms in the control of microglia activation during neuroinflammation. *Biochim Biophys Acta* **1862**, 339-351, doi:10.1016/j.bbadis.2015.10.026 (2016).

110 Borsini, A. *et al.* Interferon-Alpha Reduces Human Hippocampal Neurogenesis and Increases Apoptosis via Activation of Distinct STAT1-Dependent Mechanisms. *Int J Neuropsychopharmacol* **21**, 187-200, doi:10.1093/ijnp/pyx083 (2018).

111 Butturini, E., Boriero, D., Carcereri de Prati, A. & Mariotto, S. STAT1 drives M1 microglia activation and neuroinflammation under hypoxia. *Arch Biochem Biophys* **669**, 22-30, doi:10.1016/j.abb.2019.05.011 (2019).

112 Takagi, Y., Harada, J., Chiarugi, A. & Moskowitz, M. A. STAT1 is activated in neurons after ischemia and contributes to ischemic brain injury. *J Cereb Blood Flow Metab* **22**, 1311-1318, doi:10.1097/01.WCB.0000034148.72481.F4 (2002).

113 Haery, L. *et al.* Adeno-Associated Virus Technologies and Methods for Targeted Neuronal Manipulation. *Front Neuroanat* **13**, 93, doi:10.3389/fnana.2019.00093 (2019).

114 Grace, P. M. *et al.* DREADDed microglia in pain: Implications for spinal inflammatory signaling in male rats. *Exp Neurol* **304**, 125-131, doi:10.1016/j.expneurol.2018.03.005 (2018).

115 Olbrich, H. G. & Braak, H. Ratio of pyramidal cells versus non-pyramidal cells in sector CA1 of the human Ammon's horn. *Anat Embryol (Berl)* **173**, 105-110, doi:10.1007/BF00707308 (1985).

116 Donat, C. K., Scott, G., Gentleman, S. M. & Sastre, M. Microglial Activation in Traumatic Brain Injury. *Front Aging Neurosci* **9**, 208, doi:10.3389/fnagi.2017.00208 (2017).

117 Kaur, C., Rathnasamy, G. & Ling, E. A. Roles of activated microglia in hypoxia induced neuroinflammation in the developing brain and the retina. *J Neuroimmune Pharmacol* **8**, 66-78, doi:10.1007/s11481-012-9347-2 (2013).

118 Leng, F. & Edison, P. Neuroinflammation and microglial activation in Alzheimer disease: where do we go from here? *Nat Rev Neurol* **17**, 157-172, doi:10.1038/s41582-020-00435-y (2021).

119 Lull, M. E. & Block, M. L. Microglial activation and chronic neurodegeneration. *Neurotherapeutics* **7**, 354-365, doi:10.1016/j.nurt.2010.05.014 (2010).

120 Perry, V. H., Nicoll, J. A. & Holmes, C. Microglia in neurodegenerative disease. *Nat Rev Neurol* **6**, 193-201, doi:10.1038/nrneurol.2010.17 (2010).

121 Streit, W. J., Mrak, R. E. & Griffin, W. S. Microglia and neuroinflammation: a pathological perspective. *J Neuroinflammation* **1**, 14, doi:10.1186/1742-2094-1-14 (2004).

122 Sinha, D. *et al.* Human iPSC Modeling Reveals Mutation-Specific Responses to Gene Therapy in a Genotypically Diverse Dominant Maculopathy. *Am J Hum Genet* **107**, 278-292, doi:10.1016/j.ajhg.2020.06.011 (2020).

123 Cromer, M. K. *et al.* Global Transcriptional Response to CRISPR/Cas9-AAV6-Based Genome Editing in CD34(+) Hematopoietic Stem and Progenitor Cells. *Mol Ther* **26**, 2431-2442, doi:10.1016/j.ymthe.2018.06.002 (2018).

124 Cho, I. H. *et al.* Role of microglial IKKbeta in kainic acid-induced hippocampal neuronal cell death. *Brain* **131**, 3019-3033, doi:10.1093/brain/awn230 (2008).

125 Gordon, R. *et al.* Protein kinase Cdelta upregulation in microglia drives neuroinflammatory responses and dopaminergic neurodegeneration in experimental models of Parkinson's disease. *Neurobiol Dis* **93**, 96-114, doi:10.1016/j.nbd.2016.04.008 (2016).

126 McMillian, M. K., Vainio, P. J. & Tuominen, R. K. Role of protein kinase C in microglia-induced neurotoxicity in mesencephalic cultures. *J Neuropathol Exp Neurol* **56**, 301-307, doi:10.1097/00005072-199703000-00009 (1997).

127 Cheng-Hathaway, P. J. *et al.* The Trem2 R47H variant confers loss-of-function-like phenotypes in Alzheimer's disease. *Mol Neurodegener* **13**, 29, doi:10.1186/s13024-018-0262-8 (2018).

128 Rongo, C. A fresh look at the role of CaMKII in hippocampal synaptic plasticity and memory. *Bioessays* **24**, 223-233, doi:10.1002/bies.10057 (2002).

129 Saraf, J. *et al.* A Friend or Foe: Calcineurin across the Gamut of Neurological Disorders. *ACS Cent Sci* **4**, 805-819, doi:10.1021/acscentsci.8b00230 (2018).

130 Dos Santos, J. P. A., Vizuete, A. F. & Goncalves, C. A. Calcineurin-Mediated Hippocampal Inflammatory Alterations in Streptozotocin-Induced Model of Dementia. *Mol Neurobiol* **57**, 502-512, doi:10.1007/s12035-019-01718-2 (2020).

131 Ashpole, N. M. & Hudmon, A. Excitotoxic neuroprotection and vulnerability with CaMKII inhibition. *Mol Cell Neurosci* **46**, 720-730, doi:10.1016/j.mcn.2011.02.003 (2011).

132 Haapaniemi, E., Botla, S., Persson, J., Schmierer, B. & Taipale, J. CRISPR-Cas9 genome editing induces a p53-mediated DNA damage response. *Nat Med* **24**, 927-930, doi:10.1038/s41591-018-0049-z (2018).

133 Gimse, K. E., O'Riordan, K. & Burger, C. Induction of Metabotropic Glutamate Receptor-Mediated Long-Term Depression in the Hippocampal Schaffer Collateral Pathway of Aging Rats. *Methods Mol Biol* **1941**, 93-105, doi:10.1007/978-1-4939-9077-1_8 (2019).

134 Alfonso, J., Frasch, A. C. & Flugge, G. Chronic stress, depression and antidepressants: effects on gene transcription in the hippocampus. *Rev Neurosci* **16**, 43-56, doi:10.1515/revneuro.2005.16.1.43 (2005).

135 Szaflarski, J., Burtrum, D. & Silverstein, F. S. Cerebral hypoxia-ischemia stimulates cytokine gene expression in perinatal rats. *Stroke* **26**, 1093-1100, doi:10.1161/01.str.26.6.1093 (1995).

136 Fournier, N. M. & Duman, R. S. Role of vascular endothelial growth factor in adult hippocampal neurogenesis: implications for the pathophysiology and treatment of depression. *Behav Brain Res* **227**, 440-449, doi:10.1016/j.bbr.2011.04.022 (2012).

137 Gulbins, E. *et al.* A central role for the acid sphingomyelinase/ceramide system in neurogenesis and major depression. *J Neurochem* **134**, 183-192, doi:10.1111/jnc.13145 (2015).

138 Jiang, P. *et al.* Stress and vitamin D: altered vitamin D metabolism in both the hippocampus and myocardium of chronic unpredictable mild stress exposed rats. *Psychoneuroendocrinology* **38**, 2091-2098, doi:10.1016/j.psyneuen.2013.03.017 (2013).

139 Palop, J. J. & Mucke, L. Amyloid-beta-induced neuronal dysfunction in Alzheimer's disease: from synapses toward neural networks. *Nat Neurosci* **13**, 812-818, doi:10.1038/nn.2583 (2010).

140 Gimse, K., Gorzek, R. C., Olin, A., Osting, S. & Burger, C. Hippocampal Homer1b/c is necessary for contextual fear conditioning and group I metabotropic glutamate receptor mediated long-term depression. *Neurobiol Learn Mem* **156**, 17-23, doi:10.1016/j.nlm.2018.10.005 (2018).

141 Wang, F. *et al.* RNAscope: a novel in situ RNA analysis platform for formalin-fixed, paraffin-embedded tissues. *J Mol Diagn* **14**, 22-29, doi:10.1016/j.jmoldx.2011.08.002 (2012).

142 Gokce, O. *et al.* Cellular Taxonomy of the Mouse Striatum as Revealed by Single-Cell RNA-Seq. *Cell Rep* **16**, 1126-1137, doi:10.1016/j.celrep.2016.06.059 (2016).

143 Saha, K. *et al.* The NIH Somatic Cell Genome Editing program. *Nature* **592**, 195-204, doi:10.1038/s41586-021-03191-1 (2021).